RADIOLOGICAL AND NUCLEAR COUNTERMEASURES PROGRAM

Securing America against unconventional attacks

JULY 2009

LLNL-TR-418342

Nuisance Source Population Modeling for Radiation Detection System Analysis

Lawrence Livermore National Laboratory

PADMINI SOKKAPPA*

DAVID LANGE

KARL NELSON

RICHARD WHEELER

*925-423-3940 • sokkappa1@llnl.gov

LAWRENCE LIVERMORE NATIONAL LABORATORY

tpg
Q1011

Nuisance Source Population Modeling for Radiation Detection System Analysis

July 2009

*Padmini Sokkappa**

David Lange

Karl Nelson

Richard Wheeler

LLNL-TR-418342

*925-423-3940, sokkappa1@llnl.gov

Lawrence Livermore National Laboratory
P.O. Box 808 · Livermore, CA 94551-0808

Acknowledgements

The authors would like to acknowledge the helpful cooperation of John Mattingly and Dean Mitchell of Sandia National Laboratories throughout the course of this study. The software package GADRAS, developed by Dean, continues to play an important role in our analysis. We also acknowledge Dan Blumenthal, now with the Department of Energy, and the team at the Johns Hopkins University Applied Physics Laboratory for providing Advanced Spectroscopic Portal test data.

This work was supported by the DHS Domestic Nuclear Detection Office (DNDO) System Architecture Directorate.

Executive Summary

A major challenge facing the prospective deployment of radiation detection systems for homeland security applications is the discrimination of radiological or nuclear "threat sources" from radioactive, but benign, "nuisance sources". Common examples of such nuisance sources include naturally occurring radioactive material (NORM), medical patients who have received radioactive drugs for either diagnostics or treatment, and industrial sources. A sensitive detector that cannot distinguish between "threat" and "benign" classes will generate false positives which, if sufficiently frequent, will preclude it from being operationally deployed.

In this report, we describe a first-principles physics-based modeling approach that is used to approximate the physical properties and corresponding gamma ray spectral signatures of real nuisance sources. Specific models are proposed for the three nuisance source classes – NORM, medical and industrial. The models can be validated against measured data – that is, energy spectra generated with the model can be compared to actual nuisance source data. We show by example how this is done for NORM and medical sources, using data sets obtained from spectroscopic detector deployments for cargo container screening and urban area traffic screening, respectively.

In addition to capturing the range of radioactive signatures of individual nuisance sources, a nuisance source population model must generate sources with a frequency of occurrence consistent with that found in actual movement of goods and people. Measured radiation detection data can indicate these frequencies, but, at present, such data are available only for a very limited set of locations and time periods. In this report, we make more general estimates of frequencies for NORM and medical sources using a range of data sources such as shipping manifests and medical treatment statistics. We also identify potential data sources for industrial source frequencies, but leave the task of estimating these frequencies for future work.

Modeling of nuisance source populations is only useful if it helps in understanding detector system performance in real operational environments. Examples of previous studies in which nuisance source models played a key role are briefly discussed. These include screening of in-bound urban traffic and monitoring of shipping containers in transit to U.S. ports.

Modeling Status and Key Findings

1. Models described in this report are sufficiently developed for use in evaluation studies of detector system performance, including algorithm effectiveness.

2. *Individual source characterization.* The first-principles models developed in the current effort for all three classes of nuisance sources are sufficient for characterizing the range of individual nuisance source signatures. Initial validation has been done with available data.

- NORM – A spanning set of NORM sources was created based on materials and anticipated types and ranges of effective shielding.

- Medical – We have performed an extensive survey of nuclear medicine sources to identify what drugs are used in the medical practice and how long those drugs will be apparent in the body. We created first-principles shielding models for each of these medical sources.

- Industrial – We have developed models that span the range of possible source/packaging combinations, but have not attempted to specifically model all configurations known to be in use. For a given source type, we constructed a general model, based on transportation regulations, to set lower bounds and specific examples to determine expected upper bounds.

3. *Population frequency.* We have not found integrated data sources that provide sufficient information on frequency of occurrence of the various nuisance sources. Current frequency estimates are based on published studies, surveys, required registries and limited detector deployments, usually without ground truth.

    - NORM – We used 14 days of PIERS manifest data to characterize seasonal and port-to-port variation in NORM cargo. With the aid of field measurements from the Advanced Spectroscopic Portal test program, we have estimated the frequency of each source (or equivalent sources) in the spanning NORM model. With the aid of manifest data linked to field measurements, this methodology could be used to estimate detector performance at venues with differing source frequencies corresponding to different cargo distributions.

    - Medical – We have used drug application frequency data from Germany along with the frequency of U.S. procedures to create a first-principles population model. Initial application of this model resulted in good agreement with field measurements.

    - Industrial – We have identified a range of data sources for estimating frequency of occurrence, including manufacturer specifications, market surveys, and trade association and regulatory agency reports.

4. Significant data gaps remain. Previous studies have identified the need for more comprehensive, correlated data sets.

    - The size of an input data sample limits the number of records that can be simulated without oversampling, and thus the minimum false alarm rate that can be assessed.

    - Radiation detector data combined with ground truth for the objects screened would provide valuable validation information. For example, when used with more readily available commodity frequency data (such as

shipping manifests), these ground truth data allow a NORM model developed with data from one venue to be applied to another venue, even though the NORM populations may differ significantly.

- For medical sources, data on procedures done in Germany is a reasonable starting point for source term characterization. Comparable U.S. data would be very useful, but are not readily available.

- For industrial sources, the National Source Tracking System, may provide relevant frequency data for Category 1 and 2 sources, but is not fully operational at present. Expansion to include smaller sources (Category 3-4) has been proposed.

Next Steps

1. Case studies should be conducted to demonstrate the utility and limitations of the current nuisance source models.

2. Sensitivity analysis should be done for all nuisance source models. This could identify the impact of uncertain parameters on the simulated populations and help prioritize efforts to obtain better data.

3. NORM

    - Individual models for specific cargo types need to be developed so that a population model can be applied to multiple locations with different distributions of arriving cargo (and hence NORM).

    - Frequency estimates for the entire NORM populations at various sites need to be improved using more comprehensive manifest data.

    - Verification is needed to show that the NORM model is sufficient to parameterize NORM cargo at multiple ports. The range of model parameters that account for observed NORM cargo must be determined.

4. Medical

    - Data are needed on U.S. medical procedures to better reflect the distribution of radioactive sources likely to be encountered.

    - Improved estimates of frequency of therapeutic applications, in addition to diagnostic applications, are needed.

    - Non-uniform movement of medical patients in a given area should be accounted for (e.g., roads in the vicinity of hospitals are likely to see a higher fraction of patients than roads in general).

- Shipments of medical sources should be included in the population model in addition to medical patients.

- Medical source body models should be tuned to observed field data.

5. Industrial

- The industrial source frequency data we have identified should be analyzed for relevant frequency information.

- Using the spanning set of industrial sources we have developed, we should perform a sensitivity analysis to identify which sources are the most troublesome. We should then focus on improving the source models and frequency estimates for these challenging sources.

Table of Contents

1.0 Introduction

Performance of a radiation detection system depends upon a number of components, including the operational scenario, the threat sources to be detected, the population of other radioactive sources that could trigger nuisance alarms, background radiation at the deployed site, and the radiation detector hardware and alarm algorithms that are used. **Figure 1-1** illustrates the relationship among these components for a generic passive detection system[1]. Proper characterization and modeling of each of these components is needed to model the performance of radiation detection systems.

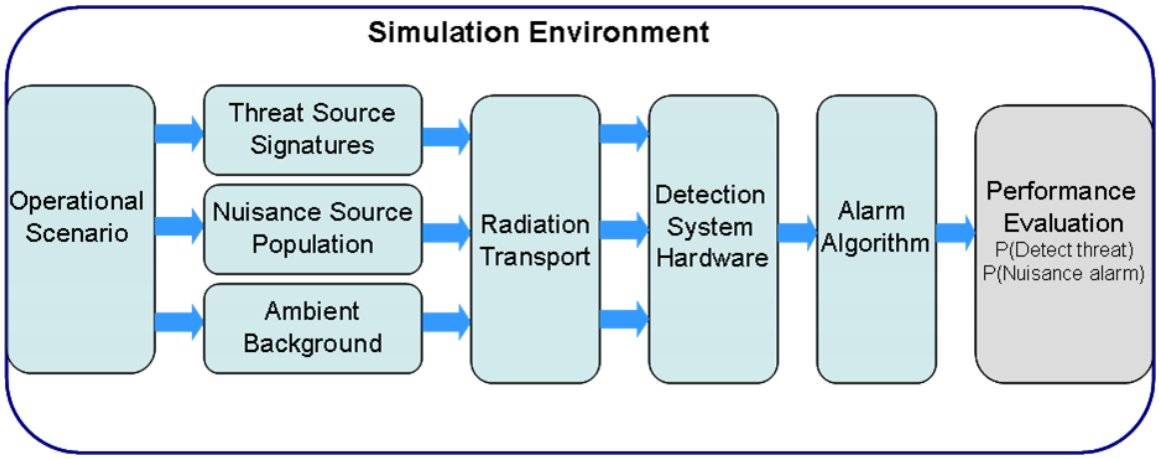

Figure 1-1. Components affecting passive radiation detection system performance.

This report focuses on nuisance source populations. The nuisance source population for an operational scenario is the population of legitimate radioactive sources that pass through the detection system. In this report, we consider only the gamma ray emissions from such sources. Legitimate sources include naturally occurring radioactive material (NORM), medical isotopes and industrial sources. The frequency of nuisance alarms from legitimate sources is often the limiting operational factor for a radiation detection system. Analysis to predict nuisance alarm rates requires a representation of the nuisance source population. This representation must include both the frequencies of the various nuisance source types and their characterization in terms of either radionuclide composition and activities or spectral signatures.

We have developed statistical models or modeling approaches for the three types of nuisance sources. A general modeling approach, described in the following section, is applied for the three different types of nuisance sources, NORM, medical, and industrial. Section 3 provides information on the data sources that we use to support nuisance source population modeling. The remaining sections describe the status of our modeling efforts

[1] Active detection systems involve directing energy toward the object being screened and collecting a resulting signature. Performance evaluation of these systems requires representing this interaction in addition to the radioactive source term emissions on the detector. The individual nuisance source term models described in this report apply to passive detection systems.

for each of the three nuisance source types. Whether one, two, or all three of the population models are applicable for a system performance study depends on the particular operational scenario. For example, for an urban monitoring scenario, all three of the populations are likely to be relevant. On the other hand, for a cargo monitoring system, only the NORM and industrial source populations would be relevant. For pedestrian monitors, the medical source population would be most important.

2.0 General Approach to Nuisance Source Population Modeling

Our goal is to create a statistical model of a radiation nuisance source population based on a representative set of measurements from that population. If the measured data is representative of the true population, then the statistical model allows us to generate arbitrarily large samples from that population for use in performance evaluation studies. Typically we have a small, but reasonably representative, set of field measurements containing up to a few thousand observations of members of the population. These observations are in the form of spectra obtained from a radiation detection system. Our general approach is to build a physics-based model of the nuisance sources that spans the range of variation present in the population. We use this physics-based model to create a random population of nuisance sources. We then apply a test to determine whether the population generated by the model spans the measured data. Next, using the measured data, we apply weights to the members of the modeled population such that a random sample drawn from the population using these weights will produce data which is statistically similar to the measured data.

2.1 Physics-based model

In our paradigm, a conveyance (or person) carrying a nuisance source is scanned using a spectroscopic detector. The nuisance source has a given physical geometry, activity, and age, which determines the source flux. Before reaching the detector, radiation from the source may pass through intervening material, which attenuates some of the energy lines and downscatters those energy lines into other energies. The detector observes the radiation in the form of a single integer-valued vector $Y \in Z^{512}$, which is the gamma energy spectrum sampled with 512 energy bins (windows), typically ranging from 0 – 3 MeV.

To represent the population we create a simplified physics-based model that represents a nuisance source, either a point source or a distributed source consisting of one or more radionuclides distributed in some material, and a shielding configuration. Although nuisance sources may have varying geometries, we use a simple spherical model consisting of concentric layers in which the innermost layers represent the radiation source and subsequent layers represent engineered and/or incidental shielding. The variables in the model represent the range of physical properties (composition, thickness, radionuclide activity) that impact the observed spectra. **Figure 2-1** illustrates the generic spherical model. The innermost layer is a void that is used to account for the self-shielding characteristics of non-spherical sources by varying the surface area to mass ratio of the radiation source. The next layer represents the radiation source. This is followed by a void to account for variability of scattering in the subsequent layers. Subsequent layers represent shielding or intervening materials between the source and the detector. The presence of voids, the arrangement and composition of shielding layers, and the range of thickness for each of these layers depend on the particular class of nuisance source being modeled. Likewise, the choice of composition, mass or thickness, radionuclides, and radionuclide activities for the radiation source also depends on the

class of nuisance source. A model for a particular class of nuisance sources is defined by the arrangement of layers and the distributions to be used for each of the variables (e.g., presence, composition, thickness, radionuclide activity).[2]

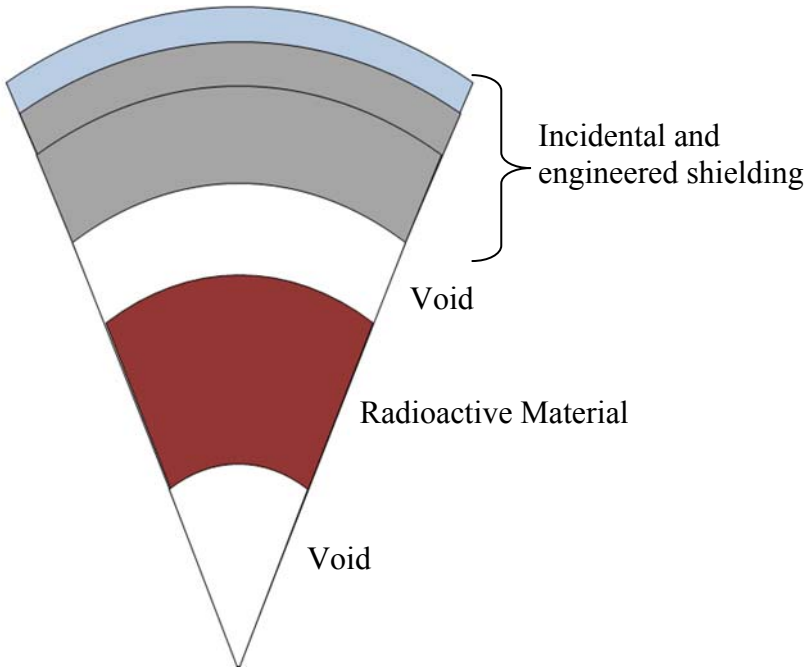

Figure 2-1. One-dimensional spherical model of a radioactive source and packaging.

We use our model to generate a random set of sources, transport their radiation to the detector, and apply the appropriate detector response function (based on the measured data set that we are using) to produce their spectral signatures. The number of samples generated is large relative to the number of measured observations in our data set. To simplify our model of nuisance sources, we break the signatures down into a shape vector and a scalar intensity. This is because we often view the same shape with a different intensity when more or less radioactive source is present. The intensity of any individual spectrum is normalized resulting in a population of spectral shapes. A complete population model would have an intensity distribution associated with each spectral shape.

2.2 Testing whether model spans measured data

Once we have generated random set of nuisance sources using our physics-based model, we perform a test to assure that the model does in fact span the measured population. Our

[2] This same basic model has also been used to generate statistically representative "threat" sources for a nuclear smuggling scenario **[Nelson 2008]**

modeled set of sources is denoted by $\boldsymbol{\theta}$ with elements θ_j and our measured data set is denoted by $\mathbf{Y}$ with elements Y_i. To perform this analysis, we compute the Mahalanobis distance d_j between each θ_j and its closest neighbor in the set $\boldsymbol{\theta}$ to generate the distribution of these intra-set distances. We also compute a distance δ_{ij}, between each pair Y_i and θ_j. The distance metric used is the Mahalanobis distance between Y_i and $\alpha_{ij}\theta_j + \beta_{ij}B_i$ where α_{ij} is a scaling factor for intensity, B_i is the background estimate for the measured data, and β_{ij} is a scaling factor to account for background suppression. The values of α_{ij} and β_{ij} are set so as to minimize δ_{ij} subject to the constraint $0.8 < \beta_{ij} < 1.0$. This constraint was set based on typical observed background suppressions of 0 to 20 percent. To check whether or not each measured data point Y_i is represented by modeled population, we compare the minimum distance $\min_j \delta_{ij}$ across the set $\boldsymbol{\theta}$ to the intra-set distance distribution. If the distance is large (above the 99th percentile) relative to the intra-set distance distribution, then the observation Y_i is not represented by the modeled population and must be addressed separately. If this occurs for too many observations (>1%), then our modeled population does not span the measured population and either a larger population must be generated in order to produce less frequent members or the model parameters need to be revised to expand its range.

2.3 Use of data to weight modeled population and compute intensity distributions

Once we have verified that our modeled population spans the measured population, we wish to derive, for each θ_j in the modeled population, a weight w_j and a probability density function of intensities such that a set of random samples drawn from the modeled population will be statistically similar to the measured population. The weight w_j can be interpreted as the posterior probability $P(\theta_j \mid \mathbf{Y})$. We can compute the posterior probability of each of the models using Bayes rule:

$$P(\theta_j \mid \mathbf{Y}) = \sum_i P(\theta_j \cap Y_i) = \sum_i P(\theta_j \mid Y_i)P(Y_i) = \sum_i \left(\frac{P(Y_i \mid \theta_j)P(\theta_j)}{\sum_k P(Y_i \mid \theta_k)P(\theta_k)} \right) P(Y_i)$$

Where the prior probabilities are $P(\theta_j) = 1/M$ where M is the number of samples in the modeled population and $P(Y_i) = 1/N$ where N is the number of observations in the measured data set. The probability of an observation given a model $P(Y_i \mid \theta_j)$ is estimated based on the assumption of normal statistics. That is, assuming each of the κ channels is independent, we can compute the expected variance in that channel based on the expected variance from a Poisson process plus the variance in the estimated background. This forms a κxκ covariance matrix $\boldsymbol{\Lambda}$ which can be used to compute $P(Y_i \mid \theta_j)$ using the probability density function for the multivariate normal distribution:

$$P(Y_i \mid \theta_j) = \frac{1}{(2\pi)^{\kappa/2}\boldsymbol{\Lambda}^{1/2}} \exp\left(-\frac{1}{2}\left(Y_i - \alpha_{ij}\theta_j - \beta_{ij}B_i\right)^T \boldsymbol{\Lambda}^{-1}\left(Y_i - \alpha_{ij}\theta_j - \beta_{ij}B\right) \right)$$

$$\text{Thus, } P(\theta_j \mid \mathbf{Y}) = \frac{1}{N}\sum_i \left(\frac{\exp\left(-\frac{1}{2}\left(Y_i - \alpha_{ij}\theta_j - \beta_{ij}B_i\right)^T \mathbf{\Lambda}^{-1}\left(Y_i - \alpha_{ij}\theta_j - \beta_{ij}B_i\right)\right)}{\sum_k \exp\left(-\frac{1}{2}\left(Y_i - \alpha_{ik}\theta_k - \beta_{ik}B_i\right)^T \mathbf{\Lambda}^{-1}\left(Y_i - \alpha_{ik}\theta_k - \beta_{ik}B_i\right)\right)} \right).$$

Finally, we need to compute the distribution of intensity for each model θ_j. This is done by using the intensity scaling factors α_{ij} weighted by the probability of the fit $\frac{P(Y_i \mid \theta_j)}{\sum_k P(Y_i \mid \theta_k)}$ multiplied by a normalization factor such that the total probabilities sum to one. We then fit a piecewise linear curve to this discrete distribution in order to generate a continuous distribution for the intensity factor.

After describing in Section 3 data sources and data samples used in the nuisance source population modeling, we discuss the application of the model and the data to NORM, medical and industrial sources in Sections 4, 5 and 6.

3.0 Data Sources

Characterization of nuisance source populations relies on the availability of data regarding the frequency and radiation characteristics of the variance types of nuisance sources. We utilize three types of data in our modeling efforts: empirical data collected from deployments of radiation detection systems, manifest data from shipping records, and literature regarding nuisance source frequencies and characteristics. In this section, we give an overview of the data sources that are currently available to us (shown in **Table 3-1**) and, for the case of radiation detection system data, describe the processing that must be done to make it usable. All of these data sets, except for the Lincoln Tunnel, pertain to cargo screening and are therefore primarily useful for NORM modeling.

Table 3-1. Data currently being used in our nuisance source population modeling efforts.

Sample	Dates collected	Measurement time	Number of samples	Type	Detector characteristics
CMTB I	3/04-6/04	~100 sec.	261	Secondary	NaI(Tl)
CMTB II	9/04-10/05	~100 sec.	795	Secondary	NaI(Tl)
Lincoln Tunnel	10/05-11/05	Varies (few sec.)	92,000	Primary	NaI(Tl)
PIERS	7/04-6/05	N/A	500,000	Manifest	N/A
NYCT ASP	3/07-3/07	Varies (5-10 sec)	1000	Primary and secondary	PVT, NaI(Tl), HPGe

3.1 Empirical radiation detection data from NYCT ASP

In this section, we describe a data set collected in early 2007 at the New York Container Terminal (NYCT) using the Advanced Spectroscopic Portal (ASP) test systems. Other empirical data sets, collected under the DHS Science and Technology Directorate CounterMeasures Test Bed (CMTB) program (e.g., CMTB I, CMTB II and Lincoln Tunnel in **Table 3-1**), have been utilized in prior studies and are summarized in those reports **[Edmunds 2007, Sokkappa 2008, Lange 2008, Wheeler 2009]**. The NYCT test campaign for the ASP systems lasted for approximately three months and had systems from three vendors. Each vendor fielded multiple systems, which were deployed in both primary and secondary screening facilities **[DNDO 2007, Monetti 2006]**. **Figure 3-1** shows the layout of these systems as deployed.

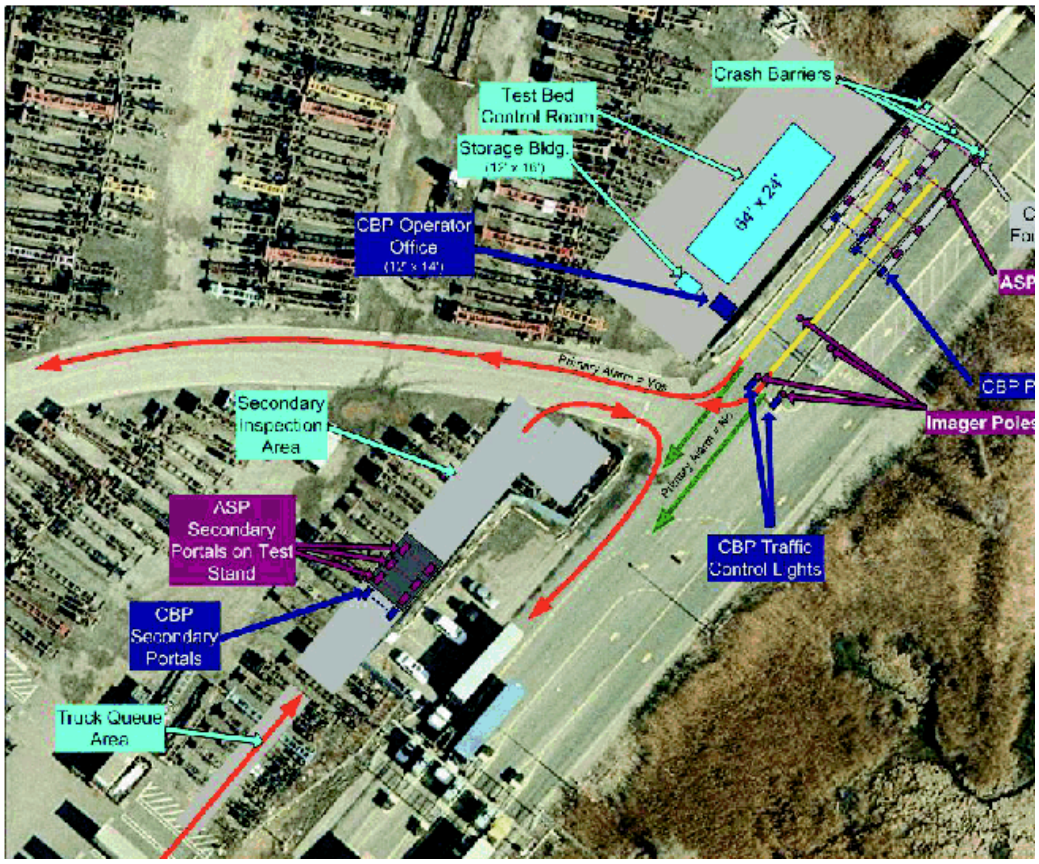

Figure 3-1. Layout of NYCT ASP test systems.

For the purpose of developing our NORM model, we obtained data from one of the NaI(Tl)-based systems used in the test. The data included spectra from primary and secondary inspection for all vehicles screened during the five days, as well as approximately 45 days of data for vehicles that alarmed, based on the alarming criteria defined for the test. The current modeling effort is focused only on the spectral characteristics and frequency of NORM, and not on detector performance. Therefore, we were not interested in the actual alarm frequencies reported, which would be very dependent on specific algorithms used for the test. All data were verified and provided to us by the John Hopkins University Applied Physics Laboratory (APL). Subsequent to receiving these data, additional data, in some cases with more complete information, have become available. We have not included them in our current analysis.

3.1.1 ASP calibration procedure

For analysis, data collected, either from different instruments or over a period of time, must be corrected for various detector effects and for differences between the expected detector response and that observed for each individual detector crystal. For example, the

GADRAS[3] DHSIsotopeID algorithm applies a linear gain correction to account for any gain drift in detector response. Each spectrum is corrected as part of the specialized algorithm using the detector response function for the ASP detector as the basis for the expected response. The gain correction is derived by comparing the location of prominent peaks (in particular, the ^{40}K line at 1460 keV) in the individual spectra to that expected from the detector model.

In order to apply generic algorithms for NORM analysis and to provide a further level of data quality checks, we apply a similar energy correction procedure and then combine data from all detectors to tabulate a single spectrum for further analysis. This, together with NORM spectra corrected by the detector response function, allows us to use generic algorithms that do not incorporate many of the radiation detection physics details that would otherwise be required. The cost of this approach is the additional work required to perform a reliable calibration. In our experience, each new data sample has some anomalous behavior that must either be fixed through the calibration procedure or removed from the final data sample.

In more detail, our calibration procedure is:

1. Determine the set of features (peaks) in the energy spectrum that can be used for calibration. As discussed below, in this case we were limited to only the ^{40}K peak at 1460 keV.
2. For each feature, use the GADRAS detector model for the ASP crystals to determine the expected energy channel of each feature (e.g., ^{40}K peak).
3. For each detector and each data record, determine the actual location of each feature. We used the background spectrum included with each data record for this step to increase the available counting statistics for this determination. The ASP system frequently updated the background spectrum such that it was a good representation of the actual energy calibration for each record.
4. Apply a least-squares minimization to determine the overall correction that best aligns the calibration features with their expected locations based upon the measured location for each feature.
5. Rebin the spectra for each detector and each data record according to this correction. For a good calibration, each rebinned spectrum will be completely compatible with the detector model.
6. Sum the spectra from each detector into the final spectrum for analysis.

Figure 3-2 shows an example determination of the ^{40}K peak location for one detector. Given the embedded calibration source, the peak location is clear and can be determined with a small uncertainty.

[3] The Gamma Detector Response and Analysis Software (GADRAS) toolkit, developed by Dean Mitchell at Sandia National Laboratories, is a multi-purpose computer code to assist in interpreting spectra generated by radiation detector systems.

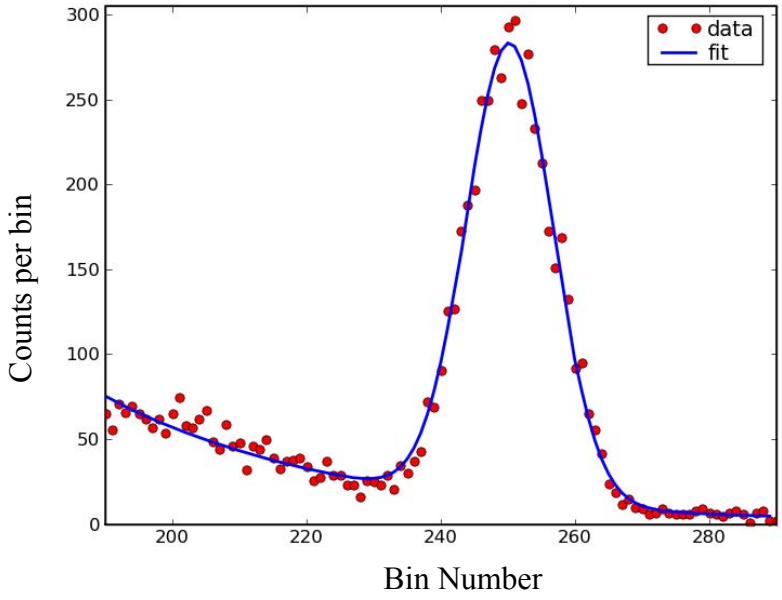

Figure 3-2. Example spectrum near the 1460 keV ^{40}K line used for calibration. The blue curve represents the result of the peak fit.

In the case of the ASP data, we observed that the gain for two of the 16 detectors was very far from the expected range for approximately 50% of the data sample. **Figure** 3-3 shows the spectra for each detector, summed over the entire five days of data that we have obtained. The ^{40}K peak, due to both NORM background and an embedded calibration source, is the most prominent feature and is the primary source of a good calibration.

One additional difficultly with this data sample is that we cannot distinguish between the three separate ASP systems used to screen vehicles. This apparent gain variation problem is likely only present in one of the systems; however we have not yet confirmed that this was actually the case. To avoid applying a large, and thus unreliable, correction using only the single ^{40}K peak, we have excluded these two crystals from the data set for our NORM analysis. Given 16 total crystals in each system, removing these two crystals from our final calibrated spectra will not have a large effect on our sensitivity to NORM sources (the SNR for a source will decrease only by 6% on average).

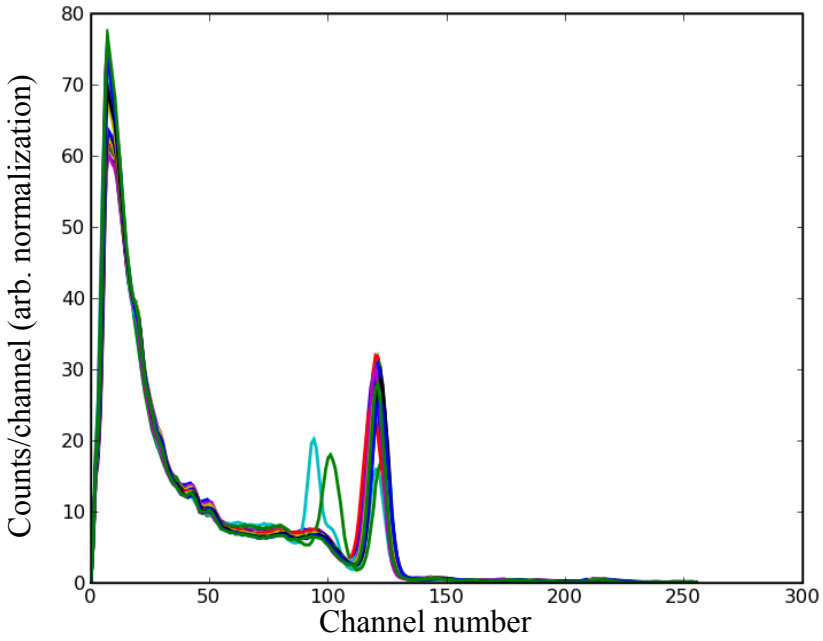

Figure 3-3. Spectra from each ASP crystal summed over all available data records.

The other problem caused by not being able to distinguish the data from each of the three ASP systems is that we could not reliably combine records from consecutive measurements to improve the statistics of the sample used for each calibration. Ideally, we would combine enough samples to achieve a good calibration using the ^{232}Th 2614 keV peak as well as the prominent ^{40}K peak. Without this additional calibration peak, we could not make adjustments to the detector model itself or consider anything beyond the simplest gain correction calibration.

Figure 3-4 shows an example of a poor calibration result due to these effects. In this vehicle, a bright NORM source primarily consisting of ^{226}Ra and ^{232}Th is observed in addition to the background radiation. While the measured spectrum and the expected spectrum (the colored, stacked histograms) from this source are well aligned at the ^{40}K peak, in other areas the measured peaks and the expected peaks are not well aligned. We observe that the data peak at an energy value below that expected for prominent peaks both above and below the ^{40}K peak. The observed effect is only at the level of a few bins; however this is sufficient to create problems for some components of our analysis.

Nevertheless, the calibration result for the ASP data suits the needs of our current work. For future efforts, we will revisit these effects in order to improve the detector model and the calibration for each record as to further improve the data used for our analysis. More detailed data records for the ASP detector data are now available from APL. Most importantly, these data will allow us to distinguish between each of the detector systems and thus we can carry out the more detailed calibration procedure described above. In turn, this will allow us to enhance the simplistic detector response model for the ASP NaI detectors that is provided with the version of GADRAS we have used.

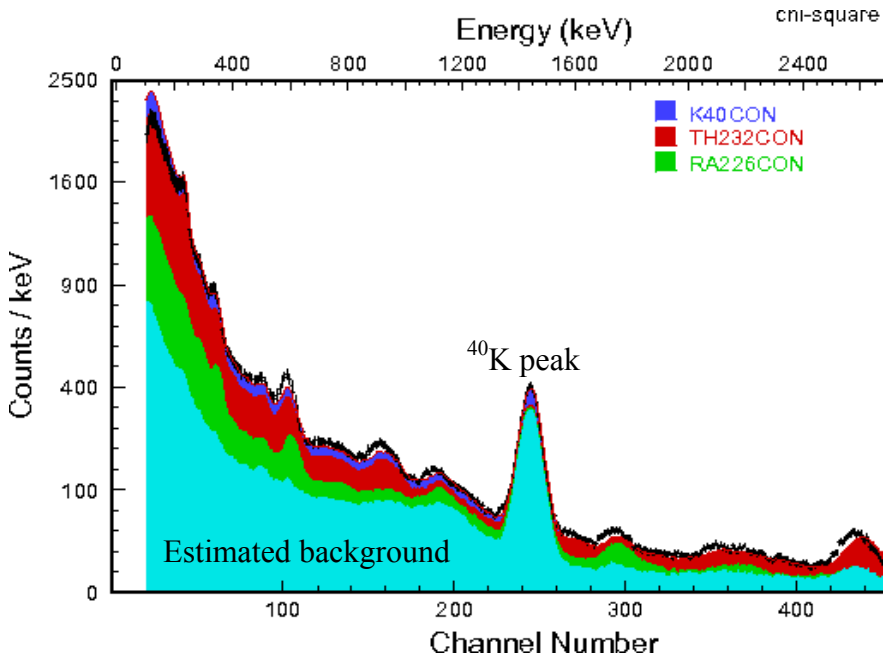

Figure 3-4. : Example spectrum after energy calibration procedure. Colors illustrate results of multi-linear regression analysis.

3.2 Shipping manifest data

A large set of container ship cargo manifest data was obtained from PIERS Global Intelligence Systems, a company that maintains a fairly comprehensive database of information on cargo moving through U.S. ports based on the bills of lading **[Descalle 2006]**. Our data set from PIERS describes shipments into the United States for 14 days in a period between July 2004 and June 2005. Twelve of the days are the single most active day in each month. The remaining days are the next two busiest days of the year. Each record describes a single shipment, which may consist of a partial container or multiple containers. In all, approximately 500,000 records, representing a total of approximately 1,000,000 twenty-foot equivalent units (TEUs), are included. Over one third of the records represent shipments of less than a half a TEU, while the vast majority of cargo is shipped in large quantities. For each shipment, a commodity description, a total weight, and the number of TEUs are given. The commodity description consists of three fields, the Harmonized Transport Code (HTS), the commodity code, and a text field.

While this comprehensive data set is useful for understanding frequency of commodity shipments to various ports, it does not contain any information specific to the natural radioactivity of any commodities.

3.3 Literature

Our modeling of medical and industrial source populations relies heavily on information obtained from literature searches. This includes academic papers, trade journals, documents and databases from regulatory agencies, and market surveys. These sources are described further in Sections 5 and 6.

4.0 Naturally Occurring Radioactive Material (NORM)

In this section, we discuss our analysis of several of the data sets shown in **Table 3-1.** We then apply the population modeling approach described in Section 2 to NORM. The physics-based model presented is a generalized NORM model and weights are calculated for this model using the ASP data. This modeling approach would be more useful if applied to specific NORM types. In this case, we would use measured data to develop a population model for each of a number of NORM types. Although we have already illustrated that the frequency of various NORM types varies with location, it may be reasonable to assume that the population of NORM signatures within a NORM type is fairly consistent. This is discussed further in Section 4.3.

4.1 Variability of NORM populations

We have used PIERS manifest data to examine a number of issues regarding NORM populations, including port to port variability, seasonal variations, and the impact of limited data on derived population characteristics. Using a list of 68 NORM commodity types that was developed based on the NYCT secondary inspection data and literature, each record in the PIERS database was assigned a NORM commodity type based on its HTS code, commodity code, and commodity description text field or determined to be outside of this set of NORM types **[Sokkappa 2008]**. (Note that not all NORM cargo falls within these 68 types.) The frequency of these NORM commodities was then examined, with focus on the impact of location and date.

Looking at the distribution of cargo types across all cargo represented in the PIERS data set, we find that out of 99 possible cargo types, as represented by the first two digits of the HTS code, only seven of them comprise 50% of the cargo shipped. Likewise, out of the 68 NORM types, three of them account for 50% of the NORM cargo and 13 represent 90% of the NORM cargo. This is illustrated in **Figure 4-1**.

When we examine the percentage of total cargo in the 68 NORM commodity types, we find that this percentage varies significantly from port to port with the value being ~4% across all ports. **Figure 4-2** shows the variability of NORM as a percentage of total cargo across all ports. We note the disproportionately high frequency of NORM at the ports Houston and Miami. On further investigation, we find that this high percentage of NORM is due primarily to shipments of tile. **Figure 4-2** also shows the variability of NORM as a percentage of total cargo when tile is excluded from the NORM population.

In addition to the variability in the overall frequency of NORM, we also find that the prevalence of particular NORM types varies significantly from port to port, tile being one example. **Figure 4-3** shows the frequency of tile as a percentage of total cargo for the various ports. Looking at the volume of tile shipped to Miami on each of the 14 days, we see that there is also significant day to day variation and that two of the 14 days are responsible for the majority of the tile seen at Miami. If our data set contained records from a different set of days, the NORM statistics for Miami would probably be quite different.

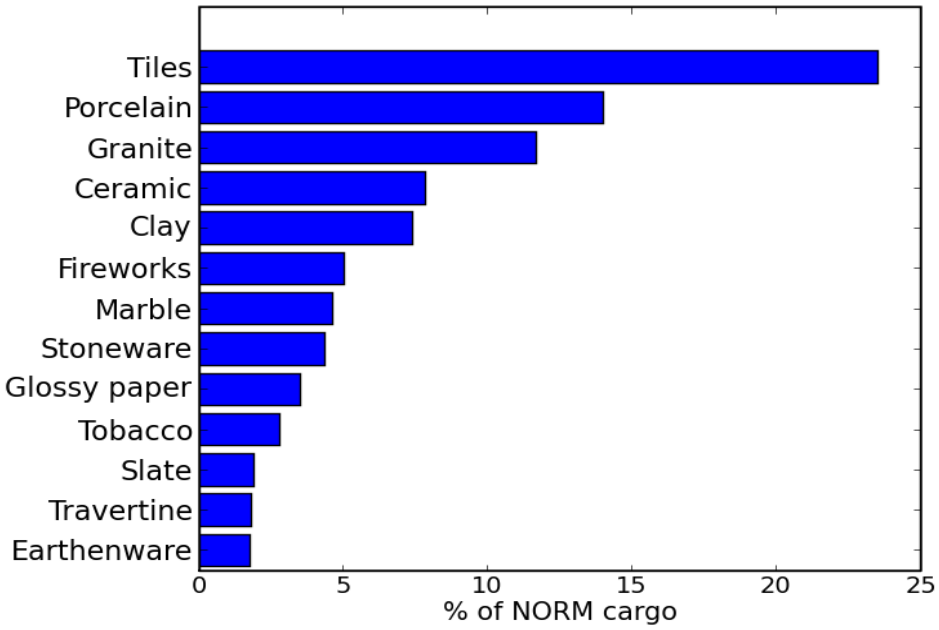

Figure 4-1. Top 13 categories of NORM cargo and their percentage of the total cargo in the 68 NOM categories.

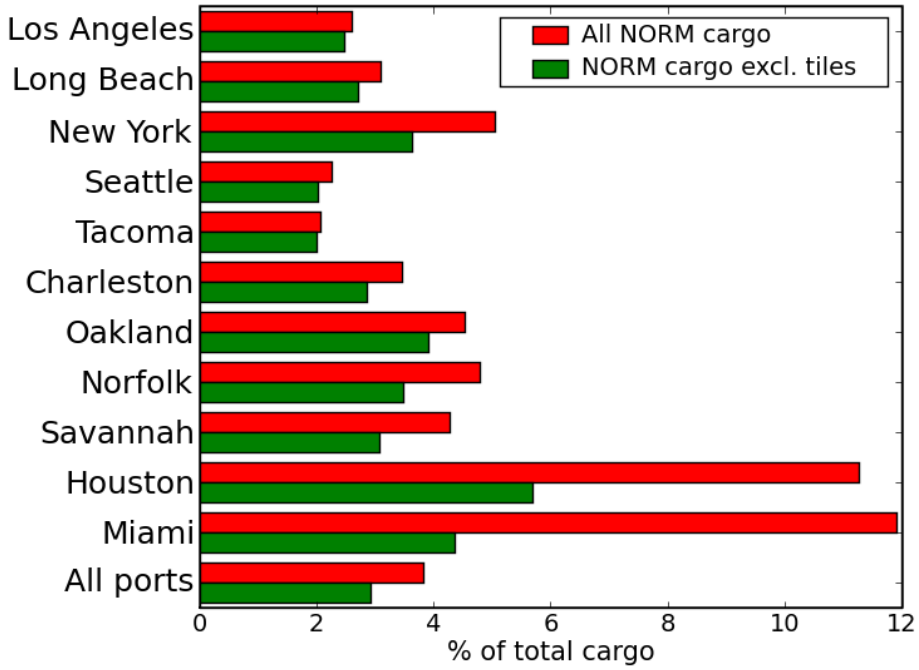

Figure 4-2. Percentage of total cargo that is in the 68 NORM commodity types for the highest volume ports and for all ports in aggregate.

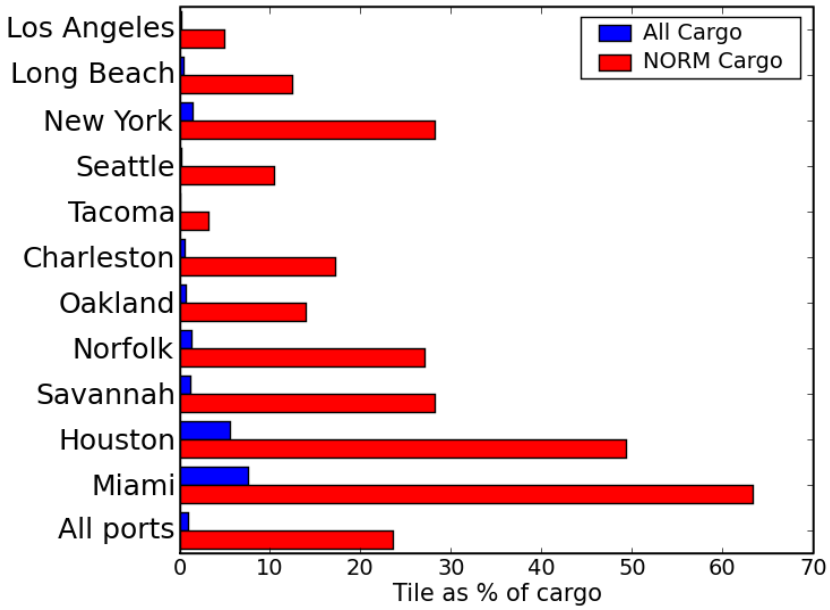

Figure 4-3. Frequency of tile as a percentage of all cargo and as a percentage of cargo in the 68 NORM types for the highest volume ports and for all ports in aggregate.

Another example of a commodity that varies significantly across ports is tobacco, which has a much higher frequency at the ports of Charleston, Norfolk, and New York compared to the frequency across all ports (**Figure 4-4**). Examination of the day to day variations in the volume of tobacco for the 14 days represented in our data set (**Figure 4-5**) indicates that the statistics are strongly driven by the particular days selected. When the dates 2/18 and 9/17 are excluded from the data, the frequency of tobacco at New York and Norfolk is below average.

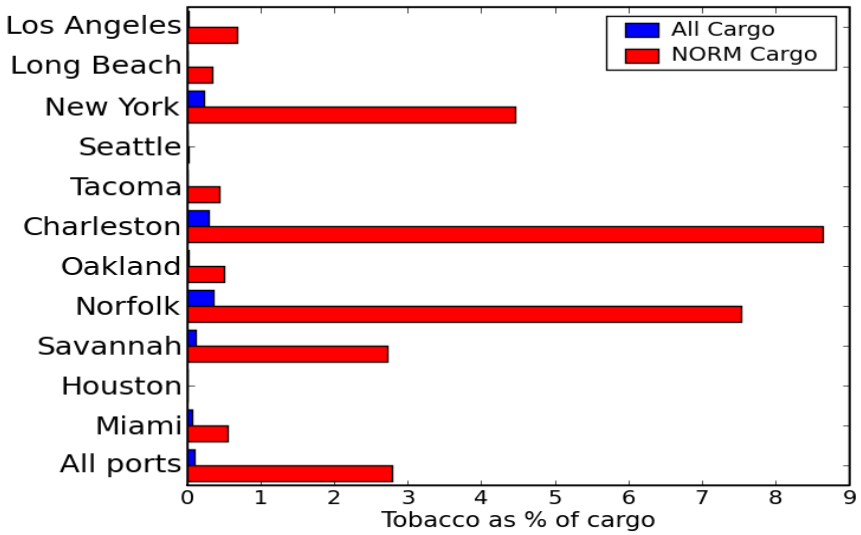

Figure 4-4. Frequency of tobacco as a percentage of all cargo and as a percentage of cargo in the 68 NORM types for the highest volume ports.

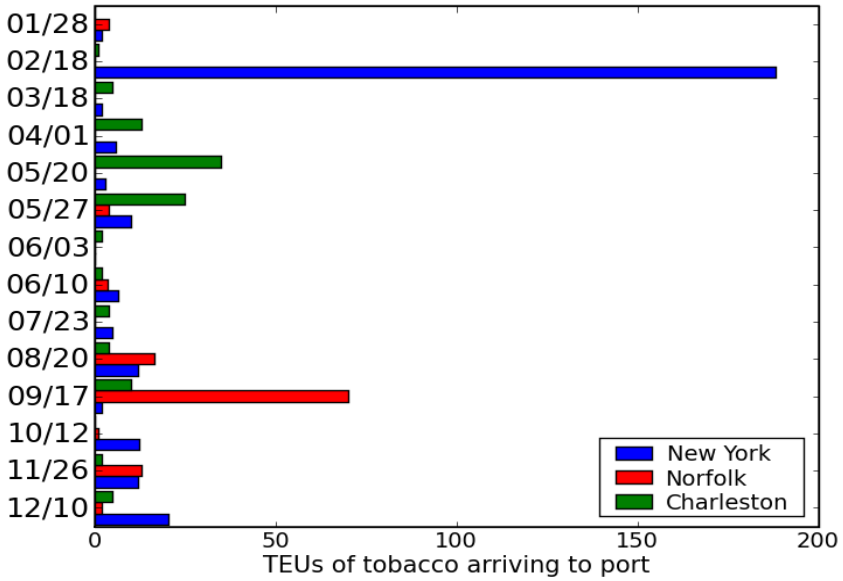

Figure 4-5. Volume of tobacco arriving at the ports of New York, Norfolk, and Charleston for each of the 14 days in our data set.

In our data set, we find that the port of Los Angeles is essentially the only port receiving shipments of fireworks and that fireworks represents over 20 percent of all cargo in the 68 NORM commodity types for Los Angeles. This result may be somewhat dependent on the days represented in the data set, but it is clear that the mixture of NORM cargo at Los Angeles differs from other ports. When looking at the day to day variations in the volume of fireworks arriving at Los Angeles (**Figure 4-6**) we see a large seasonal variation. We assume that this variation in volume is related to the timing of the two major holidays when fireworks are prevalent, Chinese New Year and Independence Day.

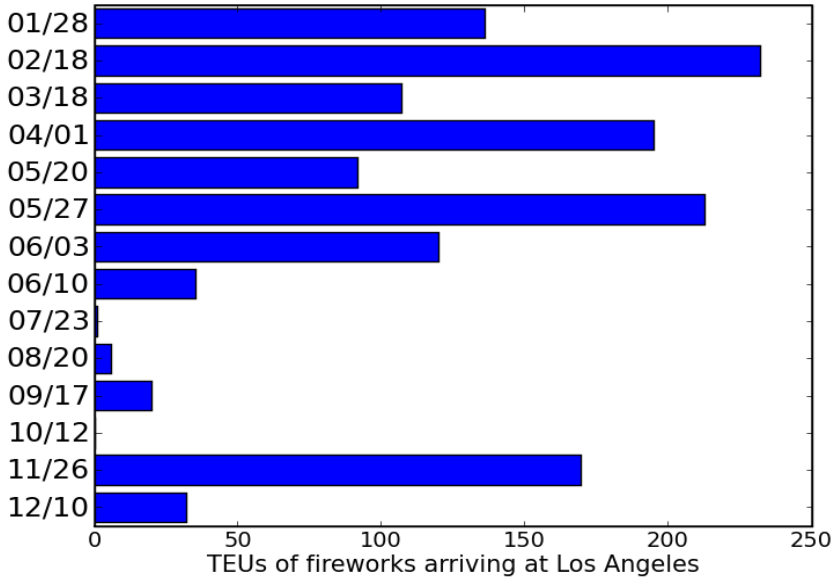

Figure 4-6. TEUs of fireworks arriving at the port of Los Angeles for each of the 14 days in our data set.

Our analysis of the variability of frequencies for the various NORM commodity types has significant implications for the data required to support NORM population modeling. Unless we have reason to believe that the NORM populations at two different ports are similar, a NORM model based on data collected at any particular port, or even at a number of ports, is unlikely to be a good representation of the NORM population at a different port. Furthermore, NORM population models based on a limited data set may not provide an accurate representation of the NORM population for the port at which it was collected. Because of day to day and seasonal variation in NORM shipments, we estimate that data must span at least a year and contain a large number of days distributed evenly over the year in order to provide an accurate representation of the NORM population. Ports with smaller volumes of cargo would require longer time periods of data than larger ports in order to obtain a sufficient sample size.

4.2 Comparison of data sets

In this section we compare the ASP spectral data with previously analyzed data (CMTB I and CMTB II), also from the NYCT. This focus of this comparison is to examine differences in spectral signatures due to different CONOPS (e.g., primary screening vs. secondary inspection) as well as variations in NORM cargo seen over time at NYCT. The previously analyzed data were collected as part of the CounterMeasures Test Bed project and were the basis of previous NORM modeling work **[Sokkappa 2007]**.

4.2.1 Gross count comparison

Figure 4-7 shows the gross count rate over the mean background level for both the combined CMTB I and CMTB II data sets and the ASP data set (alarms only). The data have been rescaled to have the same median number of gross counts in order to be more directly comparable. This procedure is required due to the different procedures used to collect the data as well as the different detector characteristics. For the CMTB data, the detection system was operated in a long-dwell mode, positioned in close proximity to an identified hot spot in the detected radiation from each vehicle. On the other hand, the ASP data was collected during a slow pass-by.

Figure 4-7 illustrates an additional difference between the two data sets due to the primary screening CONOPS. The CMTB data were collected in secondary inspection after a primary screening with a PVT portal system. The primary system alarmed based on a gross count threshold above nominal background. The ASP data is mostly primary screening data and that was processed with a spectral alarming algorithm. The spectral alarming algorithm produces an alarm when the spectral signature is distinct from the background, regardless of whether the count rate would exceed the gross count threshold in the PVT system. As we observe in **Figure 4-7**, this results in additional low count rate data in the ASP data. Thus, we can construct a more complete NORM model from the ASP data.

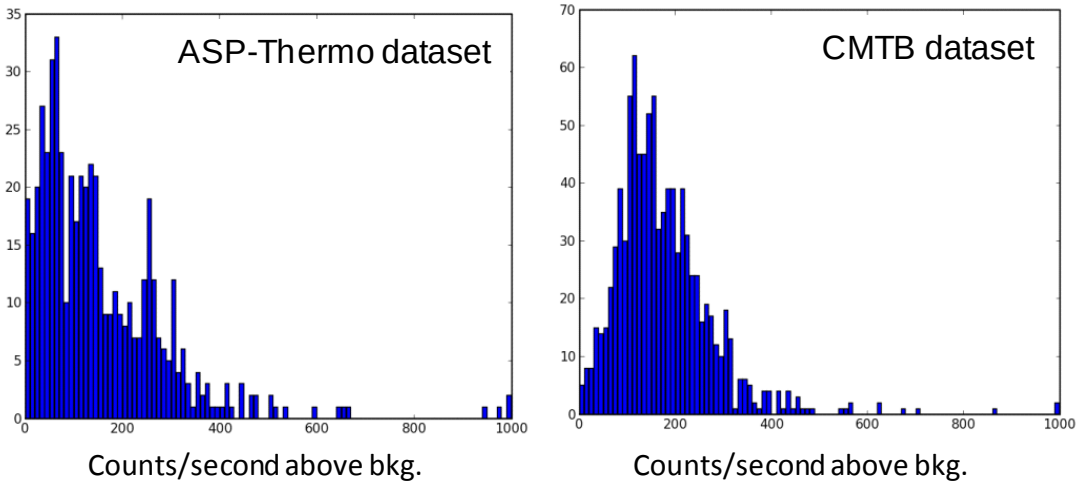

Figure 4-7. Comparison of gross counts above background for ASP and CMTB data samples.

In addition to the radiation detector data from the ASP detectors, we have obtained a small amount of manifest data for vehicles that underwent secondary inspection. We will describe this data in more detail in Section 4.2.3; however, the manifest data obtained do not directly correspond to the type of information provided by the PIERS manifest records.

4.2.2 Comparison of NORM model results

Our previously applied NORM model determined the relative frequency and composition of ^{40}K, ^{226}Ra and ^{232}Th in a given data set **[Sokkappa 2007]**. The model used the multi-linear regression tool in GADRAS to determine the relative contributions of ^{40}K, ^{226}Ra and ^{232}Th in each spectrum. These results were then clustered according to a k-Means procedure **[Hartigan 1975]** to identify the underlying features of the population.

In more detail, our procedure was:

1. A model of ^{40}K, ^{226}Ra and ^{232}Th was created from the GADRAS detector model. We modeled a 1 m radius concrete ball for each nuclide and determined a corresponding spectral template after applying the detector response function to each model.
2. The resulting spectra, together with the background spectrum, were the basis given to the GADRAS multi-linear regression tool for application to each data sample. The best fit hypothesis between the nominal background contribution and combinations of the three nuclides is determined. The normalization and corresponding uncertainty for each nuclide template and the level of background suppression are determined. However, any calibration sources integrated into the detection system and counted as part of the background spectra are not fully accounted for in this procedure. These sources are not attenuated when the background is suppressed by the vehicle being inspected. As long as the

background suppression is small, this is not a large effect. However, for some cargo, background suppression of more than 10% is observed. We have corrected this shortcoming in our new NORM model formalism. **Figure 4-8** shows a compares the results of this analysis for the CMTB and ASP data sets.

3. The results for ^{40}K, ^{226}Ra and ^{232}Th normalizations are renormalized onto a unit sphere. We then apply a k-Means clustering algorithm, which uses an iterative procedure to optimally group the data into a predefined number of clusters, summarized in **Figure 4-9**. Starting from an initial set of seeds, data are grouped based upon their proximity to each seed and a new centroid is computed for each cluster. This procedure is then repeated until no data change from one cluster to another.
4. The distribution for the normalization of each cluster is then determined from the unnormalized data corresponding to each cluster. A sigmoid function is used as the functional form for the cumulative distribution of the normalization.

Figure 4-10 shows the results of this NORM modeling procedure for both the CMTB and the ASP data samples. We observe a number of differences between these samples. Both data sets show a large cluster of ^{40}K samples. In addition, the ASP data sample has a large population along the ^{232}Th-^{226}Ra axis (no ^{40}K). This is due to having neglected the calibration source correction in our multi-linear regression analysis. These data also illustrate a deficiency of the clustering approach. The data closest to the no-^{40}K line are clustered into three separate clusters, each of which includes both data on the no-^{40}K axis as well as data away from it. The other prominent difference is along the ^{40}K-^{232}Th line (no ^{226}Ra). This difference is not easily related to known differences in the way the data sets were collected. We previously observed variation between the two CMTB data samples, especially in their ^{226}Ra content **[Sokkappa 2007]**. In addition, **Figure 4-8** shows this same difference between the CMTB and ASP samples. It is not known to what extent the differences between the two data sets are due to the inclusion of low count rate NORM in the ASP data set and to what extent they are due to other factors.

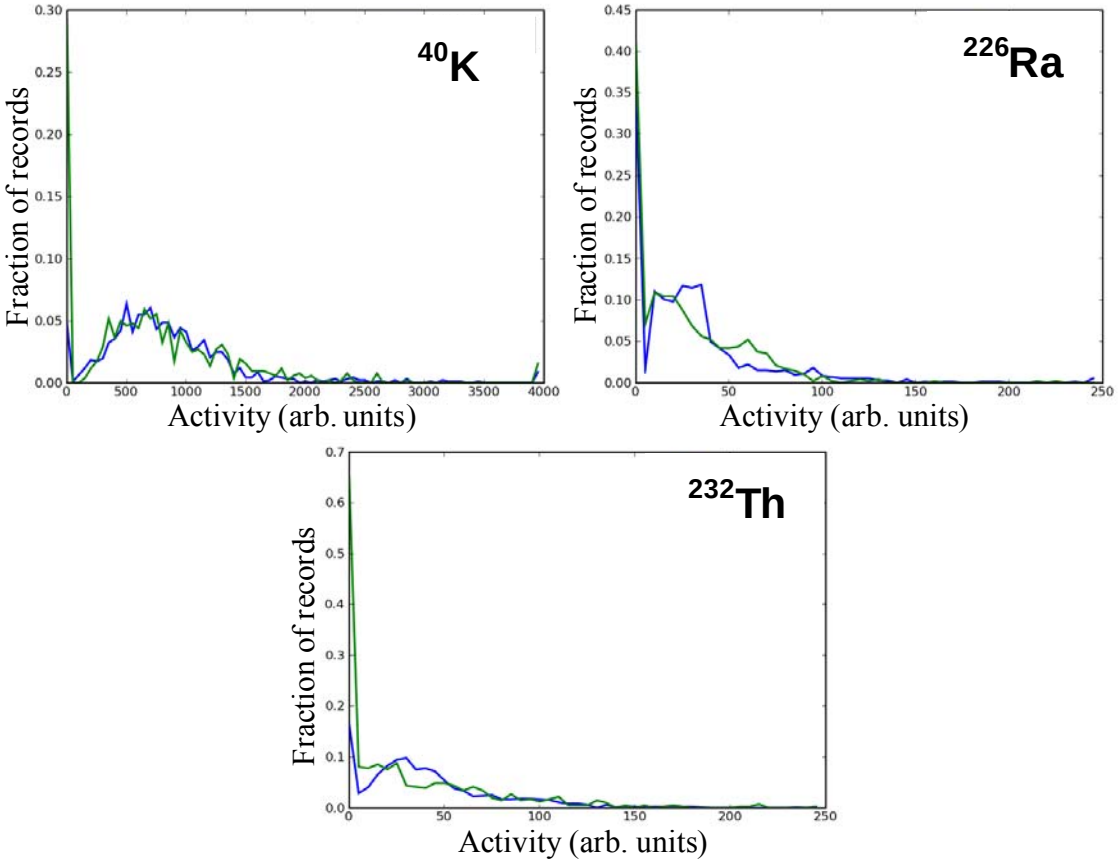

Figure 4-8. Distributions of activity level for ^{40}K, ^{226}Ra and ^{232}Th in the CMTB (blue) and ASP (green) data sets.

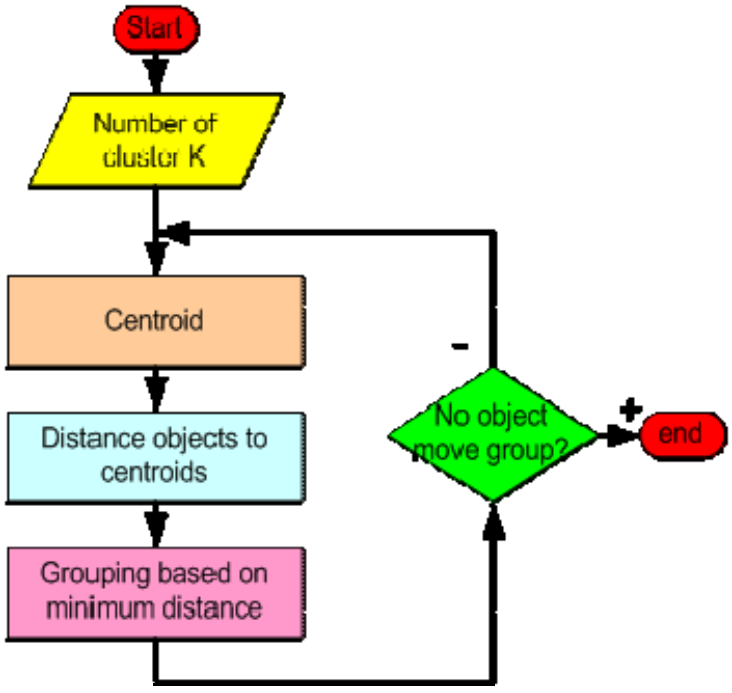

Figure 4-9. Flow diagram for k-Means clustering analysis.

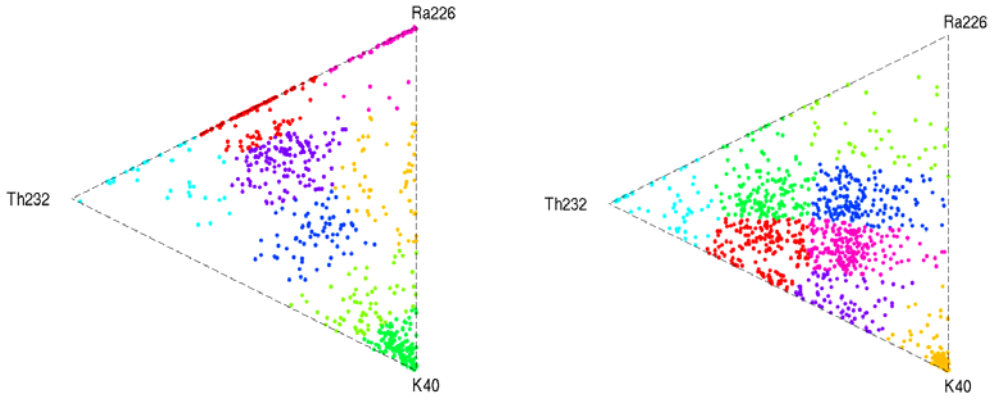

Figure 4-10. NORM model results for ASP (left) and CMTB (right) data sets.

4.2.3 Combination of spectral and commodity data from ASP test campaign

Ideally, a NORM population model would be based on representative spectral characteristics for each commodity shipped in the stream of commerce and a frequency with which each commodity occurs in that stream. Unfortunately, associating measured spectra with specific commodities requires ground truth. Short of inspecting every container, this can only be approximated using other available sources of information on container contents, such as shipping manifest data. As described above, we have commodity (manifest-like) data for approximately 190 of the ASP primary inspection alarm records for which we also have spectral data. While this is a very small data sample, it provides a basis for a limited comparison of the expected NORM population from our PIERS analysis to the set of ASP spectra. Each manifest data entry is in the form of a free text string. Entries that occurred more than one time in the commodity data are shown in **Table 4-1**. Given the low statistics of this sample, we grouped these data into four categories: food, stone, housewares and other items.

Table 4-1. Summary of commodity types for the ASP data.

Grouping	ASP manifest	Primary	Secondary
Food	Food	40	3
Stone	Stone	31	26
	Tiles	21	20
Housewares	Sinks/Toilets	17	15
	Ceramics	17	14
	Glassware	5	1
	Pottery	4	4
	Porcelain	3	2
	Kitchenware	3	2
	Houseware	3	2
Other	Other	38	25
Total		**182**	**114**

In order to compare the ASP commodity data from primary inspection (to avoid duplication of records) with the PIERS records for NYCT, we divided the PIERS records into our four categories based on the COM7 description field of the PIERS data. This procedure was done manually. Because there is no direct correspondence between the commodity information provided for the ASP data and the commodity fields in the PIERS data, this assignment may not be accurate. Furthermore, because of the limited sample size of the ASP commodity data, it may not provide an accurate representation of the distribution of NORM commodities. Because the ASP data only contains alarm data, for each commodity type, we estimated the fraction of the PIERS cargo that would have been identified as NORM by the ASP system. We assumed a cargo would be identified as NORM by the ASP system if it contributed greater than $5\sigma_b$ counts to the measured spectrum, where σ_b is the standard deviation of the unsuppressed background. To estimate the radiation characteristics for the various cargoes in the PIERS data, we used information on cargo characteristics and radionuclide activity levels that were estimated in a previous study **[Sokkappa 2008]**.

Figure 4-11 shows a comparison of fractions of NYCT cargo that fall into each of the four categories for: the NYCT PIERS data as a whole; the subset of the NYCT PIERS data that would be expected to have sufficient radiation to be detected by the ASP system; and for the ASP data. The comparable columns are the NYCT PIERS estimated alarms and the ASP alarm data. **Figure 4-12** shows the distribution of the gross counts above background observed in the ASP alarm data for each of the commodity types. The records categorized as food have significantly lower count rates than either the stone of housewares categories. Finally, **Figure 4-13** shows how the ASP data, separated by these four commodity types, populate the NORM model described in Section 4.2.2. As expected, "Food" is clustered in the ^{40}K corner. Both "Housewares" and "Stone" populate the mixed region of the space. The accuracy of our estimation of the relative contribution of the three radionuclides (determined using GADRAS) may be poor for the data points that represent low-count spectra.

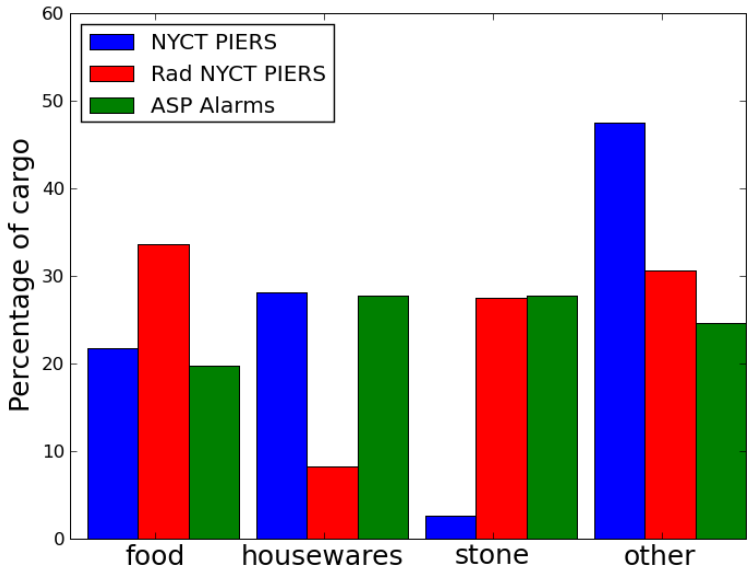

Figure 4-11. Distribution (in %) of records among the four commodity types for the ASP and PIERS data sets.

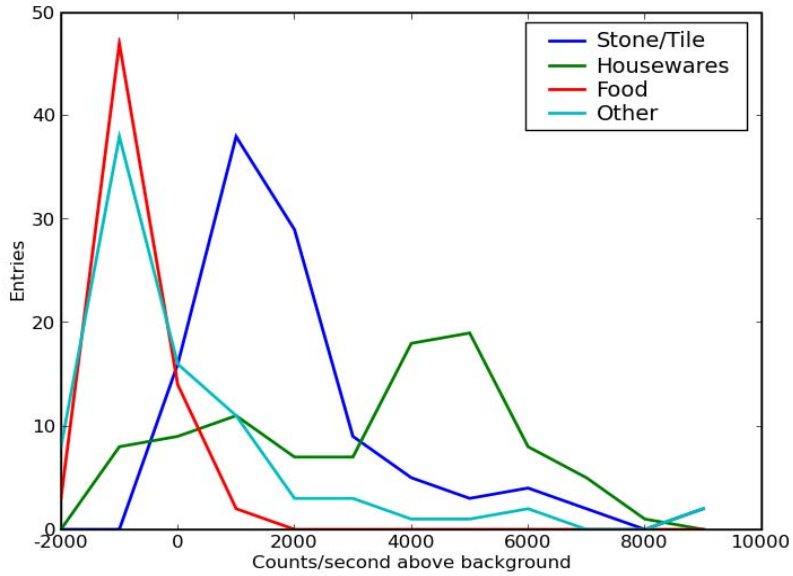

Figure 4-12. Gross counts observed above the mean background in the ASP data for each commodity type.

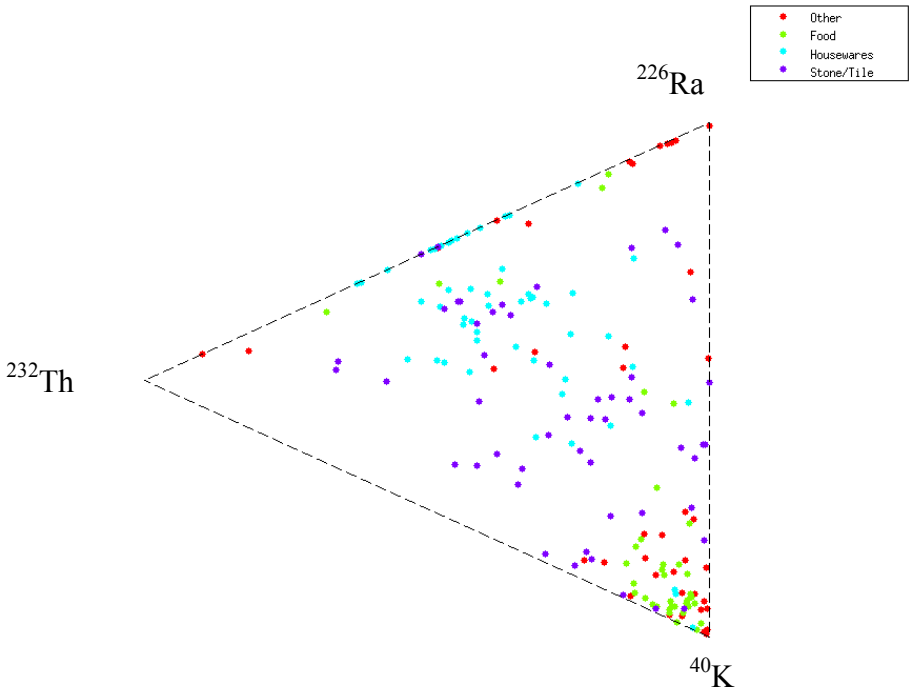

Figure 4-13. NORM model results for ASP data clustered by commodity type.

4.3 NORM population model

We have redefined our NORM modeling procedure based on the general approach to population modeling described in Section 2. The new model includes a substantially broader range of possible NORM signatures and corrects several shortcomings of our previous NORM modeling approach described and utilized in Section 4.2.2. The revised approach uses a physics-based source model to determine the range of expected spectral signatures for cargo container screening with a portal system. Measured data are used to assign frequencies and intensities to a random set of spectra generated from the physics-based model.

In this phase of work, we utilize only the spectral data from the ASP data set and do not make use of the commodity data. With sufficient manifest data linked with spectral signatures, a more refined NORM population model that includes separate models for each NORM commodity type could be developed. Such a model would enable adjustments to account for port-to-port and seasonal variations in commodity distributions based on analysis of manifest records.

4.3.1 Physics-based model of NORM

Using the approach described in Section 2.1, we have developed a physics-based model of NORM in order to span the space of possible NORM signatures for cargo containers. Our model has five layers, although some layers may be absent in random instances generated from the model. The layers are:

Layer 1–Void: We represent non-spherical sources by inserting a central void, which allows the ratio of surface area to mass of the source represented by Layer 2 to vary. The radius of the central void is uniformly distributed between 0 and 0.5 meters.

Layer 2–Distributed source: The NORM material is a distributed source ^{40}K, ^{226}Ra, and/or ^{232}Th. The relative activity levels of these radionuclides are selected from uniform distributions as defined in **Table 4-2** below. The composition of the material is selected from a distribution based on the relative frequencies of different material types seen in the CMTB I data set. The composition types and relative frequencies are given in **Table 4-3**.

Table 4-2. Range of activities for each radionuclide.

Nuclide	Minimum Activity (μCi)	Maximum Activity (μCi)
^{40}K	0	25.6
^{232}Th	0	0.93
^{226}Ra	0	1.2

Table 4-3. NORM compositions and relative frequencies for distributed source layer.

Material	Frequency	Composition
Clay	65%	$AlSi_2O_5(OH)_4$
Glass	5%	SiO_2
Wood	15%	$C_{0.5}O_{0.4}H_{0.1}$
Aqueous solution	5%	H_2O
Marble	10%	$CaCO_3$

Layer 3–Scattering layer: This is the first of two additional layers of material surrounding the distributed source to account for the attenuation that may occur due to intervening cargo. This layer is a void with a thickness uniformly distributed between 10 and 100 cm. It allows for variability of scattering in the next layer.

Layer 4–Intervening cargo: This layer represents any intervening material between the source and the container wall. This is a relatively rare occurrence and thus we give its presence a probability of 0.25. This layer, when present, is defined by its areal density, which is uniformly distributed between 2.5 g/cm^2 and 30 g/cm^2, and composition. The composition types and relative frequencies are given in **Table 4-4**. The thickness of the layer is computed from the areal density and the density of the material.

Table 4-4. Material definitions and frequencies for the attenuation layer (Layer 4).

Material	Frequency	Composition	Density
Water	10%	H_2O	1 g/cm^3
Wood	35%	$C_{0.5}O_{0.4}H_{0.1}$	1 g/cm^3
Aluminum	10%	Al	2.7 g/cm^3
Iron	45%	Fe	7.8 g/cm^3

Layer 5–Container wall: The final layer represents the outer layer of the cargo container and is present with a probability of 0.75. When present, this layer is at most equivalent to 14 gauge steel (1.9 mm) with a maximum viewing angle of 45 degrees (corresponding to 2.6 mm). Thus, the thickness of this layer is uniformly distributed between 1.9 mm and 2.6 mm.

Figure 4-14 summarizes the parameters of the NORM model. Using this model, we generated 5000 random samples.

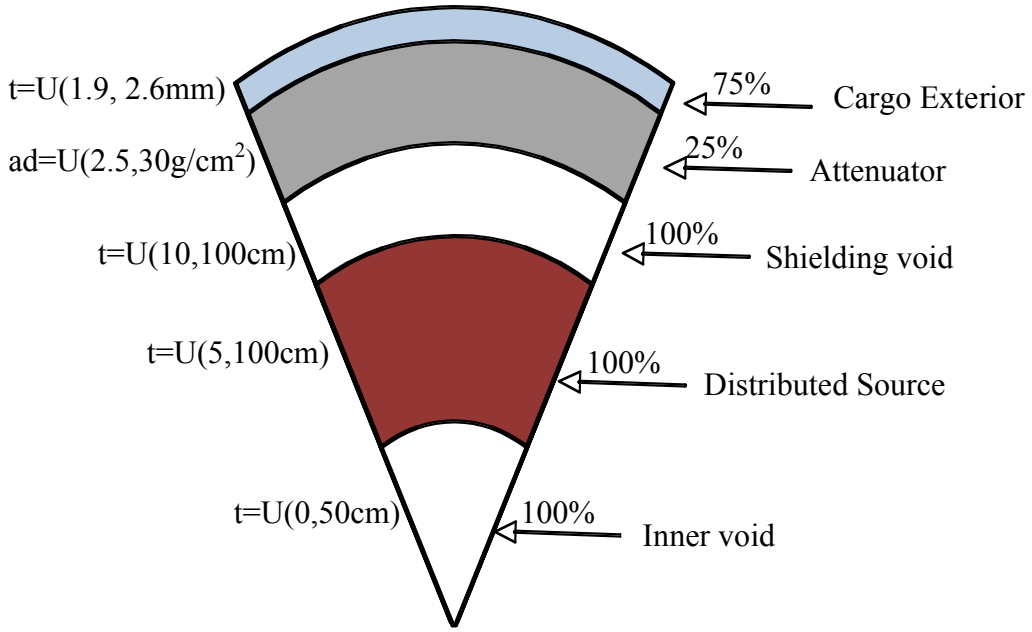

Figure 4-14. Physics-based NORM model. The numbers on the right indicate the probability of each layer being present. The numbers on the left indicate the thickness (t) or areal density (ad) of the layers.

When we attempted to fit the measured data with the modeled population, we found that our modeled population had poor coverage on the edges and corners of the trivariate $^{40}K/^{226}Ra/^{232}Th$ distribution. Our previous NORM model shows that the ASP data have large populations in these areas. To obtain good coverage, we generated 300 additional samples. For each of the corners, we generated 50 random samples where the activity level of one nuclide was selected from its range while the activity levels of the other two nuclides were set to zero. To represent the edges, we fixed the activity level for one of the radionuclides at zero and selected the other two from their appropriate ranges. These 300 additional samples were substituted for 300 randomly selected samples from the original set of 5000.

4.3.2 Use of data to determine weights and intensity distributions for modeled population

In order to assign weights to our population, we must first compute a distance metric from each measurement to each realization of the physics-based model. We use the Mahalanobis distance for our distance metric. However, as our random realizations represent spectral shapes without intensities, we must fit the intensity as a free parameter using a regression analysis. Additionally, the contributions of background to the measured spectra vary as the result of background suppression while at the same time the calibration source contributions do not change. Thus, we solve for two additional parameters, the intensity scaling factor and the background scaling factor. As before, we use the ASP data set having already calibrated each spectrum and combined the spectra from the individual detectors into a single combined spectrum. We rebin the measured

data into 64 quadratically spaced energy bins. This takes into account the better energy resolution at low energy. The best fit for each measurement Y_i compared with each model θ_j is computed by minimizing the Mahalanobis distance (δ_{ij}) given the measured spectrum $Y_i = \{y_{ik}\}$, the model $\theta_j = \{\theta_{jk}\}$, background $B_i = \{b_{ik}\}$, and calibration source $C = \{c_k\}$ distributions, where k denotes the energy bin within the spectrum. We estimate the variance of the measured data by the Poisson uncertainty in each spectral channel. As the channels vary independently, the covariance matrix is diagonal with values $1 + y_{ik}$. Thus, the square of the Mahalanobis distance is:

$$\delta_{ij}^2 = \sum_k \frac{\left(y_{ik} - (\alpha_{ij}\theta_{jk} - \beta_{ij}b_{ik} + (1-\beta_{ij})c_k)\right)^2}{1+y_{ik}},$$

where α_{ij} and β_{ij} are parameters of the minimization, representing the source intensity and level of background contribution. The final term accounts for the lack of suppression of counts from the calibration source when the background counts are suppressed by the presence of the vehicle in close proximity to the detector system. We did not include the lowest energy bins in the Mahalanobis distance minimization. These bins carry little information to differentiate the template models and also have the largest systematic uncertainties due to imperfections in the detector model. In future work, we can restore these bins given sufficient calibration source data for the detectors.

As discussed in Section 2.3, for each model, we compute the probability of producing that model given the measured data and assuming multivariate normal statistics. From the computed probabilities, we determine a weight for each model:

$$w_j = \sum_i w_{ij} = \sum_i \frac{P(Y_i \mid \theta_j)P(Y_i)}{\sum_k P(Y_i \mid \theta_k)},$$

where $P(Y_i \mid \theta_j)$ is the probability computed using data sample Y_i and model θ_j and $P(Y_i)$ is the probability of data sample Y_i, which is $1/N$, where N is the number of data samples. Thus,

$$w_j = \frac{1}{N}\sum_i \frac{\exp\left(-\frac{1}{2}\delta_{ij}^2\right)}{\sum_k \exp\left(-\frac{1}{2}\delta_{ik}^2\right)}.$$

4.3.3 Results

For this preliminary work, we have not evaluated the intraset distance metric (as discussed in Section 2.2) to verify that our physics-based model spans the measured data set. Instead we spot checked some of the results of the Mahalanobis distance minimizations to see if the models fit the measured data**. Figure 4-15** shows four

individual data records and their spectral fits resulting from the δ_{ij} minimization for the model that had the greatest probability (w_{ij}). In each case, the blue curve is the data sample, the red curve is the background and the green is the sum of the intensity-scaled model and the background contribution. Each contribution is weighted according to the best fit parameters described above. As expected, some models matched some measurements much better than others and the intensities used in the fits spanned a large range. For the most part, it appears that the data can be reasonably well fit by the models. However, the energy calibration limitations for the highest energy bins are apparent. Given the clear ^{232}Th features, we do not believe this energy calibration problem has a significant effect on our results.

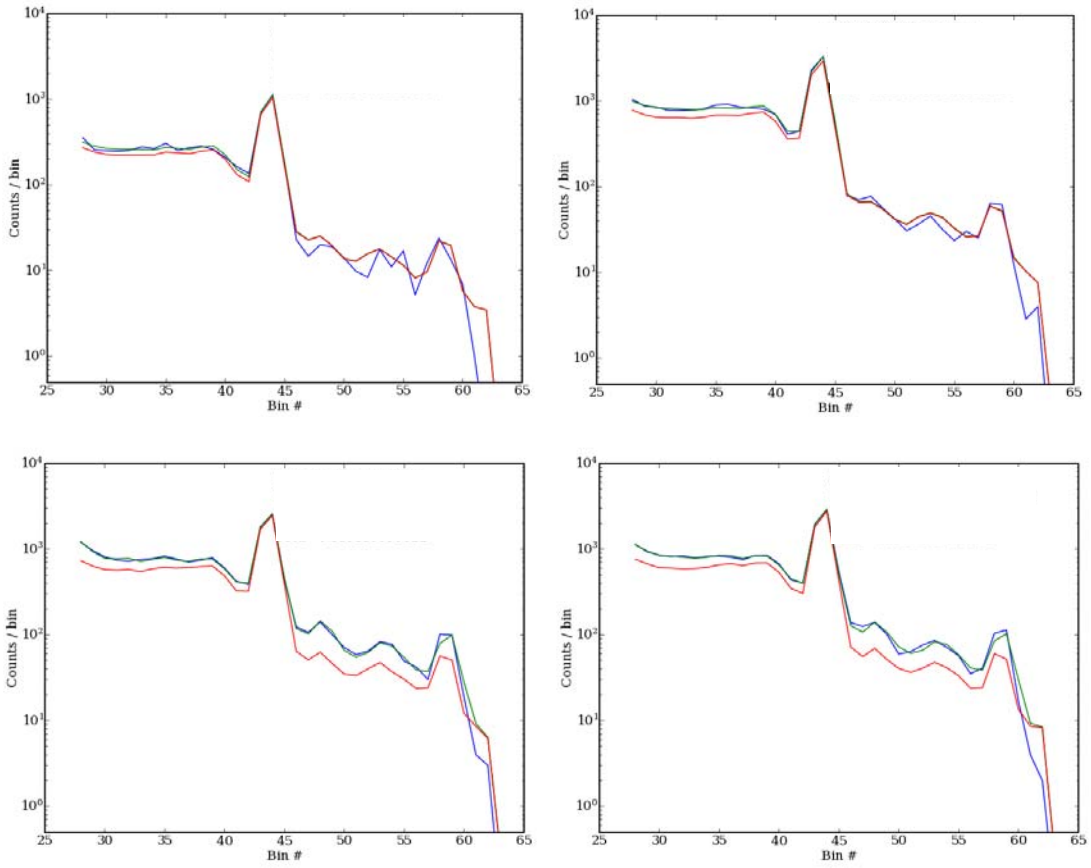

Figure 4-15. Examples of measured spectra and the best spectral fit from the modeled population. The red curves are the background estimate, the blue curves are the measured spectra, and the green curves are the best fits obtained using the models (e.g., the background estimate plus the model contribution). As expected for good quality fits, the best fit curves follow the measured spectra closely. In the top two examples, the best fit model is pure ^{40}K, thus above bin 45 (corresponding to the principal ^{40}K peak), the green and red curves are the same.

Using the fits (δ_{ij}), we computed w_j for each model. **Figure 4-16** shows these weights for each of the 5000 template models. We observe that a small number of models have weights that are significantly higher than the majority. This is not unexpected and is an indication that these members of our modeled population are a much better match to the

NORM represented in the observed population than the others. This is also consistent with observations from the previous NORM model, in particular, near the pure ^{40}K corner of the space. With these results, we have a fully described NORM model that can be applied to simulate NORM sources, at least at the NYCT venue.

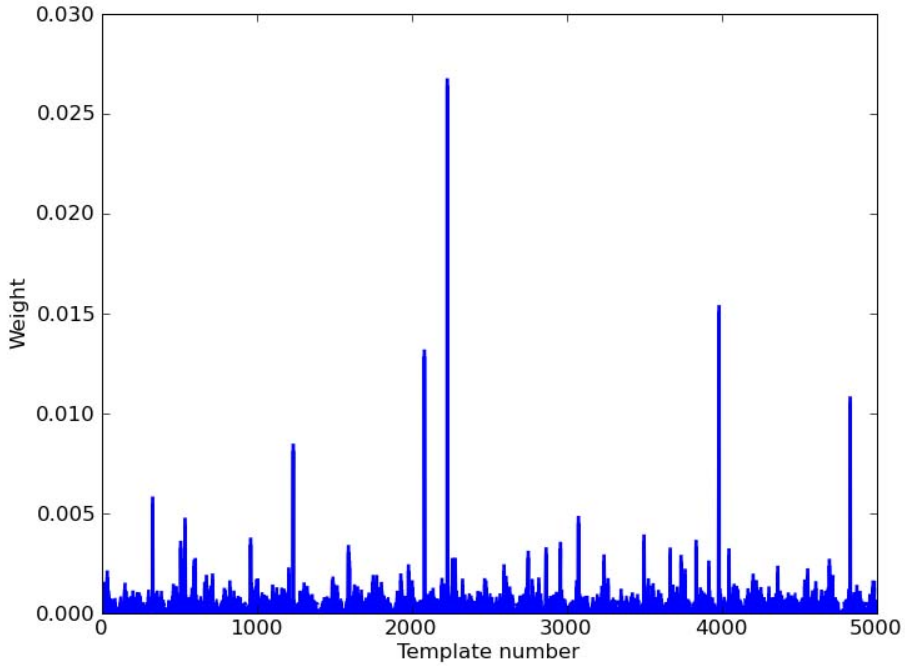

Figure 4-16. Weight, w_j , for each of the 5000 template models.

4.4 Data needs for developing a transportable NORM population model

In Section 4.3, we described a general approach to NORM population model. Using a set of measured spectra from a given location, we can develop a NORM population model for that location that enables us to generate large populations that are independent of the operational scenario associated with the measured data. This allows us to study different detection scenarios and examine sensitivity to a greater number of factors than would be possible using the measured data. However, the NORM population model is representative of the population at that particular location and is not necessarily applicable to other locations. NORM population characteristics are known to vary from location to location. While it may be reasonable to assume that the distribution of NORM characteristics for a particular type of cargo is consistent from location to location, our analysis of the PIERS data, as well as experience at various ports of entries, indicates that the frequencies of different cargo types can vary significantly across locations.

In order to develop a NORM population model for cargo that is transportable from one location to another, we would need to use the approach described in Section 4.3 to develop a separate model for each type of cargo of interest. One possibility is to develop a model for each type of cargo where the cargo type can be ascertained from manifest data. Another, but less general, approach would be to identify specific types of cargo that

are expected to produce nuisance alarms and develop models for these types only. This approach is less general because the determination of which types of cargo produce nuisance alarms depends on the resolution of the detection system and the detection algorithm that is used. However, it may be possible to make some baseline assumptions about system capability in order to reduce the number of cargo types that must be modeled.

Using these separate commodity-specific population models to model the NORM population at any particular location would require sufficient manifest data for that location in order to estimate the frequencies of the different cargo types, but would not require any spectral data from that location. However, developing the commodity-specific population models would require a sufficient amount of measured data for each commodity type. This data does not necessarily need to come from a single location, but the fields in the manifest data that are used to identify commodities must be consistent across locations and the data must be accompanied by sufficient information about the operational scenario in which they were taken.

5.0 Medical Sources

There are numerous types of medical sources which a detector may encounter in the field. These include medical devices, shipments of nuclear medicines, patients containing medical sources in their bodies, contaminated materials, and medical wastes. Medical devices are machines generally containing powerful industrial sources intended for treatment of cancer or diagnostic procedures. These devices are relatively indistinguishable from other types of industrial sources, are shipped infrequently and will be addressed in Section 6 (Industrial Sources). Medical shipments are regular deliveries of medications to hospitals. The most common encounters with medical sources are patients and contaminated personal articles. Thus the bulk of our work will focus on this area.

Medical nuclides that are commonly used for diagnostic and therapeutic procedures are shown in **Table 5-1**. We have noted the reported usage as either diagnostic (D) or therapeutic (T) or both. Those nuclides for which we have been able to estimate the frequency of application are indicated. This list is only a partial listing of nuclides in use. Several nuclides that are used in medical treatments are not likely to be detectable in a patient, as they do not produce significant gamma rays. These include ^{3}H and ^{32}P. Many other nuclides are used in medical research including ^{7}Be, ^{24}Na, ^{28}Mg, ^{35}S, ^{45}Ca, ^{46}S, ^{47}Ca, ^{48}V, ^{55}Fe, ^{59}Fe, ^{65}Zn, ^{86}Rb, and ^{123m}Te. We do not know to what extent these research nuclides would be found in general use. Other nuclides that have medical applications include ^{14}C, ^{52}Fe, ^{60}Co, ^{61}Cu, ^{64}Cu, ^{67}Cu, ^{74}As, ^{77}Br, ^{80m}Br, ^{82m}Rb, ^{85}Sr, ^{88}Y, ^{89}Zr, ^{90}Sr, ^{90}Y, ^{97}Ru, ^{103}Pd, ^{103}Ru, ^{109}Cd, ^{109}Pd, ^{117m}Sn, ^{115}Cd, ^{124}I, ^{127}Xe, ^{137}Cs, ^{145}Sm, ^{153}Sm, ^{153}Gd, ^{165}Dy, ^{166}Dy, ^{166}Ho, ^{169}Er, ^{170}Tm, ^{175}Yb, ^{177}Lu, ^{188}Re, ^{195m}Pt, ^{198}Au, ^{199}Au, ^{205}Bi, ^{206}Bi, ^{213}Bi, ^{211}At, ^{241}Am, and ^{252}Cf **[OECD 2005]**. We do not have any frequency information for these less common nuclides. Furthermore, it is not clear which of these are used for in vivo applications.

Most positron emission tomography (PET) nuclides have a very short half-life and are visible for only a short period of time. Despite this short window of visibility, PET sources have been observed in the field and thus should not be disregarded. For the purposes of modeling, we assume the minimum time between the administration of a radiopharmaceutical and observation of the patient is 2 hours. This is a critical assumption for PET procedures, but has little impact for other types of procedures.

Table 5-1. Nuclides commonly used for medical procedures. D denotes diagnostic and T denotes therapeutic usage.

Nuclide	Usage	Frequency Available	Usage
^{11}C	D	N	PET Imaging
^{13}N	D	Y	PET Imaging
^{15}O	D	Y	PET Imaging
^{18}F	D	Y	PET Imaging
$^{47}Ca/^{47}Sc$	D	N	Bone metabolism test
^{51}Cr	D	Y	Blood Volume test
^{57}Co	D	Y	B12 Test
^{58}Co	D	Y	B12 Test
^{59}Fe	D	Y	Iron metabolism test
^{67}Ga	D	Y	SPECT Imaging
^{75}Se	D	Y	Pancreas scan
^{81m}Kr	D	Y	Lung Scan
^{89}Sr	T	N	Bone Metastasis
^{99m}Tc	D	Y	SPECT Imaging
$^{106}Ru/Rh$	T	N	Brachytherapy
^{111}In	D	Y	SPECT Imaging
^{123}I	D	Y	Imaging
^{125}I	T	N	Brachytherapy
^{131}I	DT	Y	Thyroid tests and treatment
^{133}Xe	D	N	Lung scans
^{153}Sm	DT	N	Bone metastasis, SPECT Imaging
^{169}Yb	D	N	Gastrointestinal tract diagnosis
^{186}Re	T	N	Bone metastasis
^{192}Ir	T	N	Brachytherapy
^{201}Tl	D	Y	SPECT Imaging

5.1 Procedure for generating medical nuisance sources

Our general procedure for generating medical nuisance sources is to consider each person passing by a detector and determine whether he/she has undergone each class of nuclear medicine procedure in the past year, based on the yearly procedure frequency for that class. If the person is determined to have had a nuclear medicine procedure of a particular class, we then select a specific diagnostic procedure based on the relative frequencies of procedures within that class. A specific procedure is defined by a radiopharmaceutical and a dose. The dose is selected from a cumulative dose distribution for the specific procedure. We determine a time of administration using a uniform distribution from 2h to 365 days prior to the encounter and use the effective half-life of the administered drug to determine the residual radionuclide activity. We then randomly select a body model and apply the residual radionuclide activity. The following sections describe our method of

assigning frequencies to classes of medical procedures and to specific diagnostic procedures within each class, selecting the administered dose, and determining the effective half-lives.

Given the relatively short effective half-lives of most medical radionuclides, the majority of instances generated will not result in a positive detection by the detector. In our current model, we make the explicit assumption that no radionuclide treatment is visible beyond a one-year period. We note that this may not be the case for some therapeutic applications such a brachytherapy. To better understand this aspect, we would need a data source describing the medical practices that use long-lived radionuclides.

5.2 Frequency of medical treatments

5.2.1 Data sources for frequency

To estimate the frequency of medical treatments, we surveyed the literature looking for information on treatment frequencies. We found a number of different sources of data that could be used to estimate the frequency of each treatment type. These include primary data sources, industrial marketing surveys, and academic studies. None of these sources is ideal.

Primary data sources are generally raw data on treatment frequencies based on medical billing information. The availability of this data varies by country. Countries with state-run medical plans such as Canada and the United Kingdom have excellent statistics for treatments. In the United States, the main source is Medicare billing records, which cover only a segment of the population. It is not fair to assume that the population covered by private insurers is the same as those covered by Medicare. There are statistically significant differences between the two populations in terms of age and state of health. Thus, one also needs the records from private insurers. Given the large amount of work required to gather these sources of data and normalize them by population, we consider alternative sources for frequency data.

Medical market surveys are performed to help investors select investment strategies and business opportunities in growing markets. Each survey is a professionally produced report that uses primary data sources along with the research company's own surveys of industry. These reports have been normalized across public and private insurance and thus are more useful for our application. However, the primary focus of such research is to identify the market share and growth. Individual estimates of treatments, dosing and related details are not of interest for these reports. These surveys are also quite expensive. Thus, until we are certain that a particular report contains the data needed to generate our population model, we will use alternative sources.

The last type of data source is academic studies. The most relevant of these are patient dose estimates and population dose estimates. These studies focus on estimation of the risk to the general public from the use of radionuclides. The primary result of such studies is to show the effective risk either to the patient or to the general public. For

example, the typical exposure to the general public as a result of the use of medical radionuclides is less than one tenth the expected dose received from medical X-rays. To create such an estimate, the types of treatment, drug dosage and radiation exposure models must be considered. This is largely the same information we require to model the medical nuisance source population. These studies are often funded by government agencies and performed on a national scale. We have found surveys for Germany, the United Kingdom, Japan and Australia. The usage of medical radionuclides varies from one country to the next. Unfortunately, as the United States has neither a public health system nor a centralized medical record system, the dose estimates for the United States do not provide very complete information. Data on the usage of each general procedure type are available for the United States **[Mettler 2008],** but are insufficient for our purpose as each procedure type may utilize one of several different radionuclides. For example, a cardiovascular diagnostic procedure may use ^{99m}Tc or ^{201}Tl. A German paper provides a detailed breakdown of each treatment frequency, the administered dosage and the procedure type **[Hacker 2005]**. The treatments are broken down into categories that correspond to frequency information available for the United States. Thus by combining these data sources, we can provide both the frequency of each radionuclide treatment and the expected administered dose.

Even with these data, there are still deficiencies in our understanding of medical treatments. The academic dose studies only focus on diagnostic procedures and do not provide the information necessary to model therapeutic medical procedures. According to one report, therapeutic applications account for only about 2% of the total procedures **[Mettler 2008]**. As this is the only information we have, the best we could do is to create a worst case population model where we assume 2% of the procedures are therapeutic using the worst case therapeutic radionuclide and dose. In our current model, we ignore therapeutic treatments. Further, the diagnostic treatments are broken down by procedure. A typical patient often receives several of these diagnostic procedures in a relatively short time span. For example, in the German study, a total of 604,771 nuclear medicine procedures were performed on 433,709 patients. Thus a given nuclear medicine patient may have had multiple procedures. The paper gives the breakdown of these as “53.8% of the patients underwent one, 24.1% two, 10.5% three, and 11.6% four or more examinations per year.” We know from field deployments that ^{99m}Tc and ^{201}Tl are often observed at the same time. Our initial model ignores this correlation except in cases where it was explicitly reported and assumes all procedures are applied independently.

An additional difficulty is the time relevancy of our data sources. The best information that we found on the breakdown of medical treatments and doses is 8 years old and averages frequencies over a 4 year period. Thus, the data describes medical practice as it was 10 years ago. Since then, several treatment methods have fallen out of practice and new procedures have replaced them. For example, brain imaging with SPEC has been almost entirely replaced with PET imaging during the last decade.

5.2.2 Examination frequency table

For our model of treatment type frequency, we use reported data from 2005-2006 **[Mettler 2008]**. However, these data do not report procedure frequencies for the thyroid,

brain, hematology, and “other “categories. These missing categories each represent less than 2% of the procedures. For brain, hematology and “other”, we can use the reported data from the German survey to estimate the frequency expected. The estimates are each less than 2%, as expected. Thyroid procedures are unusually frequent in Germany and thus we have assigned that category a frequency of 1%. The final frequency assignments are shown in **Table 5-2**.

Table 5-2. Frequency assignments for the various types of nuclear medicine procedures.

Examination Type	U.S. Reported Procedures (in 1000’s)	U.S. Assigned Procedures (in 1000’s)	U.S. Frequency Per 1000 Population
Bone	3450	3450	11.5
Cardiac	9800	9800	32.7
Lung	740	740	2.5
Thyroid	<340	172	0.6
Renal	470	470	1.6
GI	1210	1210	4.0
Brain	<340	300	1.0
Infection	380	380	1.3
Tumor	340	340	1.1
PET	1130	1130	3.8
Hematology	<340	37	0.1
Other	<340	124	0.4

We do not distinguish between in-patient and out-patient treatments. This should result in overestimation of the number of nuclear medical treatments seen by a detector as fraction of the in-patient treatments will be below detection limits by the time the patient leaves the hospital. .

5.2.3 Radionuclide frequency for each examination type

For each examination type, we need to assign a radiopharmaceutical and dose distribution. These are based on the German medical survey for 1996-2000 **[Hacker 2005]** and reproduced in **Table 5-3**. Unfortunately, several radiopharmaceuticals were reported as “other”. We assume this was done because they do not contribute significantly to the population dose model and thus, by extension, would not be detectable by radiation detectors. In processing the data in the report, we discovered that, due to a printing error in the original article, 6275 cardiac procedures were missing (9.4%). It is unclear what details to assign to these procedures.

Table 5-3. Breakdown of medical procedures based on German survey [Hacker 2005].

Examination type	Radiopharmaceutical	%	Activity Mean (MBq)	Activity Std Dev	Activity 5th Pctl (MBq)	Activity Median (MBq)	Activity 95th Pctl (MBq)
Bone	^{99m}Tc-phosphates	100	616.4	123.3	489	600	900
Thyroid	^{99m}Tc-pertechnetate	97.4	50.8	17	37	40	74
	^{123}I-iodide	2.6	10.5	3.6	10	10	10
Renal	^{99m}Tc-MAG3	80.2	80.9	48	20	70	180
	^{99m}Tc-DTPA	8	52.5	75.7	20	40	200
	^{123}I-hippuran	4.3	37.6	23.9	2	45	69
	^{51}Cr-EDTA	1.5	7.6	2.1	5	7	11
	^{99m}Tc-DMSA	3	57.4	36.5	15	50	133
	others (2)	3					
Cardiovascular	^{99m}Tc-sestamibi	32	1,026.7	193.6	870	1,000	1,482
	^{99m}Tc-tetrofosmine	17.1	898	124.6	740	1,000	1,000
	^{201}Tl-chloride	6.4	100	34	74	90	189
	^{99m}Tc-sestamibi	3.6	439.1	125.2	275	400	600
	^{99m}Tc-tetrofosmine	2.1	394.3	58.3	370	370	550
	^{201}Tl-chloride	0.5	96.8	10	84	95	110
	^{99m}Tc-sestamibi	3	736	260.6	300	800	1,100
	^{99m}Tc-tetrofosmine	0.6	450.9	75.4	370	485	555
	^{201}Tl-chloride	0.7	90	18.4	74	80	126
	Unknown†	9.4					
	^{99m}Tc-RBC	23.8	831.8	83.5	740	820	970
	^{111}In-antimyosine	0.5	89.9	17.9	74	80	110
	^{123}I-MIBG	0.2	258.4	61.6	150	257	370
	others (2)	0.3					
PET	^{18}F-FDG	91.9	307.9	101.7	132	350	400
	^{13}N-ammonium	4.9	1,110.30	519.1	481	740	2,220
	^{15}O-water	2	3,984	1,434.90	370	4,440	4,440
	others (4)	1.2					
Lung	^{99m}Tc-MAA	68.1	142.4	53.7	43	150	223
	^{99m}Tc-HSA	3	101	10.7	100	100	100
	^{99m}Tc-technegas	14.9	54.5	24.5	20	49	98
	^{81m}Kr-krypton	6.7	832.5	305	100	1,000	1,000
	^{99m}Tc-DTPA	2.7	142.7	52.1	30	165	202
	^{99m}Tc-venticoll	1.4	12.1	6.3	10	10	20
	^{99m}Tc-nanocoll	0.1	39.9	1.2	40	40	40
	^{133}Xe-gas	3	194.6	23.4	185	200	200
	others (1)	0					
GI	^{75}Se-HCAT	0.6	1.4	2.5	0.4	0.4	7.4

Examination type	Radiopharmaceutical	%	Activity Mean (MBq)	Activity Std Dev	Activity 5th Pctl (MBq)	Activity Median (MBq)	Activity 95th Pctl (MBq)
	^{57}Co/^{58}Co B12	18.7	0.05	0	0.05	0.05	0.05
	^{99m}Tc-pertechnetate	20.3	112.9	96.8	40	75	222
	^{99m}Tc-DTPA	4.4	85.8	148.7	20	27	555
	^{99m}Tc-Ery n.d.	11.2	663.2	256.1	186	624	816
	^{99m}Tc-HIDA	16.5	162.2	119	22	140	500
	^{99m}Tc-MAA	6	107.8	79.7	75	92	200
	^{99m}Tc-nanocoll	4.5	114	51.7	50	130	160
	^{99m}Tc-sulfur colloid	6.2	34.4	39	10	20	133
	^{99m}Tc-stannous colloid	10.9	80.6	36.7	25	75	136
	others (1)	0.6					
Infection	^{99m}Tc-granuloscint	56.3	639.1	225	185	729	1,000
	^{99m}Tc-WBC	19.9	794.5	-	302	865	1,000
	^{111}In-WBC	9.6	33.2	18.8	10	31	46
	^{67}Ga-citrate	7.5	218.1	57.7	106	230	280
	^{99m}Tc-nanocoll	4.1	487.2	113.7	400	500	740
	others (2)	2.5					
Tumor	^{99m}Tc-sestamibi	27.9	538.7	195.2	300	548	800
	^{99m}Tc-tetrofosmine	1.8	566	260	129	750	800
	^{111}In-octreotide	34.4	155.9	41.9	102	166	219
	^{123}I-MIBG	22.1	203.7	95.3	59	190	370
	^{131}I-MIBG	1.2	47.7	57.3	6	18	182
	^{131}I-norcholesterol	0.9	36.5	5	30	37	40
	^{201}Tl-chloride	0.7	132.4	25	83	140	150
	^{99m}Tc-pertechnetate + ^{201}Tl-chloride	4.3	147.8	2.3	148	148	148
	^{67}Ga-citrate	3.9	138	62.9	100	100	267
	^{99m}Tc-anti-CEA	2.2	946.2	118	740	900	1,100
	others (3)	0.6					
Brain	^{99m}Tc-ECD	66.4	581.7	102.3	407	550	750
	^{123}I-IBZM	11.9	191.5	19.9	176	187	225
	^{99m}Tc-HMPAO	12	583.9	110.8	500	550	800
	^{123}I-IMT	4.5	223.2	51.4	160	220	317
	^{123}I-IPT	3.7	164.4	16.8	143	165	188
	others (6)	1.5					
Haematology	^{111}In-platelets	23.3	18	15.1	5	19	35
	^{99m}Tc-nanocoll	27	320	208.4	40	220	728
	^{51}Cr-RBC	10.7	4	2.3	1.2	3.7	9
	^{59}Fe-citrate	4.3	1.1	1.3	0.02	0.7	5
	^{99m}Tc-granuloscint	26.5	667.9	124.8	400	700	857

Examination type	Radiopharmaceutical	%	Activity Mean (MBq)	Activity Std Dev	Activity 5th Pctl (MBq)	Activity Median (MBq)	Activity 95th Pctl (MBq)
	^{99m}Tc-WBC	2.4	697.5	155.2	325	750	800
	others (2)	5.7					
Others	^{99m}Tc-nanocoll	76.6	162.3	62	58	150	291
	others (13)	23.4					

† As a result of a clerical error, 6275 cardiac treatments are missing from published table.

5.3 Statistical sampling of dose

For each radiopharmaceutical for which we have frequency data, there are statistics describing the dose distributions. We have the median, mean, standard deviation, 5th percentile and 95th percentile for the dose administered. Our dose distributions should match each of these statistics. Unfortunately, because administered doses are not normally distributed, this is an underspecified problem. More likely, administered doses have discrete distributions corresponding to one or more recommended doses depending on the case. In future work we should acquire more complete data on the dose distribution to avoid the need to construct the distributions based on coarse statistical measurements.

In order to estimate a dose distribution, we generate a series of discrete probability distributions, each of which match the specified statistics. As we have no reason to favor one potential distribution over another, we average these distributions to estimate the dose distribution.

We investigated several approaches for producing the desired distribution and selected an approach that randomly selects a set of possible doses in the range between 0.5*5th dose percentile and 1.2*95th dose percentile and then computes a set of possible frequencies for the discrete doses that is consistent with the published statistics. When selecting the random set of doses, we choose 4 doses below the 5th percentile, 4 doses above the 95th percentile and 20 between the 5th and 95th percentiles. The fitting routine for assigning frequencies uses a standard nonnegative least mean square (LMS) procedure. This procedure was repeated 1000 times. Not all of the random sets of doses could be assigned a discrete distribution that matched the desired statistics. For those that could, the resulting discrete distributions were averaged. Depending on the statistics for the particular treatment, this procedure produced one to four nominal dose ranges administered in patients. The result for ^{123}I-IPT is shown in **Figure 5-1**.

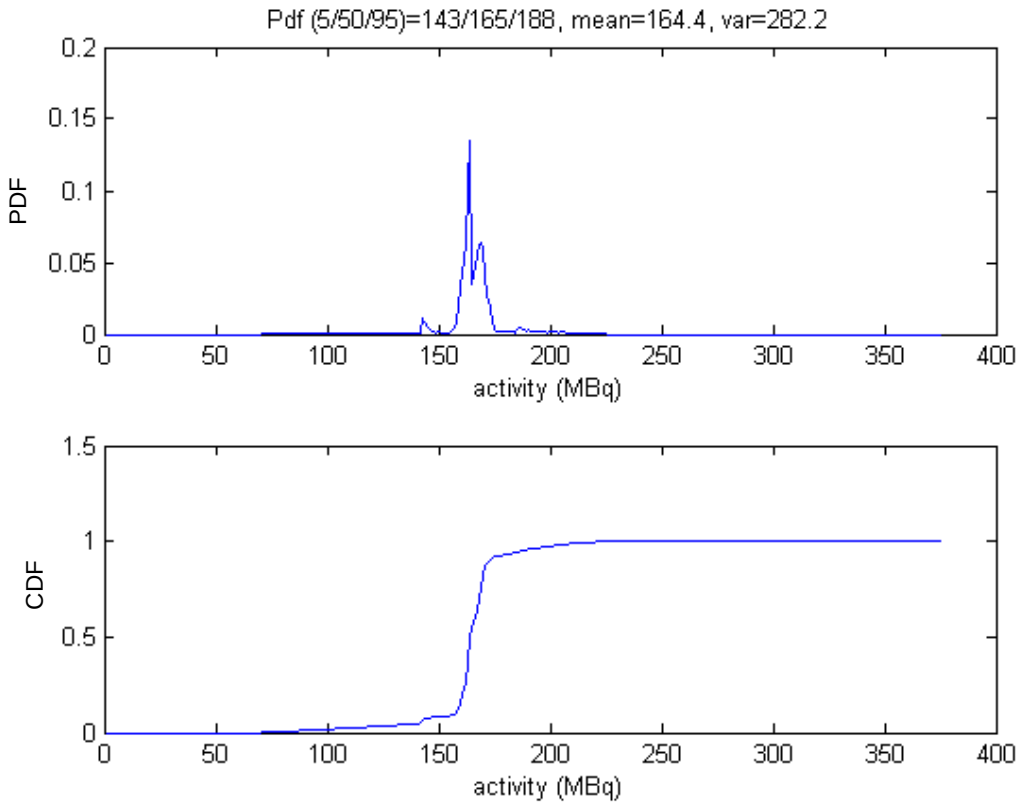

Figure 5-1. Estimated dose distribution for ^{123}I-IPT. Probability density function (PDF) is shown at top and cumulative distribution function (CDF) is shown at bottom.

5.4 Effective half-lives

For each radiopharmaceutical for which we have frequency data, we must assume an effective half-life in order to model how long it will be visible in a detector. Radionuclides used for diagnostics are generally administered as a radiopharmaceutical. As the radiopharmaceutical is broken down, the nuclide is excreted from the body. This excretion process, referred to as the biological half-life, combines with the physical half-life of the radionuclide to reduce the amount of nuclide remaining in the body. Thus, the effective half-life is often much shorter than the physical half-life of the nuclide. For some radiopharmaceuticals there are different biological half-lives depending on which part of the body is processing the drug. Biological half-life depends on the radiopharmaceutical while physical half-life depends only on the radionuclide it contains. Thus, we must determine the effective half-life for each radiopharmaceutical listed in **Table 5-3**.

We performed a literature search for each of the radiopharmaceuticals for which we have frequency data. We calculated the effective half-life by combining the physical half-life with the biological one. For some radiopharmaceuticals, multiple biological half-lives exist as a result of different biological processing paths. For example, blood directly to urine is a fast biological path while blood to liver to kidney is a slower biological path. Further, a portion of the radionuclide may be incorporated permanently into the body.

Where only excretion data exist, we have combined the rate of excretion with the physical half-life to estimate the effective half-life. Use of the 24-hour excretion rates is likely to lead to shorter effective half-lives than justified. The information we obtained is summarized in **Table 5-4**. Details on the calculation of effective half-lives for the various radiopharmaceuticals are provided in Appendix A.

Table 5-4. Effective half-lives of radiopharmaceuticals used in medical procedures.

Radiopharmaceutical	Mode	Physical Half-life	Biological Half-life	Effective Half-life
^{3}H-generic (β-)	–	12.3 y	12 d	12 d
^{13}N-ammonium	–	10 m	–	10 m
^{14}C-generic (β-)	–	5730 y	10 d	10 d
^{15}O-water	–	122.3 s	–	122.3 s
^{18}F-FDG	J	1.8 h	–	1.8 h
^{22}Na-generic	–	950 d	11 d	11d
^{32}P-generic (β-)	–	14.3 d	1155 d	13.5 d
^{35}S-generic (β-)	–	87.3 d	623 d	76.4 d
^{36}Cl-generic (β-)	–	$3.1x10^{5}$ y	29 d	29 d
^{42}K-generic (β-)	–	12.4 h	58 d	12.4 h
^{45}Ca-generic (β-)	–	164 d	49.3 y	162 h
^{51}Cr-EDTA	O	27.7 d	1d (0.95) 100m (0.0495) 7 d ($5e^{-4}$)	23 h (0.95) 100m (0.0495) 6.5 d ($5e^{-4}$)
^{51}Cr-EDTA	J	27.7 d	100 m (0.99) 7d (0.01)	100 m (0.99) 6.5 d (0.01)
^{51}Cr-RBC		27.7 d	42 d (0.9) 160 d (0.1)	16.7 d (0.9) 23.6 d (0.1)
^{57}Co B12	O	271.8 d	100 m (0.34) 1 d (0.06) 500 d (0.6)	100 m (0.34) 1 d (0.06) 176 d (0.6)
^{58}Co B12	O	70.8 d	100 m (0.34) 1 d (0.06) 500 d (0.6)	100 m (0.34) 1 d (0.06) 62 d (0.6)
^{59}Fe-citrate	O	44.9 d	1 d (0.9) ∞ (0.1)	1 d (0.9) 44.9 d (0.1)
^{67}Ga-citrate	–	3.3 d	1.25 d (0.17) 25.5 d (0.83)	22 h (0.17) 2.9 d (0.83)
^{75}Se-HCAT	O	119.8 d	2.7 d (0.97) 62 d (0.03)	2.64 h (0.97) 40.9 d (0.03)
^{81m}Kr-krypton	I	13.1 s	<1 s	0
^{99m}Tc-anti-CEA	–	6.01 h	24 h (0.5) 96 h (0.5)	4.8 h (0.5) 5.7 h (0.5)
^{99m}Tc-DMSA	–	6.01 h	2 h (0.25) 1.8d (0.25)	1.5 h (0.25) 2.8 h (0.25)

Radiopharmaceutical	Mode	Physical Half-life	Biological Half-life	Effective Half-life
			∞ (0.5)	6.01 h (0.5)
^{99m}Tc-DTPA	J	6.01 h	100 m (0.99) 7 d (0.01)	72 m (0.99) 5.8 h (0.01)
^{99m}Tc-ECD	–	6.01 h	1 h (0.9) 36 h (0.1)	51 m (0.9) 5.2 h (0.1)
^{99m}Tc-Ery n.d.	–	6.01 h	NA	6.01 h
^{99m}Tc-granuloscint	–	6.01 h	–	4.8 h (0.5) 5.7 h (0.5)
^{99m}Tc-HIDA	–	6.01 h	24 h (0.85) 30 m (0.15)	4.8 h (0.85) 27 m (0.15)
^{99m}Tc-HMPAO	–	6.01 h	1 h (0.57) 1 d (0.09) 2 d (0.2) 4 d (0.05)	51 m (0.57) 4.8 h (0.09) 5.3 h (0.25)
^{99m}Tc-HSA	–	6.01 h	6.8 h (0.8) 1.29 d (0.22) 19.4 d (0.38)	3.2 h (0.04) 5 h (0.22) 6 h (0.38)
^{99m}Tc-MAA	J	6.01 h	6 h (0.64) 3 d (0.11) 5d (0.25)	3 h (0.64) 5.6 h (0.36)
^{99m}Tc-MAG3	–	6.01 h	16 m (0.4) 32 m (0.4) 7.17 h (0.2)	16 m (0.4) 29 m (0.4) 3.3 h (0.2)
^{99m}Tc-nanocoll	IJ	6.01 h	∞	6.01 h
^{99m}Tc-pertechnetate	–	6.01 h	4.5 h (0.6) 45 h (0.4)	2.6 h (0.6) 5.3 h (0.4)
^{99m}Tc-phosphates	–	6.01 h	0.5 h (0.3) 2h (0.3) 3 d (0.4)	0.5 h (0.3) 1.5 h (0.3) 5.5 h (0.4)
^{99m}Tc-RBC	–	6.01 h	60 h	5.5 h
^{99m}Tc-sestamibi	–	6.01 h	1 d	4.8 h
^{99m}Tc-stannous colloid	–	6.01 h	∞	6.01 h
^{99m}Tc-sulfur colloid	–	6.01 h	∞	6.01 h
^{99m}Tc-technegas	I	6.01 h	8 h (0.05) 4 d (0.95)	3.4 h (0.05) 5.7 h (0.95)
^{99m}Tc-tetrofosmine	–	6.01 h	20 m (0.15) 1 d (0.85)	19 m (0.15) 4.8 h (0.85)
^{99m}Tc-venticoll	I	6.01 h	∞	6.01 h
^{99m}Tc-WBC	–	6.01 h	70 d	6 h
^{111}In-antimyosine	–	2.8 d	38 m (0.054) 3.85 h (0.13) 198 h (0.83)	37 m (0.054) 3.6 h (0.13) 50 h (0.83)

Radiopharmaceutical	Mode	Physical Half-life	Biological Half-life	Effective Half-life
^{111}In-octreotide	–	2.8 d	3 h (0.77) 2.5 d (0.21) 70 d (0.02)	2.9 h (0.77) 1.3 d (0.21) 2.7 d (0.02)
^{111}In-platelets	–	2.8 d	70 d	2.7 d
^{111}In-WBC	–	2.8 d	70 d	2.7 d
^{123}I-iodine	OJ	13.2 h	8 h (0.85) 80 d (0.15)	5 h (0.85) 13 h (0.15)
^{123}I-hippuran	–	13.2 h	25 m (0.96) 4.2 h (0.04)	24 m (0.96) 3.2 h (0.04)
^{123}I-IBZM	–	13.2 h	–	6.22 h
^{123}I-MIBG	–	13.2 h	3 h (0.36) 1.4 d (0.63) ∞ (0.01)	2.44 h (0.36) 9.5 h (0.63) 13.2 h (0.01)
^{123}I-IMT	–	13.2 h	–	60 m
^{123}I-BMIPPA/^{123}I-IPPA	–	13.2 h	1 h (0.07) 2 d (0.73) ∞ (0.2)	1 h (0.07) 10.4 h (0.73) 13.2 h (0.2)
^{123}I-IPT	–	13.2 h	6.22 h	4.2 h
^{131}I-norcholesterol	–	8.05 d	1.4 d (0.2) 13 d (0.8)	1.2 d (0.2) 5 d (0.8)
^{133}Xe-gas	I	5.2 d	22 s (0.77) 24 m (0.23)	22 s (0.77) 24 m (0.23)
^{201}Tl-chloride	–	3.0 d	7 d (0.63) 28 d (0.37)	50 h (0.63) 65 h (0.37)

J – injection, I – inhaled, O – oral

$^{(\beta-)}$ Beta source unlikely to be seen in gamma detector

5.5 Spectral models of medical sources in a human

Radionuclides administered in humans fall into two distinct categories, diagnostic and therapeutic. Diagnostic nuclides are administered in the form of a drug either intravenously, orally, or in rare cases through inhalation. These drugs are taken up preferentially by certain portions of the body. In the case of medical imaging, the patient is scanned and then discharged. Other diagnostics measure the amount of the radionuclide directly to identify the body's metabolism of the drug. Although diagnostic nuclides are preferential, some amount of the nuclide is present throughout the body. Thus, in our model for diagnostic radionuclides, the radionuclide activity is equally distributed throughout a spherical shell that has similar mass and surface area to a human. The parameters vary for each instance.

Therapeutic application is more localized. The most common therapeutic application is the treatment of cancer in the form of brachytherapy. These nuclides are administered

directly to the affected area and are most often encapsulated to prevent migration. Our model for such treatments consists of a point source encapsulated in a sphere of flesh representing the attenuation from the point source to the surface. In our current model, therapeutic applications are not included.

As described in Section 2, our model of medical nuisance sources consists of a medical radiation source surrounded by shielding in a one dimensional spherical geometry. The radiation source is a human who has been administered a medical radionuclide and is, perhaps, inside of a vehicle. Radionuclide activity is assigned to a person as described in the previous sections. The human body is modeled by a sphere of material with a central void, which is used to adjust the surface area to volume ratio. For the initial models the void radius is set to 0, resulting in the minimum surface area to volume ratio. This parameter will be adjusted as needed to cover the range of the measured data. The body composition that we use is a rough approximation of flesh given in **Table 5-5**. We select the mass of the sphere representing the body from a uniform distribution between 50 and 100 kg. Three types of shielding are used to represent vehicle doors, windows and other incidental shielding. These materials are iron, aluminum and glass. Our sampling procedure selects these materials randomly with equal probability. Areal density of the shielding material is assumed to be a uniform distribution from 0.2 to 2 g/cm^2 for glass and aluminum and 0.2 to 5 g/cm^2 for iron. Between the body and the incidental shielding is an air gap with a thickness uniformly distributed between 20 cm and 2 m.

Table 5-5. Elemental composition for body model.

Element	Mass Fraction
O	0.6143
C	0.2286
H	0.1000
N	0.0257
Ca	0.0143
P	0.0111

Observers will be quick to point out that there are few spherical people on the planet and that the shielding material representing the vehicle is likely to be distributed in a less uniform fashion. Shielding from a vehicle passing by a detector is also more complex as the shielding changes throughout the encounter. However, three-dimension geometry effects of this sort are of second order compared to the direct attenuation of the source. As most of the radiation during an encounter is received at the point of closest approach, the bulk of the signature is produced by the effective shielding at this point. Some very high count encounters may have sufficient statistics such that these second order effects will be significant. If this is the case, we will revise our model accordingly.

As described in Section 2, a population of "bodies" (humans + shielding) is generated using the parameters described above. Each "body" can be assigned any of the medical nuclides. The members of this population would then be weighted based on a measured data set. In calculating the fits used to determine the weights, the radionuclide identified in the measured spectrum is assigned to the "bodies".

5.5.1 Comparison of models with empirical data

We evaluate our "body" population model by comparing samples generated from it with the Lincoln Tunnel data records that were identified by GADRAS DHSIsotopeID as medical radionuclides. For each data record, we fit the spectra by inserting some activity level of the identified radionuclide into each of the body models and then calculating the best fit as discussed in Section 2. The Lincoln Tunnel data sample was collected from a single toll collection lane, in approximately 0.8 second measurement windows, grouped according to toll lane occupancy information. Four 2"x4"x16" NaI crystals were used to increase sensitivity to dim sources. In our analysis, we have aggregated data across time bins corresponding to a given toll lane occupancy and also across the four detectors.

For this evaluation, we use records from the Lincoln Tunnel data set that were identified as ^{18}F, ^{99m}Tc or ^{201}Tl. These are the sources for which we have the largest number of samples. In addition, we require a sufficient number of counts above the expected background and exclude low-count samples from the analysis, since these samples have a significant false alarm rate. Furthermore, even if correctly identified, comparison with modeled spectra would be more a test of the background model than the medical source models. Finally, we limited this study to the set of models representing each nuclide separately and did not consider combinations of nuclides to explain a single data record.

Figures 5-2 to **5-4** show examples of the fits for each of the nuclides that we considered. For each graph, the blue points represent the measured data with error bars based on counting statistics, the light blue curve shows the estimated background contribution, and the red curve shows a selected sample from the medical source model plus background contribution. As indicated by the figures, we found generally good agreement between the observed signatures in the Lincoln Tunnel data set and our models. However, poor fits for some of measured spectra indicate that our model is not sufficient to span all of the measured data. Our modeling approach is general enough to handle the problem cases. However, an expanded model is needed to cover all cases that we observed. Those cases that are not covered are explained below.

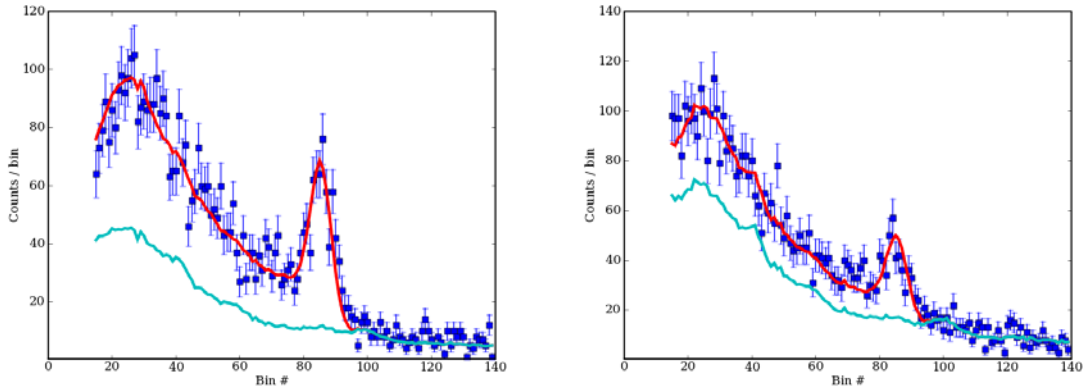

Figure 5-2. Example fits of ^{18}F models to Lincoln Tunnel records.

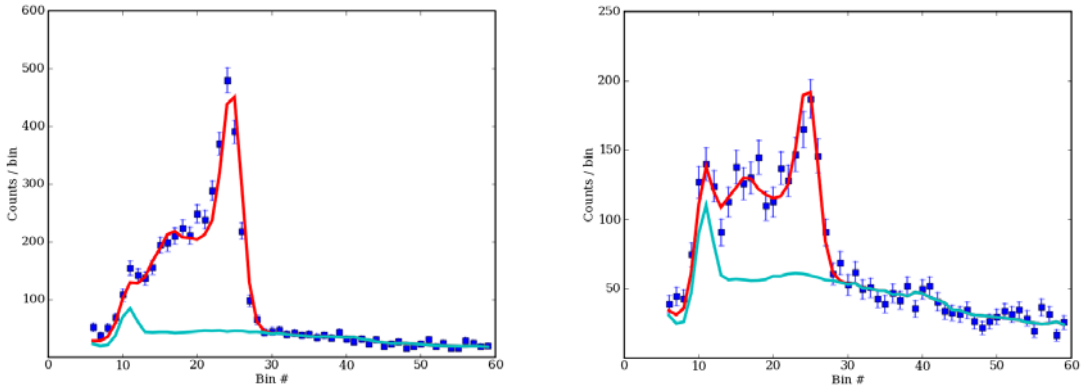

Figure 5-3. Example fits of ^{99m}Tc models to Lincoln Tunnel records.

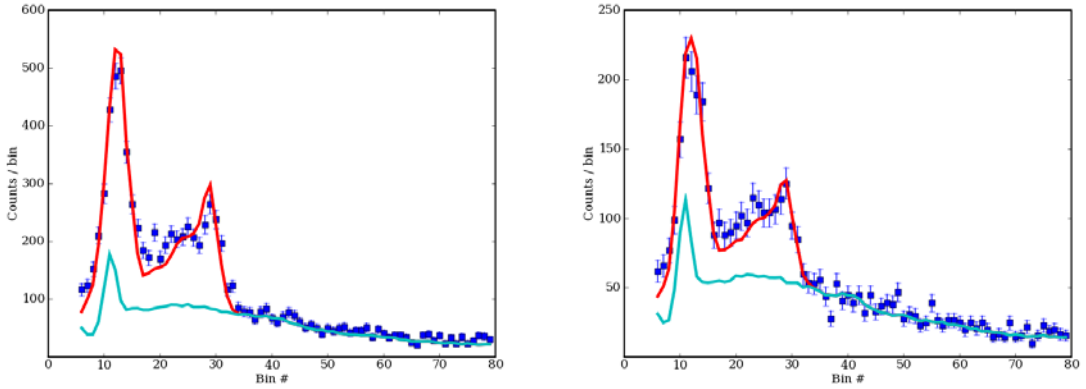

Figure 5-4. Example fits for ^{201}Tl models to Lincoln Tunnel records.

We make several observations that will guide future development of the medical nuisance source model. First, to properly explain the spectra identified as ^{201}Tl, we must also consider ^{99m}Tc in conjunction with ^{201}Tl. These two nuclides are often administered together, but, given the ratio of half-lives, the ^{201}Tl contribution will begin to dominate over time. Many of the samples that GADRAS DHSIsotopeID identified as ^{99m}Tc appear to be a combination of ^{201}Tl and ^{99m}Tc. **Figure 5-5** shows one example of this. The models can account for the two ^{201}Tl peaks, but are unable to account fully for the signal

observed between the two primary peaks. This problem would likely be corrected by adding combinations of ^{201}Tl and ^{99m}Tc to our spanning set.

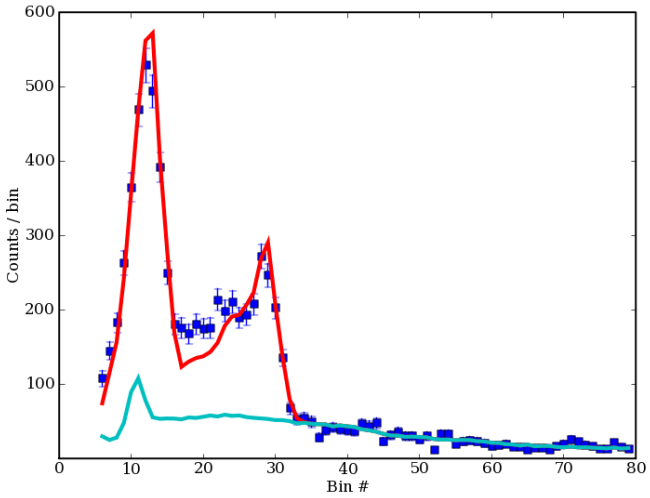

Figure 5-5. Example from Lincoln Tunnel data where a sample identified as ^{201}Tl also shows a significant ^{99m}Tc contribution.

Second, some records appear to have high shielding levels that are not included in our "body" model. We believe that this is due to out-of-lane sources, for which intervening vehicles and infrastructure such as jersey barriers can result in significantly greater shielding. Out-of-lane sources cannot be completely eliminated from the Lincoln Tunnel data sample and may represent up to 50% of the alarms due to medical nuclides.

Third, it is not uncommon for medical sources to saturate the instrument response for the detectors that were used at the Lincoln Tunnel. For example, **Figure 5-6** shows an example where clear signs of pileup are observed. These cases can be identified by their high count rates and by greater than expected count rates at high energies, where the instrument has been unable to distinguish two nearly simultaneous gammas. In the case of a ^{18}F source, as in **Figure 5-6**, pileup leads to a substantial excess over background above the 511 keV line (approximately at bin 85 in the figure) of ^{18}F. This case is not addressed by our current medical nuisance source model.

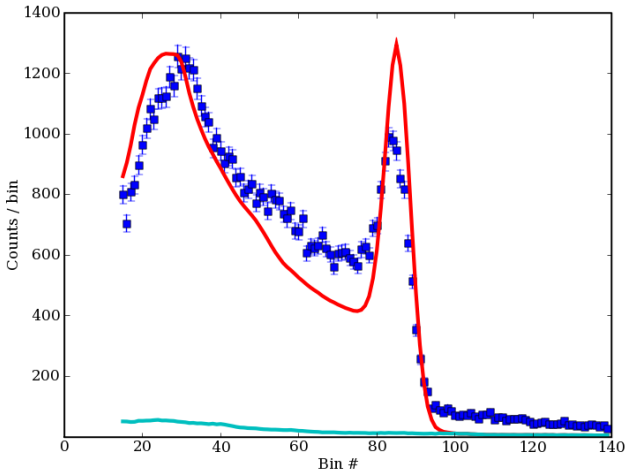

Figure 5-6. Example from Lincoln Tunnel data where pileup effects are observed due to strong passing medical source.

We did not attempt to assign weights to the modeled population using the Lincoln Tunnel data. We chose not to do this primarily because we could not definitively distinguish between sources in the instrumented toll lane and out-of-lane sources. The presence of bright, out-of-lane sources as well as sources in approaching vehicles will bias any weights calculated from these data.

Finally, good energy calibration is important when evaluating spectral fits. There is a substantial record-to-record variation in the low energy part of the spectrum where both the ^{99m}Tc and ^{201}Tl contributions are observed. If not properly calibrated, this variation will lead to poor fit probabilities and thus incorrect weights. The ^{18}F samples suffer less from this deficiency because of the higher-energy 511 keV line.

5.6 Validation of medical nuisance source population model

To complete the current work on medical nuisance source population modeling, we constructed a simulated population using the medical source frequencies and effective biological half-lives from Sections 5.2 and 5.4. We simulated ten million people passing by a typical portal monitor at a speed of 5 mph with a distance of one meter at point of closest approach. The detector used was a standard 2”x4”x16” NaI detector. For each simulated person, we first determine whether they have had a medical exam. For those that have, we determine the parameters (radionuclide, dose, date) of the exam as described in the previous sections. After aging the dose according to the biological half-life, we compute the total expected number of counts that would be registered in the detector during the encounter period. We did not simulate intervening shielding or body attenuation. Thus, the number of counts observed in our simulation will be higher than what we would expect to see in measured data. For a single crystal with a background of 600 counts per second, approximately 100 counts from the source would be required for detection. The detection threshold would drop roughly by the square root of the number of detectors for systems with multiple detectors. **Figure 5-7** shows the expected frequency of observing counts above a specified level for each of the medical

radionuclides. For a detection threshold of 100 counts or greater, we see that the most frequently detected medical source is ^{99m}Tc. This is consistent with it being the radionuclide administered most frequently and at the highest activity level. ^{99m}Tc is closely followed by ^{201}Tl. PET sources (^{18}F) can be quite bright, but their short half-lives result in a detection frequency on the order of 10 in one million.

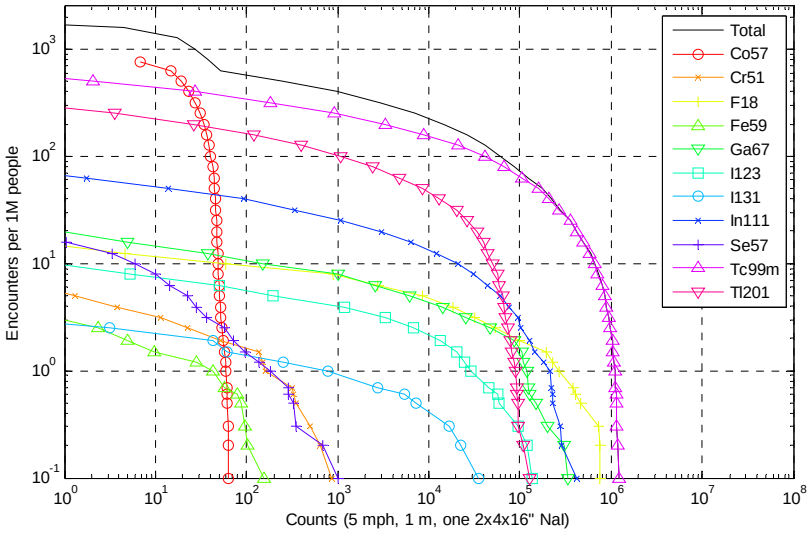

Figure 5-7. Frequency of observing counts above a specified level for each of the medical radionuclides.

5.6.1 Validation challenges

In general, we would like to validate our models against comparable empirical data. Even if extensive data were available, a number of challenges must be addressed in order to meaningfully compare to the model. These challenges include:

1) *In order to produce an accurate count of medical sources, the source must be localized to a specific vehicle.* A detector system deployed on the side of the road or in a single toll plaza lane will alarm on passing sources that are not in the vehicle closest to the detector. In addition, even a single such source could generate multiple alarms. This problem will increase the number of medical sources reported, particularly for the brightest sources.

2) *Field data generally lack ground truth and thus the source type must be inferred from the spectral data.* While it is relatively easy to identify strong sources, weaker sources are problematic.[4] If an automated algorithm is used, the results must be viewed through the error rate of the algorithm. False positives will increase the number of medical sources reported in the field; false negatives will reduce it. Even with a low error rate, false positives would be expected much more often simply because most vehicles scanned do not contain a source.

[4] Identification accuracy as a function of source strength (count rate) is analyzed in **[Labov 2004]**.

3) *Multiple medical sources may be encountered at the same time.* This presents a challenge to the automated identification algorithm, and complicates the procedure of drawing samples from models. We have ignored the correlations in medical procedures as we do not have data to estimate how frequently two procedures were performed on the same patient. We know that the average nuclear medicine patient receives 1.6 procedures, but it is not clear if these procedures are performed at the same time or many weeks apart. This effect may increase the number of medical patients encountered in our model by up to 60%. This effect will also cause confusion in the observed rates of those nuclides which are frequently administered together such as ^{99m}Tc and ^{201}Tl, as it may be difficult to identify multiple nuclides in the same sample.

4) *Field data are often taken from a single deployment and the vehicles which pass by a given location are often correlated from day to day.* This problem increases the variance in observation rates from field data. Thus one cannot assume that the statistical confidence given by the number of vehicles observed during a deployment is an accurate measure of the uncertainty in the population.

5) *Our model has ignored therapeutic uses.* This will cause an underestimate for those nuclides which are used therapeutically such as ^{125}I and ^{131}I. Literature reports cite therapeutic uses at about 2% of the total (see Section 5.2.1). This implies that we may be underestimating sources due to therapeutics by as much as 1200 per million people. Without data on the range and frequency of administered doses, we cannot estimate the fraction that would be visible to a detector.

6) *Our model omits shielding and assumes screening is performed at a fixed distance.* The impact is an increase in the expected intensity of modeled sources and the number of sources which are labeled as detectable accordingly. This will affect low energy sources such as ^{201}Tl and ^{99m}Tc more strongly. We estimate that this could result in over reporting the rate of detectable sources by roughly 25%.

7) *Our model uses literature data which may be for a different time period from the field data.* For those sources in which there was a significant increase or decrease of usage over time, due to changing medical practices, the estimated rates and observed rates may vary accordingly.

8) *We have assumed an arbitrary fixed time period prior to patient release from the hospital*. This assumption will not make a significant difference for those sources which are detectable for many days. However, for ^{18}F with a half-life of only 1.8 hours, this assumption may have a significant effect.

9) *Our model is based on German medical practice, and there are known differences between German and U.S. medical practices*. It is unclear what effect this will have on comparing results.

10) *Our model does not distinguish between inpatient and outpatient treatments.* This will tend to increase the reporting rate of our model.

Not all of these challenges affect our estimates in the same direction. Administration of multiple nuclides may cause our estimated rate to be as much as 60% more frequent than observed, lack of shielding may have increased the observed rate by 25%, and lack of data on percentage of inpatient treatments will increase our modeled rate. On the other hand, increase in the use of nuclear medicine generally (e.g. PET diagnostic procedures) and omission of therapeutic procedures may increase the observed rate. Given this, the expected frequency of occurrence in our model (one source in 2000 persons) may actually be as much as 1:1800 or as little as 1:4000. With these challenges in mind, we would still like to validate our model at some level against available field data.

5.6.2 Data sources and comparisons to the model

Unfortunately, for medical sources, only limited data are available. Previous reports do provide some data on the frequency of medical sources **[NYC Case Study 2004, Vaughn 2005, Kouzes 2006** and **Sokkappa 2007]**. Generally, these sources are useful for comparing frequencies of all medical sources in aggregate, but not individual nuclide frequencies. Data from Customs and Border Protection (CBP) radiation portal monitor deployments at the northern border suggest a frequency of total medical sources in privately owned vehicles ranging from 1:1500 to 1:3000 **[NYC Case Study 2004]**. Other observations from the northern border range from 1:500 to 1:2000 vehicles **[Kouzes 2006]**. A third estimate, based on medical procedure data and experience with detector deployments, suggests that in-lane encounters should result in approximately 1:1500 to1:2000 people carrying a detectable medical source **[Vaughn 2005]**. This corresponds to about 1:900 to 1:1200 vehicles, assuming an occupancy of 1.7 people per vehicle **[MTC 2005]**[5]. The first-principles model results shown in **Figure 5-7** indicate about 1:2000 total medical patients (or about 1:1200 vehicles) at or above the 100 counts likely to be detected. The estimated uncertainty range of the model noted above (1:1800 to 1:4000 people or 1:1000 to 1:2400 vehicles) is very consistent with these observed ranges. Finally, we note that a simple first principles model developed in **[Kouzes 2006]** estimates about 1:2600 people with a detectable source, which also lies within the range.

Although the model and data generally agree on estimated total source encounters, neither of the two sources above break down the category of medical sources by nuclide, which is necessary to validate the frequency of each nuclide. For that, spectral measurements or detailed interviews with vehicle occupants are needed. The best available spectral data we know of are from the Lincoln Tunnel data set, containing about 92,500 records [**Sokkappa 2007]**. **Figure 5-8** shows the frequency of medical sources as reported by the DHSIsotopeID identification algorithm[6] applied to this data set. The figure only shows results for reported nuclides that were also simulated in our model (and shown in **Figure 5-7**).

[5] Vehicle occupancy depends on factors such as region, time of day, day of week and type of vehicle. We have used a value of 1.7 which is the average mid-week inbound occupancy for the Lincoln Tunnel.
[6] Using the version which is included in GADRAS 14.9.1.

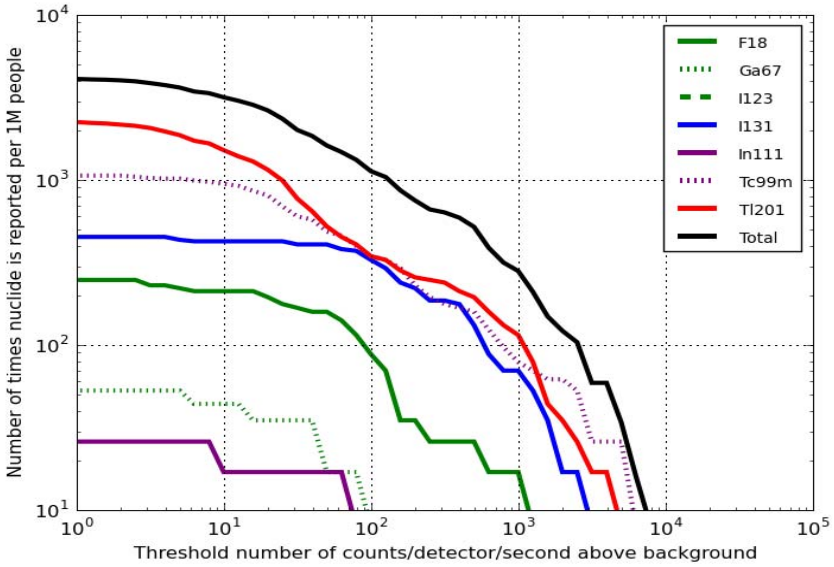

Figure 5-8. Frequency of medical sources in the Lincoln Tunnel data set.

Several of the challenges identified above are directly relevant in comparing model results to the Lincoln Tunnel data, whether by total sources or by individual nuclides.

The total of all comparable nuclides reported at or above 100 counts/sec (corresponding to a reasonable detection threshold) is about 1300 per million. Based on the CBP deployment data cited above, we would expect to see a total of between 200 and 400 per million medical sources passing through the monitored lane. There are two factors likely responsible for this discrepancy.

1) Only one lane in a multi-lane toll plaza was monitored and there was limited secondary inspection, resulting in essentially no ground truth on the source-containing vehicle. Hence, a single bright source in the vicinity of the vehicle being screened (either in-lane or out-of lane) would have generated alarms on multiple vehicles.

2) Approximately one third of the sources reported above 100 counts/sec corresponded to ^{131}I. Our model does not show ^{131}I sources either this frequent or this intense. Since ^{131}I is used for therapeutic as well as diagnostic procedures, and our model does not include therapeutic procedures, we expect to see many more therapeutic sources in the data, particularly since activity levels tend to be much higher for therapeutic applications.

The comparison by nuclide reveals both agreement and discrepancies. Both the model and the data show the most frequent sources to be ^{201}Tl and ^{99m}Tc. The much higher occurrence of ^{131}I in the data is explained both by a likely over counting of a single source and by the omission of therapeutic uses in the model, as noted above. The data also show more PET sources (^{18}F) than estimated by the model. There are two possible

explanations for this. First, medical surveys indicate a steady increase in the use of PET over the last decade **[Mettler 2008]**. Since our medical source data dates from 1996-2000, we would expect an increase in PET source encounters by 2005 when the Lincoln Tunnel data were collected. In addition, the short half-life of ^{18}F implies that it is the most influenced by our assumption of a two-hour delay prior to a patient leaving the hospital. Finally, individual nuclides were reported using an automated identification algorithm, but there was no ground truth to confirm the identification accuracy. We cannot verify the reported frequency of the expected infrequent sources (e.g. ^{67}Ga and ^{111}In) given the few data points in the sample.

Despite the discrepancies, we are encouraged by the comparison of the model results with the Lincoln Tunnel data. To our knowledge, this is the first attempt at modeling the range and frequency of medical sources, at the level of individual nuclides, based on first principles. The similarity between the observed frequencies in the modeled population and the Lincoln Tunnel data is reasonable given the limited data. In future work, we hope to incorporate better frequency estimates derived from U.S. data sources. We also plan to use measured data for the most frequently encountered sources, ^{201}Tl and ^{99m}Tc, to properly weight the parameters of our human body and incidental shielding model (Section 5.1). Once complete, this medical source population model should produce an excellent representation of medical sources for use in detector performance evaluation, in particular algorithm training and evaluation.

5.7 Other considerations

5.7.1 Medical shipment frequency

For each medical treatment there must have been a medical shipment that brought the radiopharmaceutical to the facility where it was administered. For frequently administered medical procedures, sufficient doses for all the treatments administered at that facility during the course of a week would be transported at the same time. Less frequently administered radiopharmaceuticals are transported to a facility on an as needed basis. Radiopharmaceuticals generally have only a limited window of usefulness due to the short half-lives of the radionuclides. Surveying the drug administration sheets for a number of radiopharmaceuticals, we find the typical application window for most nuclides is between 3 and 7 days. The activity levels shipped must be sufficient to administer the recommended dose on the expiration day of the medication. This often means a shipment of even a single dose will be shipped at an activity level 10 times greater than what is administered. We do not currently include medical shipments in our model of medical nuisance sources, but have noted shipment types and characteristics that would be used to construct such a model.

5.7.2 Location bias of frequencies

Our model of medical nuisance sources frequencies is based on medical literature and, thus, at best represents the averages expected when viewing the population of the United States as a whole. As noted above, when actual detectors have been deployed, the observed frequencies of vehicles have been found to be somewhere between 1 in 1500

and 1 in 3000 depending on location.[7] One reason for this wide discrepancy in estimated source frequency is differences in the installation and types of detectors used. However, there are other significant factors that can bias the observed frequencies. Nuclear medical procedures are most often performed at a hospital rather than a clinic. Detectors placed on traffic routes leading from a hospital are much more likely to observe medical sources than would be expected in an observation of the general population. Another source of location bias would be associated with commuter traffic. People do not move at random but rather follow a routine. Measurements of the frequency of medical sources taken over a period of less than a month may include observations of the same person many times over the course of the campaign. Thus only observations taken over a time period greater than the expected detectable lifetime of a particular nuclide would contain independent samples. Our population model ignores these effects.

5.7.3 Contamination effects

In our literature search, we noted additional effects which may have an impact of nuclide identification performance. In particular, many nuclear medicines contain contamination. Typically, when one is intending to produce a certain nuclide, other nuclides will be produced at the same time. Most of these undesired nuclides are separated out chemically during the purification process. However, isotopes of the desired nuclide or nuclides with similar chemistry will not be separated out. These contaminants may have a shorter half-life than the desired nuclide and, thus, are not likely to be observed except in the cases of a medical shipment. Other contaminants will have a longer half-life than the desired nuclide. As the administered dose is designed to give a specified amount of the desired nuclide, the amount of these contaminants will increase the later the dose is administered. For example, ^{202}Tl has a longer half-life than ^{201}Tl. On the day of expiration for a Thallous Chloride injection, the amount of ^{202}Tl administered in solution has risen from 1% to close to 3%. Thus, a medical patient administered a dose on the expiration date may have a different radioactive signature than a patient whose dose was administered earlier. These spectral differences will grow larger as the ^{201}Tl decays. Unfortunately, we do not have any data that we can use to estimate a distribution of administered doses relative to the expiration date.

For purposes of developing nuclide identification algorithms, we recommend that developers design their algorithms to handle a maximum level of contaminant corresponding to the amount present at the date of expiration. The fraction of contaminant can vary over the detectable lifetime of the administered dose, so an algorithm must also address any possible fraction. The worst case levels of contamination we have found based on ICRP-52 and manufacturer supplied information sheets are given in **Table 5-6 [ICRP53 1987]**. ICRP-53 lists a number of impurities, but does not give the expected levels. We note that for some treatments only the contaminants will be detectable.

[7] Unpublished data have shown even lower observed frequencies, which could result from smaller detectors deployed or higher detection threshold settings used.

Table 5-6. Worst case contaminant levels for medical radionuclides.

Medical Radionuclide	Worst case contaminants administered
^{201}Tl	3% ^{200}Tl, 3% ^{201}Tl + ^{203}Pb
^{123}I	12.5% ^{125}I , <0.1% ^{121}Te, <10^{-4}% ^{124}I, <10^{-4}% ^{126}I
^{111}In	0.25% ^{114}In/^{114m}In /^{65}Zn
^{133}Xe	0.02 ^{131}I
^{67}Ga	1.0% ^{65}Zn
^{57}Co	^{56}Co, ^{60}Co
^{52}Fe	^{52m}Mn, ^{55}Fe
^{47}Ca	^{47}Sc
^{59}Fe	^{55}Fe, ^{60}Co
^{99m}Tc	^{99}Mo, ^{99}Tc, ^{131}I
^{113m}In	^{113}Sn
^{198}Au	^{199}Au
^{197}Hg	^{197m}Hg, ^{203}Hg

6.0 Industrial Sources

Thus far we have considered naturally occurring radioactive material (NORM) and medical sources. A third type of nuisance source is industrial sources. We define industrial sources as radioactive materials used in machinery and electrical devices. Industrial sources are a diverse class ranging from a tiny check source embedded in a fire alarm to a large irradiator source. Many industrial sources are installed permanently at facilities and will not be seen in transport except on rare occasions. Others are transported regularly and thus might be encountered frequently in the course of routine commerce. The largest industrial sources are considered to be potential RDDs. Whether an alarm on one of these sources is considered a nuisance or a legitimate alarm will depend on the application. Several thousand of these potential RDD sources are located in the United States. There are a much larger number of smaller industrial sources that do not pose any radiological threat. Unlike NORM and medical sources, there are not many estimates of the frequency of encounter for industrial sources. Modeling the industrial source population requires four basic tasks: cataloguing the different types industrial sources; building a physics-based model for each type of industrial source accounting for the activity of the source and its shielding; estimating the frequency of encounter for those sources that are visible to a detector once engineered shielding is taken into consideration; and, finally, determining scenario specific encounter parameters, such as the distance from the source to the detector and incidental shielding.

6.1 Types of industrial nuisance sources

Our first task in developing an industrial source population model is to categorize different sources based on their applications. There are two key characteristics to consider, mobility of the source and the hazard the source poses to the public. We have already touched briefly on mobility. Different sources are used for different applications and the application determines the frequency of transport. Mobile sources include items such as portable gauges, radiography sources, and some calibration sources. Fixed sources include facility gauges and irradiators. The IAEA categorizes industrial sources based on the source activity and potential hazard **[IAEA 2003]**. As each radionuclide poses a different level of hazard, the IAEA defines an activity level, referred to as the D value, for each radionuclide such that the D value of each radionuclide poses an equivalent risk to humans. For an industrial source, the ratio of the source activity to the dangerous quantity for that radionuclide is referred to as the A/D ratio. Two different types of source with the same A/D ratio are considered to be equally hazardous. Based on these ratios the IAEA defines specific categories of materials as shown in **Table 6-1**.

Table 6-1. IAEA categorization of industrial sources.

Category	Typical Source Application	Activity ratio (A/D)
1	Radioisotope thermoelectric generators, Irradiators, Teletherapy sources	A/D>1000
2	Industrial radiography sources, well logging sources, high dose brachytherapy sources	1000> A/D > 10
3	Fixed industrial gauges, Well logging gauges	10 > A/D > 1
4	Low does brachytherapy source	1 > A/D > 0.1
5	Brachytherapy eye plaques, X ray fluorescence (XRF) devices, electron capture devices, PET check sources	0.1 > A/D > exempt

As described by the NRC **[NRC 2006]**, "Category 1 sources are typically used in practices such as radiation therapy (e.g., teletherapy, stereotactic radiosurgery), and in devices such as radio-thermal generators and irradiators. By contrast, Category 2 sources are typically used in blood irradiators, industrial gamma radiography, and some well-logging applications." Category 1 sources are likely to be permanently mounted in a facility and thus the material is only transported when the device is being installed or refueled. Further, these sources will most certainly fall under the DOT Type B Quantity or Highway Route Controlled Quantity **[CFR 2005]**. These sources must be transported by an exclusive use (contract carrier) vehicle and require placarding. Stopping such a vehicle and verifying that it contains a legitimate shipment would be required. Thus this type of source would not be considered a nuisance source and would not be included in our population model.

Our model considers only those sources which are Category 2 and below. Category 2 sources include two mobile applications, radiography and well logging. Sources used for these applications could be encountered during transportation, usually on private carrier vehicles. However, as these sources pose a significant harm to humans if not controlled, they might be considered to be potential RDDs. Category 3 sources and below are unlikely to be an effective RDD device from the perspective of potential damage to human life, but still may be used as a terror weapon to scare the population. Whether or not a particular source category is considered a nuisance or a potential RDD will depend on the location and operating policy of the operator of the radiation detection system.

The NRC defines nine categories of industrial uses **[NRC 2007]**:

- industrial radiography
- irradiators
- well logging
- gauging devices
- other measuring systems
- research and development
- service providers

- source material
- special nuclear material.

Our focus will be on radiography, well logging, gauging devices and other measurement systems. Research and development is a widely varying category that should be encountered rarely. The category of service providers refers to waste disposal and decontamination and is not covered in our current model. Source material includes industrial use of thorium and uranium and is covered in our NORM population model. For our purposes, special nuclear material is a potential threat and is not considered a nuisance source. In addition to the five industrial source categories defined by the IAEA, there are also exempt quantities of nuclear material such as check sources and industrial uses of natural materials. The natural materials are covered by our NORM model. We will not endeavor to characterize check sources because there is a large variety with differing characteristics and we have no information on their frequencies.

6.2 Physics-based model of industrial sources

For each industrial source type, we will define a physics-based model that can be used to generate a random sample of the radiation output from a source of that type. As with our NORM and medical models, we will use a spherical model for each source type. Each model will specify the ranges of shielding, activity and materials that can be used to represent the industrial source, including its physical packaging. Unlike NORM and medical sources, industrial sources may be point sources or distributed sources, with the majority being point sources. Industrial radionuclides, with the exception of uranium, have a fairly short half-life ranging from a few months to tens of years. Short half-lives correspond to high specific activity, and thus only a few grams are required for most applications. Even when mixed with an oxide to form a ceramic, industrial sources are very small. As with our NORM and medical models, a physical model for an industrial source consists of a radionuclide, an activity associated with that nuclide, an engineered high-Z shielding used to reduce radiation exposure, and incidental shielding which is application dependent. Our challenge is to determine the ranges of materials, activities and engineered shielding that should be used to model each type of industrial nuisance source.

Our approach to modeling industrial sources requires us to consider both the source as it is designed for use in its application and how that source is transported. Source descriptions for different industrial applications can be obtained from safety sheets filed with the NRC and the various state regulatory agencies. Physical packaging models can be inferred based on guidelines from the Department of Transportation (DOT). Once we have identified a sufficiently large set of source configurations for a given industrial source type, we can create a parameterized physics-based model.

6.2.1 Source descriptions

For each industrial source type manufactured and licensed in the United States there is a safety sheet in the "Registry of Radioactive Sealed Sources and Devices" **[NRC 2009]**. These sheets contain a description of the source along with activity ranges. For industrial

devices, the entries contain data on the shielding incorporated in the design of the device. In addition, the sheets may contain radiation measurements for the purpose of dosimetry. The total number of active sources and devices being manufactured is quite large. The index listing the entries is 179 pages long. However, many products are covered under the same registration number. Currently, access to this database is restricted as a result of heightened security concerns. It was previously available to the public and we expect to be able to obtain access to this database for use in constructing our industrial source models.

We should also be able to obtain a fairly good description of each industrial application by augmenting the safety sheets from this database with product sheets obtained from the manufacturers. Unfortunately, extracting this information will be a considerable task. Many of the sources in this database do not need to be included in an industrial nuisance source population model. For some, this is because they are well below the detection levels of the types of scenarios that we are considering. Others are Category 1 and 2 sources, which would best be modeled as potential RDD sources rather than nuisance sources. Further, this database does not have searchable fields, and thus the information must be extracted by reading each of the safety sheets. As each sheet is between 4 and 20 pages in length, it is a considerable effort to extract the useful information. We have extracted information from the subset of safety sheets that are publicly available. This information is given in Appendix B.

Some sheets contain sufficient data to develop a source model while others merely describe a generic class of products that a vendor may sell. Only those sheets that describe a unique source will be of use in constructing a nuisance source population. For the sources that are well described, only a few types describe the packaging. Thus to construct a model of sources in transport, we would need to apply the required engineered packaging used for transportation.

6.2.2 DOT regulations

For the majority of sources in the sealed source and device registry the safety sheets do not provide sufficient information to create a physics-based model. In addition to the activity and physical form, we require information about the shielding materials surrounding the source. We will infer this information based on the DOT regulations for transporting radioactive materials **[CFR 2005]**. These regulations prescribe the maximum allowable radiation exposure based on the type of carrier and the required survivability of the packaging based on the radionuclide and activity level.

The DOT regulations are designed to minimize hazards to the public posed by the transportation of radioactive sources. The DOT defines the packaging requirements based on the type of carrier that will be handling the package. The regulations define three categories of carrier type--common carrier, contract carrier and private carrier. Common carriers include services such as FedEx or UPS. The driver is assumed to have minimal training and thus common carrier limits are the strictest. Exposure limits are set for the outside of the package. A contract carrier is a private company contracted to exclusively deliver a radioactive source. Controls for contract carriers are defined based on the

location of the driver relative to the source and the expected exposure to the general public. Larger sources and greater exposure are allowed for contract carriers. Private carriers are businesses that own the source and are responsible for its control at all times. Private carriers must be licensed with the NRC.

Packaging must be engineered to meet the exposure limits defined for the carrier. The controls used to reduce exposure are distance and shielding. Greater shielding results in less radiation exposure. However, increased shielding also increases the mass of the shipment. For many modes of transport, such as air, mass is an overriding concern. Thus, distance is also used as engineering control. By increasing the size of the package in excess of the size of the object being shipped, the radiation exposure is reduced by the square of the distance from the source to the outer edge of the packaging. This is referred to as "overpack." With these two engineering controls, the radiation exposure is kept within the specified limits. However, a safety factor beyond the requirement is often desired. Exposure limits are defined based on the maximum exposure anywhere on the package. Some portions of the package will have greater shielding or overpack due to shape and mechanical or structural concerns. Further, as packaging is generally not custom-made for a particular shipment, the radioactivity of the item shipped is often less than the absolute limits for the packaging. This is especially true for radiography sources where the same package is used for the entire lifetime of the source.

In addition to meeting radiation exposure limits, packaging must also meet survivability requirements to ensure that the radioactive materials are contained in the event of an accident. Based on the level of radioactivity, the DOT defines five categories of material with different packaging requirements. These are shown in **Table 6-2**. This survivability requirement results in additional low-Z shielding beyond the high-Z shielding required to satisfy exposure limits. Low-Z shielding does not stop significant amounts of radiation, but it does downscatter radiation making detection more difficult. Typical Type A packages include a shielding pot surrounded by packing foam with a minimal protective casing. Type B packages may have additional protective packing foam and accident resistant casings.

Table 6-2. Material categories for defining packaging requirements.

Classification	Description
Non-radioactive	Material has less than 0.002 μCi per gram.
Limited Quantity	Material is less that 1/1000 of the Type B quantity. Package must be able to survive routine handling.
Type A	Material is greater than the limited quantity, but less than the Type B requirement. Shipment requires Type A package which should survive a minor accident.
Type B	Material is greater than DOT specified hazardous activity for radionuclide and form (sealed, solid, liquid). Shipment requires Type B package which should survive a serious accident.
Highway Route Controlled Quantity	Material is greater than 3000 times the Type B limit. Shipment requires Type B package and carrier must be trained. State officials must be notified if material is waste.

Based on these regulations, for a given radionuclide activity level, we are able to determine the minimum required shielding with and without overpacking, and other additional packaging requirements. By surveying manufacturers of radiation packages, we can develop representative models for each of these different packaging types. Each source package type in the United States is issued a "Certificate of Compliance." Further, the DOT maintains a list of recommended packages for sources. Thus we can construct a representative physics-based model for each source type including its expected packaging.

6.2.3 Generalized source models

Creating an exhaustive list of the different source and package combinations would be a very large task due to the number of sources types and the packaging options for each. Fortunately, we do not require an exhaustive list but can develop models that span the range of possibilities. For a given source type, regulations imply lower bounds on packaging such as minimum required shielding. As the regulations define only the minimums, we use specific examples to determine expected upper bounds. With a few representative samples from each category of industrial use, we construct a generalized model of that category.

Figure 6-1 shows an example of how we would create a general model of a radiography source. Based on the radiation emissions from ^{192}Ir, we can estimate the minimum amount of lead shielding required with and without overpack as a function of activity. We can then use the sealed source and device registry to locate specific instances of radiography sources and look up the certified packages recommended to carry these sources. Based on this, we define ranges for the source activity and shielding and assume uniform distributions across these ranges. As radiography sources decay over their useful lifetime, we need to adjust the activity level based on the source's age. The age of a radiography source is assumed to be uniformly distributed between 0 and the length of its usable lifespan.

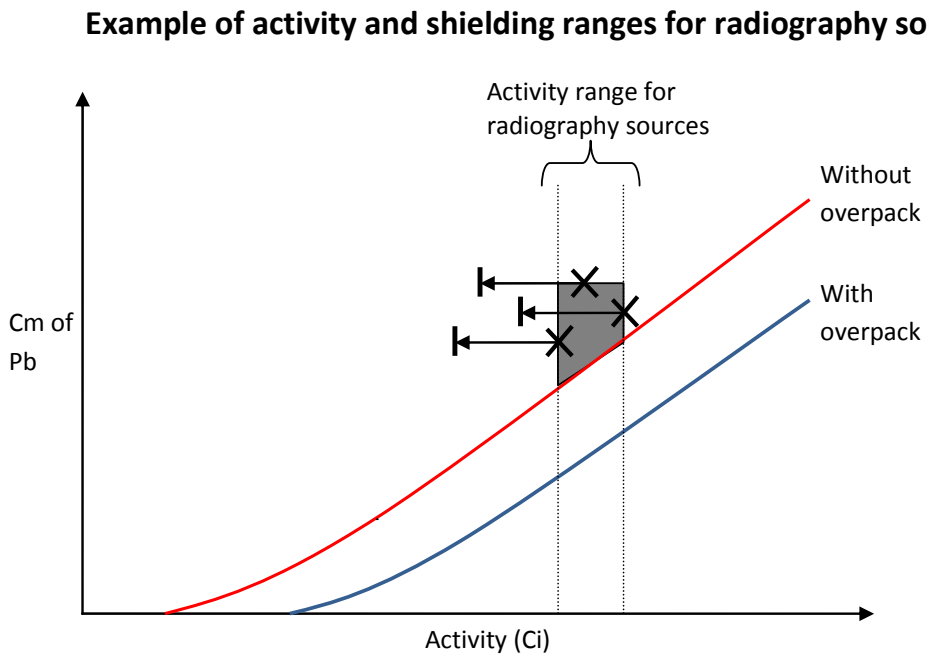

Figure 6-1. Minimum shielding required (based on exposure limits) with and without overpack as a function of radionuclide activity. The X's represent specific instances of actual radiography sources from the Registry of Radioactive Sealed Sources and Devices in their recommended packages. The arrows represent the activity range of each source over its usable lifespan. The shaded area shows the shielding range as a function of activity.

6.3 Development of frequency estimates

An even greater challenge is to estimate appropriate frequencies for industrial nuisance sources. We have identified several possible data sources that could be used to estimate industrial source frequencies. These include:

- Manufacturers of sources and devices
- Market surveys
- National Source Tracking System and interim inventory reports
- Web-based licensing program
- Trade associations
- Production estimates
- Radioactive materials in quantities of concern (RAMQC) reports

Independently, none of these data sources will provide all of the required information to build an industrial source frequency model, but hopefully by pursuing each of them we will be able to form a more complete picture.

6.3.1 Manufacturing frequency

The best method of obtaining frequency information would be to survey the manufacturers of the devices. If we know the production quantity of each item and whether it is intended for a fixed installation or for a mobile application, we can construct a good representation of the relative frequency of mobile sources as well as the frequency of transport for fixed sources. Combining this with field data on the observed frequency of known sources, we would be able to estimate the absolute frequencies required for our population model. Unfortunately, manufacturers consider information on their production rates to be proprietary. At best, a direct survey of the manufacturers would provide a rough number of sources produced from a handful of cooperative vendors.

6.3.2 Marketing surveys

The alternative to surveying vendors directly would be to utilize marketing surveys produced by private research organizations. Much like the reports produced on medical procedures, these are professional surveys designed to estimate the current capacity and potential growth for a given sector of industry. These reports tend to be quite costly, but may be less expensive than the cost of surveying the manufactures directly. Unfortunately, we would not be able to identify if the information we require is available in any particular report without first purchasing it. Reports such as "Nondestructive Testing, New Developments and Growth Opportunities (Technical Insights)" from Frost & Sullivan or "The 2009-2014 World Outlook for Computed Radiography (CR) Equipment" from Market Research may contain information that could be of use in constructing the frequency model.

6.3.3 NRC resources

Private ownership of radioactive sources requires a license issued by the NRC. These may be either general licenses for a broad class of sources or specific licenses for a specific source type. Specific source licenses are required only for certain large sources. Most licenses are general licenses. Individual sources are not tracked under either the general or specific licensing programs. The National Source Tracking System (NSTS) began tracking Category 1 and 2 sources in January 2009 **[NRC 2006]**. For periods prior to its operation, interim inventory reports are available that provide information on the number of sources per state by application. Unfortunately, neither the NSTS nor the interim reports will supply us with information on the smaller nuisance sources that we are attempting to model. It was proposed to expand the NSTS to Category 3 and 4 sources, but this proposal has not been acted on to date.

The NRC is currently developing a new system called web-based licensing. This is a modernization of the current licensing program. As such, it will be able to track individual sources. This program may be of some application to our problem, but is at least a year from implementation and it may be even longer before the data base is populated.

6.3.4 Trade associations

Another possible source of frequency information is the trade associations associated with the use of particular classes of industrial sources. For example, the American Society for Non-destructive Testing may have information about the number and types of sources used for radiography applications. This information would be useful in constructing a population model, but it is fairly limited. Only a few types of devices are likely to have a relevant trade association.

6.3.5 Production estimates and import records

The final approach to this problem would be to examine the production of radionuclides rather than the manufacturing of sealed sources or devices. Many radionuclides are produced outside of the United States and imported. We import large quantities of radioactive materials from Russia, Canada and the Netherlands. In addition, we produce some radionuclides domestically at government and university research reactors. If we know the bulk production that is being used to supply the manufacturers, the average amount of each radionuclide that is consumed by a particular application, and a rough marketing ratio to determine the relative frequency of each application, we could estimate the number of sources and devices produced. Unfortunately, like the device manufacturers, producers of radionuclides are likely to treat such information proprietary. This problem may be more tractable in that there are fewer radionuclide producers. Rough market estimates of the value of different nuclides produced are available. By assigning a cost per curie, one can estimate the total production capability **[Connell 2006]**.

Rather than contacting the producers directly, there is an alternative approach. Imports of large quantities of radionuclides must be reported to customs. These reports are called radioactive materials of quantities of concern (RAMQC) and are provided to the NRC. By adding the total of these shipments over a one year period, we could measure a significant fraction of the total production. This approach has the significant downside that it would require access to either NRC reports or customs data that are tightly controlled.

6.3.6 Practical limitations of frequency estimates

By applying each of these approaches in parallel, we believe we can develop an estimate of the industrial source frequencies that is sufficient for our modeling effort. Though the methods we are applying may seem somewhat crude, they are the best one could hope to apply given the data limitations. It will never be possible to accurately determine the actual nuisance source frequency for any given detector deployment without field measurements. In practice, the actual frequency of a particular source type observed by a detector depends on how many sources are in the locality and whether a particular source travels near the detector deployment. A detector that happens to be installed between a construction site and an instrument's storage facility may see the same source multiple times a day. Many sources are concentrated regionally. For example, the vast majority of well logging sources are located in Texas where they are used for the oil industry. It would be highly unlikely to find one in an urban setting such as Chicago.

The lack of an ability to make a definitive nuisance source population model should not detract from the utility of the effort. Without some representative population, it is not possible to either design or evaluate nuclide identification codes that might be deployed. A nuisance source population model with a large uncertainty is still useful for determining tradeoffs between different detector concepts. Further, one can use the population model to establish worst-case bounds on performance by simply increasing the nuisance source encounter rate to be significantly higher than estimated.

7.0 Applications of Nuisance Source Models

In the preceding sections, we described a comprehensive approach to modeling NORM, medical and industrial sources. These sources constitute the primary source of alarms in numerous radiation detection applications, from cargo monitoring at ports of entry to traffic screening at urban chokepoints to pedestrian screening at large event venues. Alarms due to pure background fluctuations are typically negligible compared to alarms due to these nuisance sources. Among the various types of nuisance sources, the most significant depend strongly on the application and detection scenario. Properties of the stream of traffic to be monitored, the threat under investigation, and characteristics of the detection system determine whether a particular type of nuisance source is problematic. Here we describe several prior analyses that we have performed where nuisance source modeling has played an important role and where the limited fidelity of nuisance source models limited the accuracy of the results.

For the DNDO Securing the Cities program, LLNL performed two analyses of alternatives for traffic screening systems. In one instance, a high-speed highway scenario was considered **[Lange 2008]**; in the other, radiation detection systems utilizing existing infrastructure at a toll plaza were considered **[Wheeler 2009]**. In both cases, the detection systems were required to detect, localize and classify threat sources in real time as they passed the detector system. In these analyses, a very large population of nuisance sources was required to probe the required false alarm rate of one false alarm across the system per day. The Lincoln Tunnel data sample corresponds to less than one day of traffic for the high-speed screening analysis performed. Thus, using this data sample directly limited the false alarm rate that could be considered. Nuisance source modeling of both medical and industrial sources allowed the study of lower false alarm rates (though with the caveat that infrequent and potentially problematic nuclides not in the original Lincoln Tunnel data would also not be in the model). While the suppression of alarms from background was found to be straightforward, estimates for both medical and industrial source characteristics and frequencies governed the system performance results and, thus, the preferred system alternatives. In particular, medical sources posed a challenge to the localization algorithms, where the source-carrying vehicle must be distinguished from other vehicles in the field of view. Both medical and industrial sources present challenges for the system requirements for classification - where benign nuisance sources must be distinguished from threat nuclides.

Another example is from a study on the feasibility of a long dwell in-transit radiation detection concept for monitoring shipping containers at sea **[Sokkappa 2008]**. For this type of system, a very low false alarm rate was required - one false alarm per year across all cargo containers on all ships entering the USA. In contrast to the Securing the Cities analyses, the NORM nuisance source population presented the primary challenge. In this analysis, we combined small samples of measured NORM data (the NYCT I and II samples), PIERS manifest data, and information from literature to generate a population model. This model was then used to estimate false alarm rates for the systems under consideration. The limitations imposed by small data sets determined the lowest reasonable false alarm rate that could be probed by this analysis approach.

As a final example, NORM modeling plays an important role in the study of international rail. Similar to a POE, NORM sources are the primary contribution to alarms for any radiation detection system monitoring trains entering the USA. It is expected that the distribution of NORM at rail POEs will differ from seaports and be location specific due to the different geographic origins of the material being transported. Given a NORM model based upon sea port of entry data and manifest information (as described in Section 4), a NORM model appropriate for international rail could be developed, assuming sufficient information on the distribution of commodities in the rail cargo population is available. Our approach to NORM modeling is particularly well suited in that we can naturally reweight the spanning templates based upon commodity information. However, this would rely on commodity information at both the POE where existing detectors are deployed as well as that from the prospective international rail monitoring site.

8.0 Conclusions and Next Steps

The current project has generated much of what is needed for achieving a comprehensive nuisance source population modeling capability. Source terms have been developed from first principles for NORM, medical and industrial sources. Initial estimates of frequency of occurrence have been made for NORM and medical populations, but not for industrials. These models are sufficiently developed for use in detector performance studies. We have identified a number of topics for further model development or use, including the following:

1. Case studies should be conducted to demonstrate the utility and limitations of the current nuisance source models.

2. Sensitivity analysis should be done for all nuisance source models. This could identify the impact of uncertain parameters on the simulated populations and help prioritize efforts to obtain better data.

3. NORM

    - Individual models for specific cargo types need to be developed so that a population model can be applied to multiple locations with different distributions of arriving cargo (and hence NORM).

    - Frequency estimates for the entire NORM populations at various sites need to be improved using more comprehensive manifest data.

    - Verification is needed to show that the NORM model is sufficient to parameterize NORM cargo at multiple ports. The range of model parameters that account for observed NORM cargo must be determined.

4. Medical

    - Data are needed on U.S. medical procedures to better reflect the distribution of radioactive sources likely to be encountered.

    - Improved estimates of frequency of therapeutic applications, in addition to diagnostic applications, are needed.

    - Non-uniform movement of medical patients in a given area should be accounted for (e.g., roads in the vicinity of hospitals are likely to see a higher fraction of patients than roads in general).

    - Shipments of medical sources should be included in the population model in addition to medical patients.

    - Medical source body models should be tuned to observed field data.

5. Industrial

    - The industrial source frequency data we have identified should be analyzed for relevant frequency information.

    - Using the spanning set of industrial sources we have developed, we should perform a sensitivity analysis to identify which sources are the most troublesome. We should then focus on improving the source models and frequency estimates for these challenging sources.

REFERENCES

[Bhattacharya 1991] Bhattacharya, S. and A. Lahiri, *Clinical role of indium-Ill antimyosin imaging*, **European Journal of Nuclear Medicine 18**, 1991.

[CFR 2005] *Shippers – General Requirements for Shipment and Packagings, Class 7 (Radioactive) Materials*, Code of Federal Regulations - Title 49: Transportation - 49 CFR 173.401-477, Dec. 2005.

[Connell 2006] Connell, L.W., *Prospect for Radiological Terrorism, A Risk Based Approach (U)*, briefing to DHS Secretary Chertoff, Sandia National Laboratories, 2006.

[Descalle 2006] Descalle, M.-A., E. Manatt, and D. Slaughter, *Analysis of Recent Manifests for Goods Imported Through US Ports,* Lawrence Livermore National Laboratory, UCRL-TR-225708, 2006.

[DNDO 2007] Domestic Nuclear Detection Office, *Report on testing conducted at the New York Container Terminal in support of the Advanced Spectroscopic Portal production decision*, 200-TPNYC-103720v4.00, 2007.

[Edmunds 2007] Edmunds, Thomas, et. al., *Urban Perimeter Defense*, Lawrence Livermore National Laboratory, UCRL-TR-229202, March 2007.

[Hacker 2005] Hacker, M., et al, *Radiation exposure of patients undergoing nuclear medicine procedures in Germany between 1996 and 2000. Multicenter evaluation of age and gender-specific patient data*, **Nuklearmedizin 44**, 2005.

[Hartigan 1975] Hartigan, J. A., **Clustering Algorithms**, ISBN 0-471-35645-X, Wiley, 1975.

[IAEA 2003] *Categorization of radioactive sources—Revision of IAEA TECDOC 1191 Categorization of radioactive sources*, IAEA TECDOC 1344, International Atomic Energy Agency, 2003.

[ICRP53 1987] International Commission on Radiological Protection, *Publication 53*: *Radiation Dose to Patients from Radiopharmaceuticals*, **Annals of the ICRP**, Vol. 18, No. 1-4, 1987.

[ICRP62 1993] International Commission on Radiological Protection, *ICRP Publication 62: Radiological Protection in Biomedical Research*, 1993.

[ICRP80 1998] International Commission on Radiological Protection, *Publication 80: Radiation Dose to Patients from Radiopharmaceuticals-Addendum 2 to ICRP 53*, **Annals of the ICRP**, Vol. 28, No. 3, 1998.

[ICRP106 2009] International Commission on Radiological Protection, *Publication 106: Radiation Dose to Patients from Radiopharmaceuticals*, 2009.

[Kouzes 2006] Kouzes, Richard T. and Edward R. Siciliano, *The response of radiation portal monitors to medical radionuclides at border crossings*, **Radiation Measurements 41,** 2006.

[Kuikka 1994] Kuikka, Jyrki T., Kim A. Bergström, Aapo Ahonen, and Esko Länsimies, *The dosimetry of iodine-123 labelled 2β-carbomethoxy-3β-(4-iodophenyl)tropane***, European Journal of Nuclear Medicine and Molecular Imaging 21**, 1994.

[Labov 2004] Labov, Simon et al., *Foundations for Improvement to Passive Detection Systems—Final Report*, UCRL-TR-207129, October 2004.

[Lange 2008] Lange, David, Thomas Edmunds and Richard Wheeler, *Securing the Cities: Analysis of Alternatives for Fixed-site High Speed Traffic Screening*, Lawrence Livermore National Laboratory, LLNL-TR-403911, March 2008.

[Mettler 2008] Mettler, Fred A., et al., *Nuclear Medicine Exposure in the United States, 2005-2007: Preliminary Results*, **Semin Nucl Med (W.B. Saunders) 38,** 2008.

[Monetti 2006] Monetti, M., *Test Plan for the New York Container Terminal Test of Advanced Spectroscopic Portal Engineering Development Model (Draft)*, DHS Doc #101870085.00, December 2006.

[MTC 2005] New York Metropolitan Transportation Council, *Congestion Management System 2005 Status Report* (*Appendix H –River Crossings 24 Hour Counts and Vehicles Occupancy Data*), August 2005.

[Nelson 2008] Nelson, Karl and Padmini Sokkappa, *A Statistical Model for Generating a Population of Unclassified Objects and Radiation Signatures Spanning Nuclear Threats*, LLNL-TR-408407, September 2008.

[NRC 2006] Nuclear Regulatory Commission, *10 CFR Parts 20 and 32, National Source Tracking of Sealed Sources*, **Federal Register**, Vol . 71, No. 216, Nov. 8, 2006.

[NRC 2007] *Industrial Uses of Nuclear Materials,* Nuclear Regulatory Commission, 2007.

[NRC 2009] *Registry of Radioactive Sealed Sources and Devices Active Vendors/Active Products by Vendor Name,* Nuclear Regulatory Commission, 2009.

[NYC Case Study 2004] Lawrence Livermore National Laboratory, Los Alamos National Laboratory, Pacific Northwest National Laboratory and Sandia National Laboratories, *Metrics and Evaluation Framework for Radiological and Nuclear Threat Countermeasures: An Interim Report and Case Study*, SAND 2004-6261P, December 2004.

[OECD 2005] *Nuclear Development Beneficial Uses and Production of Isotopes: 2004 Update (Complete Edition - ISBN 9264008802)*, **OECD Nuclear Energy Journal**, Vol. 2005, No. 1, Feb. 2005.

[Schmidt 1997] Schmidt, Daniela, et al., *Whole-body kinetics and dosimetry ofl-3-[123I]iodo-α-methyltyrosine*, **European Journal of Nuclear Medicine and Molecular Imaging 24,** 1997.

[Smith 1999] Smith, T., R. Senior, U. Raval, B. Dasgupta, and A. Lahiri, *Biodistribution, radiation dosimetry and pharmacokinetics of 111In-antimyosin in idiopathic inflammatory myopathies*, **Journal of Nuclear Medicine 40** , 1999.

[Sokkappa 2007] Sokkappa, Padmini, et. al., *Radiation Detection Modeling and Operational Analysis: Benchmarks, Nuisance Source, Algorithm and Resolution Studies*, Lawrence Livermore National Laboratory, LLNL-TR-401531, Dec. 2007.

[Sokkappa 2008] Sokkappa, Padmini, et. al., *Assessment of Long-Dwell, In-Transit Radiation Detection Systems for Cargo Ships: Final Report*, Lawrence Livermore National Laboratory, LLNL-TR-405924, July 2008.

[Vaughn 2005] Vaughn, Andrew C., Ofelia P. Bredt, Eleanor T. Dixon, Robert G. Hillaire, Hugh L. Scott, Alan Sicherman, Mark F. Tardiff, and Randy M. Walker, *Radioactive Nuisance Sources Report (Project Pitchfork)*, Sandia National Laboratories, SAND 2005-4183, July 2005.

[Wheeler 2009] Wheeler, Richard, Karl Nelson, David Lange and Thomas Edmunds, *Securing the Cities: Analysis of Alternatives for Urban Traffic Screening at a Bridge or Tunnel*, Lawrence Livermore National Laboratory, LLNL-TR-409922, January 2009.

Appendix A Calculations of Effective Half-lives

For each medication we have documented our calculation of the effective half-life based on biokinetic data used to calculated patient dose. These models are intended for a more complicated estimate of distribution as it is critical in dosimetry to understand which organs have taken up the radionuclide. Often the models are too sophisticated for our simple purpose. Early models prior to 1980 used biological half time as the metric of retention. Later models assume non-exponential distributions to more accurately reflect dose. However, the older models are better suited for our needs. Thus wherever possible we have used the total body retention model. As we should generally consider these treatments to be given to individuals with a poor state of health, we generally prefer to assume an unhealthy model. This will generally favor a longer retention of the labeled drug. The exception is for those cases in which retention is the result of a rare or secondary health problem. Most body models only fit the first few days after dosing after which the residual dose has faded below health concerns. Unfortunately, this may not be below the level detectable with a radiation detector.

^{51}Cr-EDTA

Chromium ethylene diaminetetraacetic acid (Cr-EDTA) may be administered either as intravenously or orally. From the blood stream, the total body retention has a half time of 100 min (0.99) and 7d (0.01) and is excreted in the urine. Oral doses have only 1-5% uptake. **[ICRP53 1987, p105]**. We assume a 24h half time for GI tract. Thus the injected effective model will be 100 m (0.99) and 6.5 d (0.01). The oral model will be 23 h (0.95), 100 m (0.049), and 6.5 d ($5e^{-4}$).

^{51}Cr-RBC

Chromium-labeled erythrocytes are cells labeled with a radioactive nuclide. The cells die with a half-life of 42 d and are then taken up by body tissues. Of the portion taken up by the body 90% is eliminated with a half-life of 10 d and the remainder is assumed to have a half live of 160 d. **[ICRP53 1087, p111]**. This is a complex process but for this we will simply take the longest half-life. This gives us a biological model of 42 d (0.9) and 160 d (0.1). The effective half-life will thus be 16.7 d (0.9) and 23.6 d (0.1).

^{57}Co/^{58}Co Vitamin B_{12}

Four uses are listed for this drug. If administered intravenously without a carrier, the total body model is given as 1.0 d (0.1) and 500 d (0.9). With a carrier this shifts to 1.0 d (0.9) and 500 d (0.1). However, these uses do not seem to fit GI examinations we have in our examination table. For a GI intake test, the dose is given orally with or without flushing. Oral without flushing 30% passes to the GI tract and the remainder has the same body model as without carrier given as 1.0 d (0.1) and 500 d (0.9). Flushing reduces the retained portion to 100 m (0.34), 1 d (0.06) and 500 d (0.6) **[ICRP-53 1987, pp127-133]**. We will assume the flushing model assuming minimizing dose to patient is standard practice.

^{59}Fe-citrate

No ICRP model given for citrate form, however the citrate dissociates into the ion form. Oral administration of iron is taken up by the body between 0.1 and 0.5 depending on the health of the patient. No retention model is given for iron as the body uses iron for a number of important biological processes. We will thus assign this as 1 d (0.9) and ∞ (0.1).

^{67}Ga-citrate

This nuclide is of particular concern as it emits several lines that could be interpreted as indicative of fissile material. We have heard of multiple incidences where a patient was detained as the result of improper identification. The total body model for gallium is 1.25 d (0.17) and 25.5d (0.83) **[ICRP-53 1987, p141]**. The effective half-life will be 22 h (0.17) and 2.9d (0.83).

^{75}Se-HCAT

This nuclide is of some concern as it is a dual use nuclide. It is found in several industrial sources and may be used in a potential RDD. It has a fairly long half-life and thus may be in the patient long after the dose is administered. The whole body retention model for ^{75}Se is given as 2.7 d (0.97) and 62 d (0.03) **[ICRP-53 1987, p153]**. It has a physical half-life of 119.8 d, thus the effective half lives would be given as 2.6 d (0.97) and 41 d (0.03).

^{81m}Kr-krypton

Krypton gas is inert and has a very short physical half-life (13 s). It is produced from a gas generator which we will need to model separately. Given the very short half-life, we do not believe there is any reason this will ever be seen in a patient **[ICRP53 1987, p. 159]**.

^{99m}Tc-anti-CEA

This is a radio labeled antibody (anti-carcinoembryonic monoclonal antibody). We were not able to identify a specific model for this particular drug in the ICRP. Antibodies are relatively large molecules and are described as slowly clearing from the body. We will used the biological model for monoclonal tumour-associated antibodies **[ICRP106 2009, p115]**. This gives a biological half-life to metabolism of 24 h (0.5) and 96 h (0.5). Assuming that the free nuclide is quickly excreted, this gives us an effective half-life of 4.8 h (0.5) and 5.7 h (0.5).

^{99m}Tc-DMSA (2,3-dimercaptosuccinic acid)

The whole body retention function for this nuclide is given as 2.0 h (0.25), 1.8d (0.25), ∞ (0.5) **[ICRP53 1987, p185]**. With the physical half-life of 6.01 h, this will result in an effective half-life of 1.5 h (0.25), 2.8h (0.25), and 6.01 h (0.5).

^{99m}Tc-DTPA

This drug has two common methods of administration. Intravenous administration of Tc-diethylenetriaminepentaacetatic acid has a total body retention given as 100m (0.99) and

7 d (0.01) **[ICRP53 1987, p187]**. It is also given intrathecal as part of a spinal exam. We will assume the intravenous method for both GI and renal examination types. The effective half-life is thus calculated as 72 m (0.99) and 5.8 h (0.01).

^{99m}Tc-ECD

This drug (Ethyl cysteinate dimer) is used for brain imaging and thus is intended to be retained in the brain for the duration of imaging. There is no total body retention function given for this drug and thus we must imply it from the individual organs **[ICRP106 2009, p106]**. Summing up the organs we find the biological half-life to be given roughly by 1 h (0.9) and 36 h (0.1). This gives us an effective half-life of 51 m (0.9) and 5.2 h (0.1).

^{99m}Tc-Ery n.d.

We were not able to locate any drugs that fit this description. We will thus need to assume that the effective half-life is the physical half-life of 6.01 h.

^{99m}Tc-granuloscint

We were not able to find the exact description of this particular drug in the literature. However, in several papers it was referred to as ^{99m}Tc labeled anti-NCA-95 antibody (anti-CD66/CD67). These are a type of labeled antibody. This is a large molecule that clears slowly from the body. We will use the model for monoclonal tumour-associated antibodies **[ICRP106 2009, p115]**. This gives us an effective half-life of 4.8 h (0.5) and 5.7 h (0.5).

^{99m}Tc-HIDA

This drug is used in liver diagnostics and has a wide range of biological half lives depending on the condition of the liver. There is no total body retention model given for this drug. The primary organ is the liver which takes up about 0.85 of the total dose. The release time is between 45 m for a healthy individual to 8 d for an individual with occlusion of the common bile duct. Liver dose goes to the GI tract with an effective 24 h half-life **[ICRP53 1987, p201]**. We have no frequency data to support which of the various models are best to use though clearly one of the diseased models should be preferred. We will assume a rough average of the different models where the liver is not blocked. The assumed model will be 24 h (0.85), and 30 m (0.15). This gives us an effective half-life of 4.8 h (0.85) and 27 m (0.15).

^{99m}Tc-HMPAO (Ceretec)

This drug is intended for brain imaging and is designed to cross the brain-blood barrier for an extended period of time. There is no total body retention model given and thus we will need to use the individual organ totals **[ICRP62 1993, p11]**. Assuming an adult 0.55 is taken by the body tissues with half-life of 1 h (0.35) and 2 d (0.65). The other tissues with long half-life include the brain 4d (0.05), kidneys 1 d (0.09) and lungs 3 d (0.085). We will assume the remainder has the half-life of 1 hr. This gives us a total model of 1 h (0.57), 1 d(0.09), 2 d (0.2), 3 d (0.09), and 4 d (0.05).

^{99m}Tc-HSA

This is a radiolabeled albumin. The total body retention model given for HSA is 6.8 h (0.4), 1.29 d (0.22) and 19.4 d(0.38) **[ICRP53 1987, p285]**. These are all long relative to the half-life so our effective half-life model will be 3.2 h (0.04), 5 h (0.22), and 6 h (0.38).

^{99m}Tc-MAA

This drug is administered intravenously and then immediately absorbed in the lungs. There was not total body retention function given for this chemical. One quarter of the dose ends up in the liver with half-life of 5 d. The rest is released from the lung with half-life of 6 h (0.85) and 3 d (0.15) **[ICRP53 1987, p223]**. We will thus assign total body retention to 6h (0.64), 3 d (0.11) and 5d (0.25). The physical half-life is 6.01 h. Thus the effective half-life would be 3 h (0.64) and 5.6 h (0.36).

^{99m}Tc-MAG3 (mertiatide)

This is a replacement for labeled hippuran for imaging of the renal functions. As such it is very quickly excreted. With impaired function the half lives are increase. We will assume the impaired function for this model. The ICRP total body retention with impaired function is 17 m (0.4), 32 m (0.4) and 7.17 h (0.2) **[ICRP62 1993, p15]**. This would give us an effective half-life of 16 m (0.4), 29 m (0.4) and 3.3 h (0.2). The last component would change to 38 m in a healthy individual.

^{99m}Tc-nanocoll

These are a type of colloid as such that biological half-life is long compared to the physical one. Thus the effective half-life will be 6.01 h.

^{99m}Tc-pertechnetate

The ICRP total body retention for this radiopharmaceutical is given as 4.5 h (0.6), and 45 h (0.40) **[ICRP53 1987, p197]**. It is given both intravenously and orally. The difference between these two methods is relatively small as 80% of the oral dose is absorbed. This gives us an effective half-life of 2.6 h (0.6), and 5.3 h (0.40)

^{99m}Tc-phosphates

The ICRP total body retention for this radiopharmaceutical is given as 0.5 h (0.3), 2 h (0.3) and 3 d (0.4) **[ICRP53 1987, p213]**. This model is complicated as some diseases will block the metabolism and excretion of this drug. We will assume the health case which will give us an effective half-life of 0.5 h (0.3), 1.5 h (0.3) and 5.5 h (0.4).

^{99m}Tc-RBC

The ICRP model for this drug is a simple 60h half-life **[ICRP53 1987, p209]**. This gives us an effective half-life of 5.5 hr.

^{99m}Tc-sestamibi (MIBI, Haxamibi, Cardiolite)

This drug is used in imaging of the heart. It is either administered for a stress test or a rest test. The biological uptake depends on the type of the test, but this has little difference for

the purpose of whole body retention. No total body retention function is given and thus we must depend on the totals from the individual organs. Aside from minor organs all the biological half lives are given as 1 d for this drug and thus our effective half-life will be 4.8 h **[ICRP62 1993, p15]**.

^{99m}Tc-colloid

Colloids denote multiple types of labeled drugs including sulphur colloid, tin colloid and minimicroaggregated albumia, and antimony suphide colloid. As such multiple uses are listed for a broad range of chemicals. The primary listed use is in liver diagnostics. This drug is not excreted from the body and thus its effective half-life is the physical half-life **[ICRP53, p179]**. The other use of a colloid is in tumor diagnostics. In this case the drug is removed with the tumor and thus will not be visible in the patient. As our data is for GI examinations we will assume this is entirely liver diagnostics.

^{99m}Tc-technegas

This is an aerosol which is inhaled for lung imaging. The particles settle in the lung and are retained. It is not clear what fraction is exhaled, and it does not appear to be listed as a factor for technegas. For a related drug, pertechnegas, 75% is exhaled with a half-life of 10 m. Of the fraction that remains in the lungs, the biological half-life is long compared to the physical one and is given as 8 h (0.05) and 4 d (0.95) **[ICRP80 1998, p31]**. This gives us an effective half-life of 3.4 h (0.05) and 5.7 h (0.95).

^{99m}Tc-tetrofosmin (Myoview)

This is a drug used in myocardial profusion studies. No total body retention function is given for this drug in the ICRP. We will thus use only the other organs and tissues model which accounts for 80% of the total activity. The tissues model is given with a half-life of 20 m (0.15) and 1 d (0.85) **[ICRP80 1998, p35]**. This gives us an effective half-life of 19 m (0.15) and 4.8 h (0.85).

^{99m}Tc-venticoll

This appears to be a trade name for a type of nanocolliod. We will consider the effective half-life to be the same. Colloids are not absorbed by the body and thus the effective half-life is 6.01 hr.

^{99m}Tc-WBC

These are nuclide tagged white blood cells. There was not total body retention function given for this form **[ICRP53 1987, p229]**. Thus we will adopt the same model as ^{111}In-WBC with a 70 d half-life. The biological half-life is long compared to the physical one of 6.01 h. Thus the effective half-life is simply 6 h.

^{111}In-antimyosine

This drug is used to image necrosis most commonly associated with damage to the heart. It is an antibody product otherwise known as indium-*111 (In*-111) monoclonal *antimyosin* antibody. Antibodies have relatively long retention times as they are large molecules. The total body retention model for this drug is given as biological retention

rates as 1.09 hr^{-1} (0.054), 0.18 hr^{-1}(0.13), 0.0035 hr^{-1}(0.83) **[Smith 1999]**. We need to convert this from rates to half lives giving us a biological half-life of 38 m (0.054), 3.85 h (0.13), 198 h (0.83). We combine this with the 2.8 d physical half-life to get the effective half-life of 37 m (0.054), 3.6 h (0.13), 50 h (0.83). This drug may be used with dual isotope imaging with ^{201}Tl to observe perfusion **[Bhattacharya 1991]**.

^{111}In-octreotide

This is a peptide used for diagnostics of brain and GI tumors. The label remains tied to the peptide. There is no whole body retention function given and thus we will need to add up the individual organs. Fortunately, all of the half lives given are similar time base and thus we can sum them directly to get 3h (0.77), 2.5 d (0.21), and 70 d (0.02) **[ICRP80 1998, p43]**. The physical half-life is 2.8 d. This gives us an effective half-life of 2.9 h (0.77), 1.3 d (0.21) and 2.7 d (0.02).

^{111}In-platelets

The ICRP biokinetic model does not give a total body retention function for this drug thus the model will need to be based on the individual organs **[ICRP53 1987, p253]**. As platelets are not disposed of directly but rather broken down by the body and recycled, excretion is very slow and in the ionic form. This means the biological half-life is 70 d. This gives us an effective half-life of 2.7 d (1.0).

^{111}In-WBC

These are radionuclide labeled white blood cells. No whole body model is given for this pharmaceutical product, thus we will need to model the retention from the individual tissue retentions **[ICRP53 1987, p255]**. All tissues are assumed to have a retention half-life of 70 d for the purposes of dose, thus our effective half-life is given as 2.7 d (1.0).

^{123}I-hippuran

This chemical administered intravenously and immediately is excreted from the renal system. The biological half-life is a mere 25 min. At the worst case 0.04 is retained by the liver with a half-life of 4.2 h. **[ICRP53 1987, p305]**. We would thus compute the effective half-life as 24 m (0.96) and 3.2 h (0.04). Given the short half lives involved this chemical is unlikely to be seen in this form.

^{123}I-IBZM

ICRP-53 does not include this radiopharmaceutical thus we used published literature instead. The whole body retention has an effective half time of 6.22 h **[Kuikka 1994].**

^{123}I-IMT (*alpha-methyl tyrosine*)

ICRP-53 does not include this radiopharmaceutical thus we used published literature instead. This tracer is used in combination with sodium perchlorate to prevent absorption in the body. As such the body excretes the radiopharmaceutical quickly with an effective half-life based on renal estimations of about 60 m. **[Schmidt 1997]**.

^{123}I-MIBG (meta-iodobenzylguanidine)

Total body retention models for this pharmaceutical is given as 3h (0.36), 1.4 d (0.63) and ∞ (0.01) **[ICRP53 1987, p329]**. Combine with the physical half-life of 13.2 h, gives us an effective half-life of 2.44 h (0.36), 9.5 h (0.63) and 13.2h (0.01)

^{123}I-BMIPPA/^{123}I-IPPA

These are labeled fatty acids used to study the function of the heart. The model for this drug is quite complex and there is no total body retention function given. We will thus need to add up individual organs to get the total **[ICRP106 2009, p137]**. The organ summed model is 1h (0.07), 48 h (0.73), and ∞ (0.2). This gives us an effective half-life of 1h (0.07), 10.4 h (0.73), and 13.2 h (0.2).

^{131}I-norcholesterol

This radiopharmaceutical has a biological half-life given as 1.4 d (0.2) and 13 d (0.8) **[ICRP53 1987, p317]**. We combine this with 8.05 d physical half-life to get effective half-lives of 1.2 d (0.2) and 5 d (0.8).

^{123}I-IPT (tropane)

This is a drug with a binding affinity to the brain receptors for dopamine with structural similarities to cocaine. The total body retention function is given with a half-life of 6.22 h for this compound **[Kuikka 1994]**. This gives us an effective half-life of 4.2 h.

^{133}Xe-gas

This is a gas and thus is not retained significantly. In the worst case, with a 10 min rebreather treatment, the biological retention is given as 22 s (0.77) and 24 m (0.23) **[ICRP53 1987, p341]**. Combining this with the physical half-life of 5.2 d, we find the effective half-life is the biological half-life. Assuming our 2 hour minimum prior to viewing by the detector, this source is unlikely to be seen in a patient.

^{201}Tl-chloride

This is the most commonly seen medical radionuclide in the field. Although it is not the most frequently administered, ^{201}Tl has a longer half-life than ^{99m}Tc and thus makes it more visible. It is administered as an injection, and the whole-body retention is given as 7 d (0.63) and 28d (0.37) **[ICRP53 1987, p371]**. It has a physical half-life of 3 d, thus this gives us an effective half-life of 50 h (0.63) and 65 h (0.37).

Appendix B Summary of Registry of Radioactive Sealed Sources and Devices

Although the centralized Registry of Radioactive Sealed Sources and Devices is not available to the public, many manufacturers provide the safety sheets on their websites. We have gathered roughly 40 of these sheets and have summarized their contents in the table below. In lieu of better data, we would propose using these sources to illustrate the modeling procedure described in this report. The following notation is used in the table:

- \- Denotes that no nuclide was specified so the category (as defined in **[IAEA 2003]**) is not applicable.
- ? Indicates sources for which there is no assigned D value in **[IAEA 2003]**. Dangerous quantity values are the basis of IAEA categories, so assignment of the category requires a D value.

Registry Number	Use	Source	Activity	Category	Shielding
CA-0208-D-102-S	Neutron Moisture Gauge	^{137}Cs	10mCi	5	NA
CA-0208-D-102-S	Neutron Moisture Gauge	^{241}Am/Be	50mCi	4	NA
CA-384-S-102-U	Radiography	^{192}Ir	100 Ci	2	Radiography Carrier
CA-406-S-102-S	Utility Neutron Source (Well logging, gauging)	^{252}Cf	5 mCi	4	Unshielded plug
CA-406-S-148-S	Gamma Calibration Source	various	10 mCi	-	None
CA-406-S-154-S	Line Source	various	300 mCi	-	None
CA-406-S-165-S	Medical Radiography Source	^{57}Co	100 mCi	5	None
CA-406-S-165-S	Medical Radiography Source	^{153}Gd	300 mCi	4	None
CA-406-S-169-S	Medical Reference Source	^{60}Co	500 μCi	4	None
CA-406-S-171-S	Medical Reference Source	^{57}Co	1 mCi	5	None

Registry Number	Use	Source	Activity	Category	Shielding
CA-406-S-172-S	Medical Reference Source	^{57}Co	300 μCi	5	None
CA-406-S-173-S	Calibration Source	^{57}Co	200 μCi	5	None
CA-406-S-180-S	Medical Reference Source	^{57}Co	20 mCi	5	None
GA-1138-D-104-S	Gamma Irradiator, Category I	^{137}Cs	4 Ci	3	4” Lead
LA-567-S-102-S	Brachytherapy Source (clinical trial)	^{192}Ir	0.5 Ci	4	45 lb Lead
LA-612-D-102-U	Radiography Device	^{192}Ir	300 Ci	2	17 kg DU
LA-612-D-102-U	Radiography Device	^{75}Se	300 Ci	2	17 kg DU
LA-612-D-102-U	Radiography Device	^{169}Yb	300 Ci	2	17 kg DU
LA-612-D-103-U	Radiography Device	^{192}Ir	240 Ci	2	16 kg DU
LA-612-D-112-U	Radiography Device	^{60}Co	300 Ci	2	~4” DU
LA-612-S-105-S	Radiography Source	^{60}Co	110 Ci	2	Radiography Carrier
LA-612-S-105-S	Radiography Source	^{192}Ir	240 Ci	2	Radiography Carrier
LA-612-S-111-S	Radiography Device	^{192}Ir	150 Ci	2	17 kg DU
LA-612-S-113-S	Radiography Source	^{60}Co	300 Ci	2	Radiography Carrier
LA-612-S-114-S	Radiography Source	^{60}Co	110 Ci	2	Radiography Carrier
MA-0555-S-101-S	Radiography Source	^{192}Ir	155 Ci	2	Radiography Carrier
MA-1059-D-127-S	Radiography Source	^{192}Ir	240 Ci	2	19 kg DU
MA-1059-D-127-S	Radiography Source	^{60}Co	120 mCi	3	19 kg DU
MA-1059-D-127-S	Radiography Source	^{137}Cs	10.8 Ci	3	19 kg DU
MA-1059-D-127-S	Radiography Source	^{75}Se	81 Ci	2	19 kg DU

Registry Number	Use	Source	Activity	Category	Shielding
MA-1059-D-127-S	Radiography Source	^{169}Yb	40 Ci	3	19 kg DU
MA-1059-D-127-S	Radiography Source	^{170}Tm	400 Ci	4	19 kg DU
MA-1059-D-334-S	Radiography Source	^{192}Ir	150 Ci	2	35 lb DU
MA-1059-D-334-S	Radiography Source	^{60}Co	65 mCi	3	35 lb DU
MA-1059-D-334-S	Radiography Source	^{75}Se	80 Ci	2	35 lb DU
MA-1059-D-334-S	Radiography Source	^{169}Yb	20 Ci	3	35 lb DU
MA-1159-D-101-B	X-Ray Fluorescence	^{109}Cd	50 mCi	5	Tungsten (<0.1 mR/hr)
MA-1159-D-101-B	X-Ray Fluorescence	^{55}Fe	40 mCi	5	Tungsten
MA-1159-D-101-B	X-Ray Fluorescence	^{241}Am	30 mCi	4	Tungsten
MA-1159-D-101-B	X-Ray Fluorescence	^{109}Cd	40 mCi	5	Tungsten
MA-1159-D-101-B	X-Ray Fluorescence	^{241}Am	30 mCi	4	Tungsten
MA-1159-D-101-B	X-Ray Fluorescence	^{241}Am	1-5 μCi	5	Tungsten
MA-1159-D-101-B	X-Ray Fluorescence	^{241}Am	5 mCi	5	Tungsten
MA-0476-S-108-S	X-Ray Fluorescence	^{109}Cd	300 mCi	5	Tungsten
MA-0476-S-108-S	X-Ray Fluorescence	^{109}Cd	100 mCi	5	Tungsten
MA-0476-S-108-S	X-Ray Fluorescence	^{109}Cd	1000 mCi	5	Tungsten
NC-356-D-101-S	Portable Moisture and Density Gauge	^{137}Cs	11 mCi	5	Complex
NC-356-D-101-S	Portable Moisture and Density Gauge	^{241}Am/Be	44 mCi	4	Complex
NC-646-D-126-S	Portable Moisture Gauge	^{241}Am/Be	44 mCi	4	Complex
NC-646-D-128-S	Asphalt Content Gauge	^{241}Am/Be	110 mCi	4	Complex

Registry Number	Use	Source	Activity	Category	Shielding
NC-646-D-128-S	Asphalt Content Gauge	^{241}Am/Be	120 mCi	4	Complex
NC-646-D-128-S	Asphalt Content Gauge	^{241}Am/Be	330 mCi	4	Complex
NC-646-D-130-S	Portable Moisture and Density Gauge	^{137}Cs	9 mCi	5	Complex
NC-646-D-130-S	Portable Moisture and Density Gauge	^{241}Am/Be	44 mCi	4	Complex
NC-646-D-130-S	Portable Moisture and Density Gauge	^{252}Cf	55 μCi	5	Complex
NC-646-D-131-S	Thin-layer Density Gauge	^{137}Cs	9 mCi	5	Complex
NC-646-D-134-S	Portable Moisture Gauge	^{241}Am/Be	11 mCi	4	Complex
NC-646-D-135-B	Laboratory Asphalt Content System	^{252}Cf	110 μCi	5	Complex
NC-646-D-137-S	Laboratory Moisture Content System	^{252}Cf	110 μCi	5	Complex
NC-646-D-830-S	Portable Moisture and Density Gauge	^{137}Cs	9 mCi	5	Complex
NC-646-D-830-S	Portable Moisture and Density Gauge	^{241}Am/Be	44 mCi	4	Complex
NC-646-D-830-S	Portable Moisture and Density Gauge	^{252}Cf	66 μCi	5	Complex
NR-112-D-111-S	Mold Level Control	^{60}Co	2-300 mCi	3	100-240 mm Lead
NR-112-D-111-S	Mold Level Control	^{137}Cs	82-500 mCi	4-5	100-240 mm Lead
NR-536-D-110-B	Detector Cell Assembly	^{63}Ni	NA	-	NA
NR-1235-S-101-S	Teletherapy Source	^{60}Co	Large	1?	NA
NR-1235-S-102-S	Medical Reference Source	^{60}Co	100 μCi	5	NA

Registry Number	Use	Source	Activity	Category	Shielding
NR-1235-S-102-S	Medical Reference Source	^{133}Ba	500 μCi	?	NA
NR-1235-S-102-S	Medical Reference Source	^{137}Cs	500 μCi	5	NA
NR-1235-S-102-S	Medical Reference Source	^{22}Na	500 μCi	?	NA
NR-1235-S-102-S	Medical Reference Source	^{57}Co	15 mCi	5	NA
NR-1235-S-102-S	Medical Reference Source	^{68}Ge	500 μCi	5	NA
WA-0406-S-202-S	Medical Radiography	^{68}Ge	13 mCi	5	NA
WA-653-D-102-S	X-Ray Fluorescence	^{57}Co	40 mCi	5	Tungsten
WA-653-D-102-S	X-Ray Fluorescence	^{241}Am	150 mCi	4	Tungsten
WA-653-D-102-S	X-Ray Fluorescence	^{109}Cd	150 mCi	5	Tungsten
CA-406S162S	Portable Moisture Density Gauge	^{241}Am	40 mCi	4	NA
CA-406-S-177-S	Gamma Gauging	^{22}Na	100 mCi	?	NA
CA-406-S-177-S	Gamma Gauging	^{57}Co	300 mCi	4	NA
CA-406-S-177-S	Gamma Gauging	^{58}Co	300 mCi	?	NA
CA-406-S-177-S	Gamma Gauging	^{60}Co	300 mCi	4	NA
CA-406-S-177-S	Gamma Gauging	^{68}Ge	50 mCi	5	NA
CA-406-S-177-S	Gamma Gauging	^{133}Ba	50 mCi	?	NA
CA-406-S-177-S	Gamma Gauging	^{137}Cs	50 mCi	4	NA
CA-406-S-177-S	Gamma Gauging	^{226}Ra	50 mCi	4	NA
CA-406-S-177-S	Gamma Gauging	^{229}Th+^{232}Th	50 mCi	?	NA

Registry Number	Use	Source	Activity	Category	Shielding
CA-406-S-177-S	Gamma Gauging	$^{230}Th+^{232}Th$	50 mCi	?	NA
CA-406-S-177-S	Gamma Gauging	^{252}Cf	1 mCi	5	NA
CA-384-S-114-S	Radiography Source	^{192}Ir	120 Ci	2	Radiography Carrier
LA-612-S-106-S	Radiography Source	^{192}Ir	140 Ci	2	Radiography Carrier